

Mitochondrial catastrophe during doxorubicin-induced cardiotoxicity: An evaluation of the protective role of melatonin.

by

Yogeshni (Jenelle) Govender

*Dissertation presented for the degree of Doctor of Philosophy
(Physiological Sciences) in the
Faculty of Science at
Stellenbosch University*



Supervisor: Prof Anna-Mart Engelbrecht

Co-supervisor: Dr Ben Loos

Co-supervisor: Dr Erna Marais

March 2017

Declaration

By submitting this thesis/dissertation electronically, I declare that the entirety of the work contained therein is my own, original work, that I am the sole author thereof (save to the extent explicitly otherwise stated), that reproduction and publication thereof by Stellenbosch University will not infringe any third party rights and that I have not previously in its entirety or in part submitted it for obtaining any qualification.

March 2017

Copyright © 2017 Stellenbosch University

All rights reserved

Abstract

Introduction: Anthracyclines, such as doxorubicin (DXR), are among the most valuable treatments for various cancers, but their clinical use is limited due to detrimental side-effects such as cardiotoxicity. The abundance of mitochondria in cardiomyocytes closely links mitochondrial function with myocardial function. Mitochondrial dysfunction has emerged as a critical element in the development of DXR-induced cardiotoxicity. In light of this scenario, melatonin (MLT) is a potent anti-oxidant, is non-toxic, is dually oncostatic and cardio-protective, and has been shown to influence mitochondrial homeostasis and function. Both endogenously produced and exogenously administered MLT during or prior chemotherapy shows great promise in this therapeutic avenue as demonstrated in several studies. Although research support the mitochondrial protective role of MLT, the exact mechanisms by which MLT confers mitochondrial protection in the context of DXR-induced cardiotoxicity remains to be elucidated.

Aims: The aim of this study was to investigate the effect of MLT on the following mitochondrial and cellular parameters: mitochondrial reactive oxygen species (ROS) production, mitochondrial membrane potential, mitochondrial fission and fusion, mitochondrial bioenergetics and biogenesis, sirtuin activity, autophagy and cell death in an *in vitro* model of DXR-induced cardiotoxicity. Furthermore, the effect of MLT on cardiac function and tumor growth was assessed in a tumor-bearing rat model of acute DXR-induced cardiotoxicity.

Materials and Methods: H9c2 rat cardiomyoblasts were pre-treated with MLT (10 μ M) for 24 hours followed by DXR treatment (3 μ M) for 24 hours. Following treatment, the above mentioned mitochondrial and cellular parameters were assessed using immunoblot analysis, mitochondrial respiration analysis, flow cytometry, fluorescence microscopy and luciferase-based assays.

Sprague Dawley female rats (16-18 weeks old), were inoculated with LA7 rat tumor cells. Animals received DXR (3 intraperitoneal injections of 4 mg/kg at 3-day intervals, 12 mg/kg cumulative dose) and/or received MLT (6 mg/kg) daily in their drinking water. Tumors were measured daily using

digital calipers and tumor volumes calculated. Animal weights were recorded daily. Rat hearts were used to conduct isolated heart perfusions to assess cardiac function and thereafter, heart tissue was used for immunoblot analysis.

Results: DXR treatment significantly increased cell death, mitochondrial ROS levels and mitochondrial fission and these effects were significantly reduced with MLT pre-treatment. Furthermore, MLT pre-treatment significantly increased mitochondrial membrane potential, mitochondrial biogenesis and cellular ATP levels reduced by DXR treatment.

Cardiac output and total work performance of the heart was significantly increased in rats treated with DXR+MLT in comparison to rats treated with DXR alone. In addition, body and heart weights were significantly reduced in DXR-treated rats in comparison to DXR+MLT treated rats. Tumor volumes were significantly reduced in DXR+MLT-treated rats on Day 8 in comparison to DXR-treated rats.

Discussion and Conclusion: The results obtained from the current study indicates that MLT treatment confers a cardio-protective effect by maintaining mitochondrial function, increasing cardiomyocyte survival and improving cardiac function during DXR-induced cardiotoxicity. Furthermore, MLT treatment alone suppresses the growth of tumors. The combination of DXR+MLT treatment rapidly reduced tumor growth, suggesting that MLT enhances the oncostatic activity of DXR. The unique ability of MLT to be both cardio-protective and oncostatic during DXR-induced cardiotoxicity is promising for the field of cardio-oncology.

Opsomming

Inleiding: Antrasikliene, soos doxorubicin (DXR), is van die mees waardevolle behandelings-opsies vir verskeie tipes kankers, maar die kliniese gebruik daarvan word deur die nadelige newe-effekte beperk, wat kardiotoxisiteit insluit. Die groot hoeveelheid mitochondria in kardiomyosiete verbind mitochondriale funksie aan kardiaale funksie. Na aanleiding hiervan, is daar al bewys dat melatonien (MLT), 'n kragtige antioksidant, nie-toksies, gelyktydig onkostaties en kardio-beskermend, mitochondriale homeostase en funksie kan beïnvloed. Dit is al in verskeie navorsing bewys dat beide endogeen geproduseerde en eksogeen toegediende MLT tydens en voor chemoterapie groot belofte as behandelings-opsie inhou. Alhoewel navorsing al die beskermende rol van MLT bewys het, moet die presiese meganisme waardeur MLT mitochondria beskerm in die konteks van DXR-geïnduseerde kardiotoxisiteit, nog bepaal word.

Doelwitte: Die doel van hierdie studie was om die effek van MLT op die volgende mitochondriale en sellulêre parameters in 'n *in vitro* model van DXR-geïnduseerde kardiotoxisiteit te bepaal: Mitochondriale reaktiewe suurstofspesie produksie, mitochondriale membraanpotensiaal, mitochondriale splyting en fusie, mitochondriale bio-energie produksie en biogenese, sirtuin aktiwiteit, autofagie asook seldood. Die effek van MLT op kardiaale funksie en tumorgroei is ook in 'n tumor-draende rot model van akute DXR-geïnduseerde kardiotoxisiteit geondersoek.

Materiaal en Metodes: H9c2 rot kardiomyoblaste is met MLT (10 μ M) vir 24 uur behandel voordat die met DXR (3 μ M) ook vir 24 uur behandel is. Na behandeling is die bo-vermelde mitochondriale en sellulêre parameters bepaal deur middel van immunoblot bepaling, mitochondriale analises, vloeisitometrie, fluoressensie mikroskopie en lusiferase-gebaseerde bepaling.

Sprague Dawley vroulike rotte (16-18 weke oud) is met LA7 rot tumorselle geïnkuleer. Die rotte het DXR (3 intraperitoneale inspuitings van 4 mg/kg met 3-dag intervalle en 'n 12 mg/kg kumulatiewe dosis) en/of MLT (6 mg/kg) daagliks in hul drinkwater ontvang. Tumore is daagliks met 'n digitale meetpasser gemeet en tumor volumes is bereken. Die rotte is ook daagliks geweeg. Rotharte is

geïsoleer en geperfuseer om kardiaale funksie te bepaal en daarna is dit vir immunoblot analises gebruik.

Resultate: DXR behandeling het seldood geïnduseer, mitochondriale reaktiewe suurstofspesie vlakke verhoog en het ook mitochondriale splyting veroorsaak. Hierdie negatiewe effekte van DXR is beduidend verminder wanneer die selle vooraf met MLT behandel is. MLT behandeling het ook mitochondriale membraanpotensiaal, mitochondriale biogenese en sellulêre ATP vlakke verhoog wat deur DXR behandeling verlaag was.

Kardiaale omset en kardiaale werkverrigting van die harte was beduidend verhoog in rotte wat met beide DXR en MLT behandel is in vergelyking met harte van die DXR behandelde rotte. Verder is die liggaamsgewig en die massas van die harte ook beduidend verlaag in vergelyking met die DXR en MLT behandelde rotte. Tumor volumes is ook alreeds beduidend verlaag op dag 8 in die DXR en MLT behandelde rotte in vergelyking met die DXR behandelde rotte.

Bespreking en Gevolgtrekking: Die resultate van hierdie studie bewys onteenseglik dat MLT behandeling sy kardio-beskermende effekte tydens DXR-geïnduseerde kardiotoxisiteit teweegbring deur mitochondriale funksie te handhaaf, asook om kardiomiosiet oorlewing en kardiaale funksie te verbeter. Verder kan MLT behandeling op sy eie ook tumor-groei onderdruk. Die kombinasie van DXR en MLT behandeling het tumor-groei vinniger geonderdruk wat moontlik 'n bewys is dat MLT die onkostatiese aktiwiteit van DXR kan verhoog. Hierdie unieke vermoë van MLT om beide kardio-beskermend en onkostaties tydens DXR-geïnduseerde kardiotoxisiteit te wees, maak van MLT 'n belowende terapeutiese opsie in die veld van kardio-onkologie.

Acknowledgements

Thank you Heavenly Father for the strength and courage you have provided me with to persevere during challenging times.

I would like to thank the following people to whom I will be forever grateful:

My supervisor, Professor Anna-Mart Engelbrecht, my gratitude to you is beyond words. Over the years, you have been an exceptional mentor, a friend, a mother and a daily inspiration to me. Your unwavering support, encouragement, patience, understanding, and faith in me, has enabled me to persevere during challenging times and to achieve my career goals. Thank you for entrusting me with this project and for allowing me the freedom to explore my ideas whilst providing insight and guidance to the very end of this PhD journey. Prof, you are truly a blessing in my life and one in a million.

My co-supervisor, Dr Ben Loos, my sincerest gratitude to you for your mentorship, assistance, advice, and expertise. You have a passionate and enthusiastic approach to research which has inspired me over the years and has kept me motivated. Thank you for always taking the time to share your insights and guide me along this journey.

My co-supervisor, Dr Erna Marais, thank you for your support, guidance and expertise. Your cheerful spirit always made me smile during those long hours at Tygerberg.

Prof Lochner, thank you for initiating the melatonin research on the heart. Your passion for research is truly inspiring.

Mev. S. Genade, a special thank you for conducting the perfusions. The moments of laughter and wonderful stories shared while working, kept me going strong.

A very BIG thank you to those who assisted in this study. I truly appreciate your technical assistance and your guidance (Ashwin Isaacs, Megan Mitchell, Zaakiya Emjedi, Dr TA Davis, Dr A Krygsman, Jurgen Kriel, Dr D Joseph, Dr P Durcan, Prof F van der Westhuizen, Hayley van Dyk, Lize Engelbrecht and Rozaan Adams, Dr L Lacerda, Dr BJN Sishi, Mev Judy Faroo, Paul Williams).

DSG and CRG research groups, thank you for your support, laughs, and discussions on research.

Academic and technical staff, thank you for the great leadership.

To my parents and family, none of this would have been possible without your unconditional love, support, and care. Thank you for all the sacrifices you have made to help me achieve my goals, for this I will be forever grateful. A special thank you to my late maternal grandparents (Mr and Mrs Pillay), my aunts (Lolly Enoch and Nellie Naidoo) and uncle (Timothy Enoch) for their guidance, love, advice, motivation and support over the years.

Andre de Bruyn, for the past six years, you have filled my life with immense joy and love. Thank you for your unconditional support and for having faith in me when I had none. You have always stood by my side even during the darkest hours and you fought along side me. Words cannot express my gratitude to you for all that you have endured with me. Thank you for your advice and undivided attention during our conversations on research, science, lab-work and life. I am truly blessed to have you in my life.

Special thanks to the NRF and CANSA for your financial support which enabled me to continue with my studies.

List of figures

Chapter 1

Figure 1.1: The effect of MLT on DXR-induced bioenergetic failure.....	10
Figure 1.2: The effect of MLT on DXR-induced free radical generation.....	15
Figure 1.3: The effect of MLT and DXR on cardiomyocyte cell death.....	22

Chapter 2

Figure 2.1: Schematic representation of the <i>in vitro</i> study design.....	24
Figure 2.2: Schematic representation of <i>in vivo</i> study design.....	38

Chapter 3

Figure 3.1.1: The effect of various DXR concentrations on the cell viability of H9c2 cardiac myoblasts	45
Figure 3.1.2: The effect of various MLT concentrations on the cell viability of H9c2 cardiac myoblasts	46
Figure 3.1.3: The effect of MLT pre-treatment on the cell viability and DXR-induced cell death....	47
Figure 3.2.1: The effect of MLT on the cell viability during DXR-induced cardiotoxicity.....	48
Figure 3.2.2: The effect of MLT on the caspase 3/7 activity during DXR-induced cell death.....	48
Figure 3.2.3: The effect of MLT on cleaved caspase-3 and PARP cleavage during DXR-induced cell death.....	50
Figure 3.3.1: The effect of MLT on autophagy during DXR-induced cardiotoxicity.....	51
Figure 3.3.2: The effect of MLT on Pink1 and PARKIN during DXR-induced cardiotoxicity.....	52
Figure 3.4.1: The effect of MLT on ROS and mitochondrial ROS generation during DXR-induced cardiotoxicity.....	53
Figure 3.5.1: The effect of MLT on mitochondrial membrane potential during DXR-induced cardiotoxicity.....	55
Figure 3.6.1.1: Fluorescence microscopy images.....	56
Figure 3.6.1.2: The effect of MLT on the mitochondrial network during DXR-induced cardiotoxicity.....	57
Figure 3.6.2.1: The effect of MLT on mitochondrial fusion proteins Mfn1 and Mfn2 during DXR- induced cardiotoxicity.....	58
Figure 3.6.2.2: The effect of MLT on mitochondrial fusion protein OPA1 during DXR-induced cardiotoxicity.....	58

Figure 3.6.2.3: The effect of MLT on mitochondrial fission proteins Drp1 and hFis1 during DXR-induced cardiotoxicity.....	59
Figure 3.7.1.1: The effect of MLT on mitochondrial respiration during DXR-induced cardiotoxicity.....	61
Figure 3.7.2.1: The effect of MLT on cellular ATP levels during DXR-induced cardiotoxicity.....	62
Figure 3.7.3.1: The effect of MLT on PGC-1 α during DXR-induced cardiotoxicity.....	63
Figure 3.8.1.1: The effect of MLT on sirtuin activity during DXR-induced cardiotoxicity.....	64
Figure 3.9.1: The effect of daily MLT administration on rat body weight during DXR-induced cardiotoxicity.....	65
Figure 3.9.2: The effect of daily MLT administration on rat tumor volume during DXR-induced cardiotoxicity.....	66
Figure 3.9.3: The effect of daily MLT administration on rat heart weight during DXR-induced cardiotoxicity.....	67
Figure 3.9.4: The effect of daily MLT administration on cardiac function during DXR-induced cardiotoxicity.....	68
Figure 3.9.5.1: The effect of daily MLT administration on cleaved caspase-3 and PARP cleavage during DXR-induced cell death.....	70
Figure 3.9.6.1: The effect of daily MLT administration on LC3 II and p62/SQSTM1 protein levels during DXR-induced cardiotoxicity.....	71
Figure 3.9.6.2: The effect of daily MLT administration on Pink1 and PARKIN protein levels during DXR-induced cardiotoxicity.....	72
Figure 3.9.7.1: The effect of daily MLT administration on Mfn1, Mfn2 and OPA1 protein levels during DXR-induced cardiotoxicity.....	73
Figure 3.9.7.2: The effect of daily MLT administration on Drp1 and hFis1 protein levels during DXR-induced cardiotoxicity.....	74
Figure 3.9.8.1: The effect of daily MLT administration on PGC-1 α protein levels during DXR-induced cardiotoxicity.....	75
Figure 3.9.9.1: The effect of daily MLT administration on SIRT1 and SIRT3 protein levels during DXR-induced cardiotoxicity.....	76
Figure 5.1: The effects of pre-treatment with MLT during DXR-induced cardiotoxicity.....	101

List of abbreviations

β -actin	Beta actin
3-MA	3-methyladenine
ADP	Adenosine di-phosphate
AFMK	N1-acetyl-N2-formyl-5-methoxykynuramine
Am	Area of mitochondrion
AMP	Adenosine monophosphate
AMPK	AMP-activated protein kinase
ANOVA	One-way analysis of variance
ATP	Adenosine tri-phosphate
Bad	Bcl-2-associated death promoter
BAF	Bafilomycin A1
Bak	Bcl-2 homologous antagonist/killer
Bax	apoptosis regulator protein
Bcl-2	B-cell lymphoma 2
Bcl-xL	B-cell lymphoma-extra large
BID	BH3 interacting-domain death agonist
BNIP3	BCL2/adenovirus E1B 19 kDa protein-interacting protein 3
BRR	Basal Respiration Rate
C3-HOM	Cyclic 3-hydroxymelatonin
CaCl ₂ .2H ₂ O	Calcium chloride dihydrate
CAT	Catalase
CCCP	Carbonyl cyanide m-chlorophenyl hydrazone
CCD	charge coupled device
c-Jun	proto-oncogene
CK	Creatine kinase

CO	Cardiac Output
CO ₂	Carbon dioxide
CPT 1/2	Carnitine palmitoyl transferase 1/2
Cr	Creatine
CTRL	Control
cyt c	Cytochrome complex
DCF	Dichlorofluorescein
dH ₂ O	Deionized water
DMEM	Dulbecco modified eagles medium
DNA	Deoxyribonucleic acid
Drp1	Dynamin-related protein 1
DSB	Double stranded DNA
DXR	Doxorubicin
DXR SQ	Doxorubicin semiquinone
ECACC	European collection of cell cultures
ECL	Enhanced chemiluminescence
EDTA	Ethylenediaminetetraacetic acid
ER	Endoplasmic reticulum
ERK 1/2	Extracellular signal-regulated kinases 1/2
ETC	Electron transport chain
EtOH	Ethanol
ETS	Electron transport system
FA-CoA	Fatty acyl-coenzyme A
FADH	Flavin adenine dinucleotide
Fas(L)	Apoptosis-stimulating fragment (ligand)
FCCP	Carbonyl cyanide p-trifluoromethoxyphenyl hydrazone
FITC	Fluorescein

Foxo3a	Forkhead box O3a
GLUT4	Glucose transporter type-4
GPx	Glutathione peroxidase
GRd	Glutathione reductase
GSH	Glutathione
H ⁺	hydrogen ion
H ₂ DCFDA	2',7'-dichlorodihydrofluorescein diacetate
H ₂ O ₂	Hydrogen peroxide
HCl	Hydrogen chloride
hFis1	Fission 1 protein
HSP-70	Heat shock protein-70 kilo dalton
mt-iNOS	Mitochondrial-inducible nitric oxide synthase
I/R	Ischemia/reperfusion
JC-1	5,5',6,6',-tetrachloro-1,1',3,3',-tetraethylbenzimidazolylcarbocyanine
KCl	Potassium chloride
KH ₂ PO ₄	Potassium monophosphate
KHB	Krebs-Henseleit bicarbonate buffer
LC3	Microtubule-associated proteins light chain-3
L-OPA1	Long-form of optic atrophic protein 1
mdivi-1	Mitochondrial fission inhibitor
Mfn 1/2	Mitofusin 1/2
MgSO ₄ .7H ₂ O	Magnesium sulphate heptahydrate
Mi-CK	Mitochondrial creatine kinase
MLT	Melatonin
MnSOD	Mitochondrial antioxidant manganese superoxide dismutase
mPTP	Mitochondrial transition pore opening
mRNA	Messenger RNA

RNA	Ribonucleic acid
MSRC	Mitochondrial spare respiratory capacity
mtDNA	Mitochondrial DNA
mTOR	Mammalian target of rapamycin
MTT	3-(4, 5-Dimethylthiazol-2-yl)-2, 5-diphenyltetrazolium bromide
NA ₂ SO ₄	Sodium sulphate
NA ₃ VO ₄	Sodium orthovanadate
NaCl	Sodium chloride
NAD	Nicotinamide adenine dinucleotide
NADC	Sodium Deoxycholate
NADPH	Nicotinamide adenine dinucleotide phosphate-oxidase
NADH	Dihyronicotinamide adenine dinucleotide
NaF	Sodium Fluoride
NaHCO ₃	Sodium bicarbonate
Nec-1	Necrostatin-1
NOS	Nitric synthase
NP-40	Nonidet-P40
O ₂	Oxygen
OCR	Oxygen consumption rate
OD	Optical density
OMA1	Zinc-metalloprotease
OPA 1	Optic atrophic protein 1
OXPHOS	Oxidative phosphorylation
P-Akt	Protein kinase B
PAO	Aortic pressure
P-p 53	Phospho tumor Protein 53
PARKIN	Parkinson protein

PARP	Poly (ADP-ribose)-polymerase
PBS	Sterile phosphate buffered saline
PCr	Phosphocreatine
PE	Phycoerthrin
PFK	Phosphofructokinase
PGC-1 α	Peroxisome proliferator-activated receptor gamma coactivator 1-alpha
Pi	Inorganic phosphate
Pink1	PTEN-induced putative kinase 1
Pm	Perimeter of mitochondria
PMSF	Phenyl-methyl-sulphonyl fluoride
PPAR-gamma	Peroxisome proliferator-activated receptor gamma
PSP	Peak systolic pressure
PTM	Posttranslational modification
PVDF	Polyvinylidene fluoride
Qa	Aortic flow rate
Qe	Coronary flow rate
RIPA	Radioimmunoprecipitation assay
RNS	Reactive nitrogen species
ROS	Reactive oxygen species
SBTI	Soybean trypsin inhibitor
SDS	Sodium dodecyl sulfate
SEM	Standard error of the mean
SIRT	Sirtuin
SOD	Superoxide dismutase
S-OPA1	Short-form optic atrophic protein 1
SQSTM1/p62	Sequestosome-1
SV	Stroke volume

TBS-T	TRIS-buffered saline-Tween
TCA	Tri-carboxylic acid
T CTRL	Tumor control
TMRE	Tertramethylrhodamine, Ethyl ester, perchlorate
TNF-alpha	Tumor necrosis factor alpha
TOM20	Translocase of outer mitochondrial membrane 20
TRAIL	TNF-related apoptosis-inducing ligand
Tris-HCl	2-Amino-2-(hydroxymethyl)-1,3-propanediol hydrochloride
Trypsin-EDTA	Trypsin-ethylene-diaminetetra-acetic
TW	Total work performance
UV	Ultraviolet
VEH CTRL	Vehicle control
V CTRL	Vehicle Control
vs	versus
YME1L	ATP-dependent metalloprotease

Units of measurements

%	percentage
A	amps
AU	arbitrary unit
cm	centimeter
cm ³	cubic centimeter
g	gram
hr	hour
kDa	kilodalton
kg	kilogram
L	liter
mg	milligram
mg/m ²	milligram per meter squared
min	minute
ml	milliliter
ml/min	milliliter per minute
mm	millimeter
mm ³	cubic millimeter
mM	millimolar
mmHg	millimeter of mercury
mmol	millimole
mWatts	milliWatts
nM	nanomolar
nm	nanometer
rpm	revolutions per minute

μg	microgram
μl	microliter
μm	micrometer
μM	micromolar
μmol	micromole
V	Volt
$^{\circ}\text{C}$	degrees celsius

Table of Contents

Chapter 1: Literature Review

1.1 Introduction.....	1
1.2 Mitochondria: a common target for melatonin and doxorubicin.....	3
1.3 The role of melatonin in doxorubicin-induced bioenergetic failure.....	5
1.4 The role of melatonin in doxorubicin-induced free radical generation.....	11
1.5 The role of melatonin on doxorubicin-induced cardiomyocyte cell death.....	15
1.6 Motivation.....	22

Chapter 2: Materials and methods

2.1 <i>In vitro</i> Study design – Phase 1.....	24
2.1.2 Cell culture and maintenance of H9c2 cell line.....	25
2.1.3 Cell culture treatments.....	25
2.1.3.1 Doxorubicin (DXR) treatment.....	26
2.1.3.2 Melatonin (MLT) treatment.....	26
2.1.4 Cell Viability Assays.....	26
2.1.4.1 MTT Cell Viability Assay.....	26
2.1.4.2 Trypan blue cell exclusion technique.....	27
2.1.5 Apoptosis assay.....	28
2.1.5.1 Caspase-Glo® 3/7 Assay.....	28
2.1.6 ROS generation.....	29
2.1.7 Mitochondrial Membrane Potential Analysis.....	30
2.1.8 Mitochondrial Network Analysis.....	31
2.1.8.1 Live Cell Imaging.....	31
2.1.8.2 Mitochondrial Network and Morphology assessment.....	31
2.1.9 Mitochondrial Bioenergetics.....	32
2.1.9.1 Cellular ATP Analysis.....	32

2.1.9.2 Mitochondrial Respiration Analysis.....	32
2.1.10 Immunoblot Analysis.....	34
2.1.10.1 Whole Cell Protein Extraction.....	34
2.1.10.2 Mitochondrial Isolation from cells and Protein Extraction.....	35
2.1.10.3 Protein Determination and Sample Preparation.....	35
2.1.10.4 Sodium Dodecyl-Sulphate Polyacrylamide Gel Electrophoresis (SDS-PAGE) and Electrotransfer.....	36
2.1.10.5 Immuno-detection.....	36
2.1.11 Statistical Analysis.....	37
2.2 <i>In vivo</i> Study design – Phase 2.....	38
2.2.1 Animal care and grouping.....	39
2.2.2 Cell culture and maintenance of LA7 cell line.....	39
2.2.3 Mammary tumor induction.....	40
2.2.4 Doxorubicin treatment.....	40
2.2.5 Melatonin treatment.....	41
2.2.6 Isolated rat heart perfusions.....	41
2.2.6.1 Perfusion technique of isolated perfused rat heart.....	42
2.2.6.2 Determination of cardiac function.....	42
2.2.7 Immunoblot Analysis.....	43
2.2.7.1 Tissue Protein Extraction.....	43
2.2.7.2 Mitochondrial Isolation from Tissue and Protein Extraction.....	43
2.2.7.3 Protein Determination, Sample Preparation, SDS-PAGE, Electrotransfer and Immuno-detection.....	44

2.2.8 Statistical Analysis.....	44
Chapter 3: Results	
3.1 Pilot study.....	45
3.1.1 The effect of various Doxorubicin (DXR) concentrations on cell viability.....	45
3.1.2 The effect of various melatonin (MLT) concentrations on cell viability.....	46
3.1.3 The effect of MLT pre-treatment on cell viability and doxorubicin-induced cell death.....	46
3.2 The effect of MLT on cell viability and apoptosis during DXR-induced cardiotoxicity.....	47
3.2.1 Trypan blue assay.....	47
3.2.2 Caspase 3/7 activity assessment.....	48
3.2.3 Immunoblot analysis of cleaved caspase-3 and cleaved PARP protein levels.....	50
3.3 The effect of MLT on autophagy during DXR-induced cardiotoxicity.....	51
3.3.1 Immunoblot analysis of autophagy proteins LC3 II and SQSTM1/p62.....	51
3.3.2 Immunoblot assessment of Pink1 and PARKIN protein levels.....	52
3.4 The effect of MLT on ROS and mitochondrial ROS generation during DXR-induced cardiotoxicity.....	53
3.4.1 Flow cytometry analysis of ROS generation with H ₂ DCFDA and MitoSox Red staining.....	53
3.5 The effect of MLT on mitochondrial membrane potential during DXR-induced cardiotoxicity.....	54
3.5.1 Flow cytometry analysis of mitochondrial membrane potential with JC-1 staining.....	54
3.6 The effect of MLT on mitochondrial dynamics during DXR-induced cardiotoxicity.....	55
3.6.1 Mitochondrial Morphometric Network Assessment.....	55
3.6.2 Immunoblot analysis of mitochondrial fission and fusion proteins.....	57
3.7 The effect of MLT on mitochondrial bioenergetics and biogenesis during DXR-induced cardiotoxicity.....	60
3.7.1 Mitochondrial respiration.....	60

3.7.2 ATP Analysis.....	62
3.7.3 Immunoblot analysis of Peroxisome proliferator-activated receptor gamma coactivator 1-alpha (PGC-1 α)	62
3.8 The effect of MLT on sirtuin activity during DXR-induced cardiotoxicity.....	63
3.8.1 Immunoblot analysis of SIRT1 and SIRT3.....	63
3.9 <i>In vivo</i> Study.....	65
3.9.1 The effect of daily MLT administration on rat body weight during DXR- induced cardiotoxicity.....	65
3.9.2 The effect of daily MLT administration on tumor growth during DXR-induced cardiotoxicity.....	66
3.9.3 The effect of daily MLT administration on rat heart weight during DXR-induced cardiotoxicity.....	67
3.9.4 The effect of daily MLT administration on cardiac function during DXR-induced cardiotoxicity.....	68
3.9.5 The effect of daily MLT administration on apoptosis during DXR-induced cardiotoxicity.....	69
3.9.5.1 Immunoblot assessment of cleaved caspase-3 and cleaved PARP protein levels.....	70
3.9.6 The effect of daily MLT administration on autophagy during DXR-induced cardiotoxicity.....	71
3.9.6.1 Immunoblot assessment of autophagy proteins LC3 II and SQSTM1/p62.....	71
3.9.6.2 Immunoblot analysis of Pink1 and PARKIN protein levels.....	72
3.9.7 The effect of daily MLT administration on mitochondrial fusion and fission during DXR-induced cardiotoxicity.....	73
3.9.7.1 Immunoblot analysis of mitochondrial fusion proteins.....	73
3.9.7.2 Immunoblot analysis of mitochondrial fission proteins.....	74
3.9.8 The effect of daily MLT administration on mitochondrial biogenesis during DXR-induced cardiotoxicity.....	75
3.9.8.1 Immunoblot analysis of PGC-1 α protein levels.....	75

3.9.9 The effect of daily MLT administration on sirtuin activity during DXR-induced cardiotoxicity.....	76
3.9.9.1 Immunoblot analysis of SIRT1 and SIRT3 protein levels.....	76
Chapter 4: Discussion	
4.1 Introduction.....	77
4.2 The effect of melatonin on cell viability during DXR-induced cardiotoxicity.....	77
4.3 The effect of melatonin on apoptosis during DXR-induced cardiotoxicity.....	78
4.4 The effect of melatonin on autophagy during DXR-induced cardiotoxicity.....	80
4.5 The effect of melatonin on Pink1 and PARKIN during DXR-induced cardiotoxicity.....	82
4.6 The effect of melatonin on mitochondrial ROS production during DXR-induced cardiotoxicity.....	83
4.7 The effect of melatonin on mitochondrial membrane potential during DXR-induced cardiotoxicity.....	85
4.8 The effect of melatonin on mitochondrial morphology during DXR-induced cardiotoxicity.....	86
4.9 The effect of melatonin on mitochondrial fission and fusion during DXR-induced cardiotoxicity.....	87
4.10 The effect of melatonin on mitochondrial bioenergetics and biogenesis during DXR-induced cardiotoxicity.....	90
4.11 The effect of melatonin on sirtuin activity during DXR-induced cardiotoxicity.....	93
4.12 The effect of daily melatonin administration on cardiac function, animal body weight and tumor growth during DXR-induced cardiotoxicity.....	95
Chapter 5	
Conclusion.....	99
References	102

Chapter 1

Literature Review

1.1 Introduction

Since its discovery in the late 1960s, the anthracycline antibiotic doxorubicin (DXR) has been one of the most effective and generally prescribed chemotherapeutic drugs for the treatment of various cancers (Weiss, 1992; Octavia *et al.*, 2012; Bonadonna *et al.*, 1970). The eminent use of this potent antineoplastic agent is subdued by several severe side effects one of which, cardiotoxicity, is of particular concern. Patients suffering from DXR-induced cardiotoxicity may clinically present with acute, subacute, or early/late-onset chronic progressive forms, all of which result in heart failure. Such a complication poses a major clinical obstacle as the prognosis for heart failure in this cohort of patients remains poor: 50% die within 2 years, emphasising the urgent need for novel or adjuvant therapeutic agents (Steinherz *et al.*, 1991; Von Hoff *et al.*, 1979; Ganz *et al.*, 2008).

Over the decades, numerous studies sought to identify the intracellular targets and elucidating the molecular mechanisms involved in DXR-induced cardiotoxicity (Minotti *et al.*, 2004; Olson and Mushlin, 1990; Singal *et al.*, 1997). These studies have contributed to the theory that it is in fact a multifactorial process that leads to cardiomyocyte death as the terminal downstream event (Minotti *et al.*, 2004; Kalyanaraman *et al.*, 2002; Fukazawa *et al.*, 2003). Mitochondrial dysfunction has become an apparent hallmark of DXR-induced cardiotoxicity (Tokarska-Schlattner *et al.*, 2006). Abnormalities in mitochondrial functions such as defects in the respiratory chain/oxidative phosphorylation (OXPHOS) system, decreased adenosine tri-phosphate (ATP) production, a switch in metabolic substrate utilization, mitochondrial deoxyribonucleic acid (DNA) damage, modulation of mitochondrial sirtuin activity, and a vicious cycle of free radical formation have all been suggested as the primary causative factors in the pathogenesis of DXR-induced cardiotoxicity (Olson and Mushlin, 1990; Tokarska-Schlattner *et al.*, 2006; Verma *et al.*, 2013). These defects act synergistically to create a bioenergetic crisis, which culminates in cardiomyocyte death.

In view of the above-mentioned, the general clinical approach to attenuate DXR-induced cardiotoxicity is to utilize antioxidants. Melatonin (MLT), also known as the 'dark hormone,' has shed light on this therapeutic avenue as demonstrated in various studies (Kim *et al.*, 2005; Sahna *et al.*, 2003; Ahmed *et al.*, 2005; Eser *et al.*, 2006). The promising effects of this pineal indoleamine are attributed to it being a free radical scavenger of high potency, having low toxicity, exhibiting good solubility in both aqueous and organic phases, influencing mitochondrial homeostasis and functioning, and being dually oncostatic and cardioprotective (Reiter *et al.*, 2008; Leon *et al.*, 2008; García *et al.*, 2014; Tengattini *et al.*, 2008). Furthermore, a number of *in vivo* studies have shown that MLT is significantly superior to the classic antioxidants, such as vitamin E, β -carotene, and vitamin C, as well as garlic oil, in enhancing free radical destruction (Gultekin *et al.*, 2001; Rosales-Corral *et al.*, 2003; Anwar and Meki, 2003). However, the exact mechanisms by which MLT confers protection and the key cellular parameters that it influences remain to be elucidated.

The role of MLT regarding the detrimental effects of DXR on mitochondrial function, such as bioenergetics failure, free radical generation, and cardiomyocyte cell death will be discussed in this literature review. Furthermore, some of the key parameters associated with mitochondrial dysfunction which lack evidence to support the role of MLT in the context of cardiotoxicity are briefly highlighted.

1.2 Mitochondria: a common target for melatonin and doxorubicin

Mitochondria, which are organelles present in all cells of the human body except erythrocytes, play a pivotal role in energy production. In addition to this vital function, mitochondria are involved in other complex processes such as heme metabolism, maintaining homeostatic control of reactive oxygen and nitrogen species production, calcium regulation, cellular metabolism and proliferation, cell division and programmed cell death (apoptosis), and in house-keeping functions of mitophagy and mitochondrial dynamics (Gustafsson and Gottlieb, 2008; Cardinali *et al.*, 2013; Szewczyk and Wojtczak, 2002; Schaper *et al.*, 1985; Ventura-Clapier *et al.*, 2004). Mitochondria are abundant in heart tissue, constituting about 45% of the myocardial volume (Marin-Garcia *et al.*, 2001; Gottlieb and Gustafsson, 2011) in comparison with other tissues. This abundance is due to the high energy demand of the heart that is satisfied during mitochondrial respiration which generates ATP, of which more than 90% is utilized by cardiomyocytes (Tokarska-Schlattner *et al.*, 2006).

The abundance of mitochondria in cardiomyocytes closely links mitochondrial bioenergetics with myocardial function and viability; thus, mitochondrial dysfunction has recently been recognized as a pivotal element in the development of DXR-induced cardiotoxicity. Supporting this notion, it has been demonstrated that DXR specifically targets mitochondria and accumulates in these organelles at concentrations 100-fold higher than in plasma (Tokarska-Schlattner *et al.*, 2007; Sokolove, 1994). This accumulation is greatly attributed to the cationic nature of DXR that has a high affinity to cardiolipin, a negatively charged and major phospholipid component in the inner mitochondrial membrane. The binding of DXR to cardiolipin leads to the formation of an irreversible complex (Goormaghtigh *et al.*, 1980; Goormaghtigh *et al.*, 1986), inhibiting oxidative phosphorylation as it renders cardiolipin incapable of acting as a cofactor for mitochondrial respiratory enzymes. MLT has been reported to protect the mitochondria by preventing cardiolipin oxidation which would otherwise promote the mitochondrial transition pore opening (mPTP), resulting in cell death (Paradies *et al.*, 2010).

In light of this scenario, mitochondria are also a common target for MLT. In fact, in a recent review by Tan and colleagues (2013), it has been hypothesized that mitochondria were the initial sites of

MLT biosynthesis during the early stages of endosymbiosis. The review summarizes crucial evidence in support of the proposed theory that mitochondria may have the ability to independently synthesize MLT (for review see Tan *et al.*, 2013). Attributed to this molecule's amphiphilic properties, MLT readily crosses all biological barriers and gains access to all compartments of the cell, thus highly concentrating in the mitochondria and the nucleus (Acuna-Castroviejo *et al.*, 2014; Venegas *et al.*, 2012; Escames *et al.*, 2010; Menendez-Pelaez *et al.*, 1993; Pablos *et al.*, 1996). It is important to note that MLT concentrations in the cell membrane, cytosol, nucleus, and mitochondria fluctuate independently of the circadian rhythm during a 24-hr period (Venegas *et al.*, 2012). It may be possible that MLT changes its levels to satisfy the antioxidant demand of each subcellular compartment. From a therapeutic perspective, clinicians should bear in mind that the subcellular levels of MLT are controlled by regulatory mechanisms, and therefore, MLT has low toxicity when administered at high doses (Venegas *et al.*, 2012). Furthermore, the use of MLT at high doses has been shown to be essential in reaching adequate subcellular concentrations to exert its pharmacological effects (Venegas *et al.*, 2012).

An emerging regulatory pathway that plays a role in controlling mitochondrial function is the posttranslational modification (PTM) of mitochondrial proteins via acetylation/deacetylation of protein lysine residues (Sack, 2011). PTM is modified by nutrient flux and redox stress, thus influencing mitochondrial proteins controlling fat oxidation, the tricarboxylic acid (TCA) cycle, the electron transport chain (ETC), and controlling redox stress (Zhao *et al.*, 2010). Three mitochondrial deacetylation enzymes have been identified, namely sirtuin-3, sirtuin-4, and sirtuin-5 (SIRT3-5) (Schwer and Verdin, 2008) with SIRT3 being found to be the most robust mitochondrial deacetylase (Sack, 2011; Lombard *et al.*, 2007). In addition to its established mitochondrial function, SIRT3 is also a nuclear NAD⁺-dependent histone deacetylase that translocates to the mitochondria in response to various stressors, including ultraviolet (UV) irradiation and the chemotherapeutic drug, etoposide (Scher *et al.*, 2007).

Interestingly, a major mechanism by which DXR elicits its antitumor activity is via double-stranded DNA breaks (DSB), and SIRT3 has been shown to protect cardiomyocytes from stress-induced cell death at least in part by deacetylating and activating the DSB repair protein (Sundaresan *et al.*,

2010). Another study demonstrated that in contrast to SIRT3, downregulation of SIRT4 expression renders mitochondria resistant to mPTP induction. Thus, the suppression of mitochondrial SIRT4 protected against mPTP-dependent cytotoxicity induced by DXR (Verma *et al.*, 2013). On the other hand, MLT was first implicated in modulating nuclear SIRT1 during the biological process of aging as well as in cancer (Jung-Hynes *et al.*, 2010; Jung-Hynes *et al.*, 2010). Such evidence potentially implies that MLT may have the ability to favourably modulate mitochondrial sirtuins during DXR-induced cardiotoxicity. However, this remains to be elucidated. In the ensuing sections of this literature review, the focus is on the adverse effects of DXR on key mitochondrial parameters and the mechanism by which MLT can potentially mitigate mitochondrial dysfunction during DXR-induced cardiotoxicity.

1.3 The role of melatonin in doxorubicin-induced bioenergetic failure

The heart is a vital organ demanding vast amounts of energy to sustain its contractile functioning. Mitochondrial respiration is responsible for generating 90% of this energy in the form of ATP via the respiratory chain (Ventura-Clapier *et al.*, 2004). The respiratory chain, which is located in the inner mitochondrial membrane, contains a series of electron carriers grouped into four enzyme complexes: complex I (NADH dehydrogenase); complex II (succinate dehydrogenase); complex III (cytochrome c reductase); and complex IV (cytochrome c oxidase). The synthesis of ATP via the respiratory chain involves two coupled processes: electron transport and oxidative phosphorylation (OXPHOS) (Mitchell *et al.*, 1967).

Disruption of cardiac energy homeostasis is a critical feature of DXR-induced cardiotoxicity. The intracellular ATP pools in the heart are very small (5 mmol/kg heart wet weight). When energy demand is increased, these ATP pools may be replenished from larger intracellular pools of phosphocreatine (PCr) (10 mmol/kg heart wet weight) (Meininger *et al.*, 1999). Creatine kinase (CK) is responsible for the conversion of creatine to phosphocreatine and acts as a modulator of the energy reservoir (Thomas *et al.*, 1994; Beer *et al.*, 2002). DXR is known to accumulate ferrous iron

which in turn induces oxidative damage to CK, disrupting energy homeostasis by decreasing both ATP and PCr levels (Ichikawa *et al.*, 2014).

In an *in vivo* study, Eidenschink and colleagues (2000) reported a 20% decrease in PCr/ATP ratio in children 4 years post-DXR treatment even in the absence of clinical manifestations of cardiomyopathy. When assessing ATP levels, it is important to bear in mind that ATP levels may also diminish due to activation of apoptosis and calcium-dependent proteases. Tokarska-Schlattner *et al.* (2005) demonstrated in an isolated perfused rat heart that acute DXR-induced cardiac dysfunction may impair energy signaling via the energy sensor AMP-activated protein kinase (AMPK), which is associated with mitochondrial dysfunction.

In addition, as mentioned previously, DXR has a high affinity for cardiolipin (Goormaghtigh *et al.*, 1980), an integral component of the inner mitochondrial membrane. The binding of DXR to cardiolipin does not allow for cardiolipin interaction with key respiratory complexes (Goormaghtigh *et al.*, 1980). As the inner mitochondrial membrane represents a critical site for DXR accumulation, the respiratory chain can be considered a potential target for DXR-induced toxicity. Numerous studies have demonstrated that DXR disrupts mitochondrial respiration at multiple levels, by inhibiting complexes of the respiratory chain or inhibiting phosphorylation steps and inducing partial uncoupling (Gosalvez *et al.*, 1974; Vidal *et al.*, 1996; Sayed-Ahmed *et al.*, 2000; Jeyaseelan *et al.*, 1997).

In particular, studies aimed at determining the sensitivity of respiratory complexes to DXR found that DXR-sensitive sites were mainly located in complex I, III, and IV, with a specific vulnerability for complexes I (NADH dehydrogenase) and IV (cytochrome c oxidase) (Goormaghtigh *et al.*, 1986; Marcillat *et al.*, 1989; Nicolay *et al.*, 1987). Other findings further indicate inactivation of complex II (Muraoka and Miura, 2003; Bianchi *et al.*, 1987); however, the variation in these results may have been influenced by the type of model used. For instance, drug distribution, binding specificity, and drug metabolism, via iron, peroxidase systems, or other metabolic pathways, are crucial parameters excluded in models of isolated mitochondria. The effect of DXR on mitochondrial respiration results in a bioenergetic decline, and this is considered a hallmark of impaired cardiac function in the onset and progression of DXR-induced cardiotoxicity.

The ability of MLT to influence mitochondrial energy homeostasis has been tested in various *in vivo* and *in vitro* models (Martin *et al.*, 2000; Tan *et al.*, 2000; Martin *et al.*, 2002; Liu *et al.*, 2013). MLT was found to increase the activity of the brain and liver mitochondrial respiratory complexes I and IV 30 min after its administration to rats, and the activity of these complexes returned to basal levels at 120–180 min post-treatment. However, the activity of complexes II and III remained unaffected (Martin *et al.*, 2000). These findings suggest that MLT has the potential to directly affect mitochondria within the hormone's half-life range. It was also found that MLT administration was able to counteract the reduced activity of complexes I and IV in the presence of ruthenium red, an inorganic polycationic complex, which causes mitochondrial uncoupling (Martin *et al.*, 2000). MLT was further found to prevent cyanide-induced inhibition of complex IV and increased ATP synthesis in both untreated and cyanide-treated mitochondria, suggesting that MLT not only directly affects mitochondrial energy metabolism but also provides a homeostatic mechanism for the regulation of mitochondrial function (Yamamoto and Mohanan, 2002).

A recent study demonstrated the impact of MLT treatment on the proliferation and differentiation of rat dental papilla cells and dentine formation by modulating the activity of mitochondrial complexes I and IV (Liu *et al.*, 2013). This finding not only supports the direct action of MLT on mitochondrial complexes I and IV, but also the versatile nature of MLT that enables it to influence various biological processes. In context of the heart, MLT increased complex IV activity, improved cardiac function with a higher left ventricular ejection fraction, and decreased the mortality rate in a model of septic heart injury (Zhang *et al.*, 2013). The exact mechanism by which MLT increases the activity of these respiratory complexes is, however, unknown, and thus, the effect of MLT at the level of gene transcription should also be considered.

Studies regarding the direct effect of MLT on the mitochondrial respiratory chain and complexes during DXR-induced cardiotoxicity seem to be lacking. As a result of the specific interaction of MLT with complexes I and IV, future studies should consider assessing the effect of MLT on the reduced activity of complexes I and IV induced by DXR, as these specific complexes are vulnerable to the toxic effects of DXR. However, the assessment of mitochondrial complex III would be equally valuable in this scenario as it plays a critical role in electron transfer and OXPHOS. The method

used currently to assess mitochondrial complex III activity involves spectrophotometrically measuring the activity of cytochrome c reductase in isolated mitochondria (Fu *et al.*, 2013). A major limitation of this method is that during the isolation process of mitochondria, the cytoplasmic microenvironment niche that contains critical regulatory mechanisms of mitochondrial function is depleted, and therefore, this method may not accurately indicate cellular mitochondrial complex III function. To overcome this experimental limitation, the use of intact cells would be highly advantageous.

Fu and colleagues (2013) have developed a novel and effective method to measure mitochondrial complex III function in intact cells. This method exploits the fluorogenic property of MLT-induced oxidation of 2, 7-dichloro-dihydrofluorescein and the use of this effective and reliable method should be considered in future research. It is important to note that the beneficial effects of MLT on mitochondrial respiration are independent of its antioxidant activity but are the result of its high redox potential (0.94 V) (Tan *et al.*, 2000). This unique property allows for MLT to interact with the complexes of the ETC and donate and accept electrons thereby increasing the electron flow, an effect not exhibited by other antioxidants (Martin *et al.*, 2000).

During DXR-induced cardiotoxicity, cardiac remodeling occurs, which initiates a switch in metabolic substrate utilization from fatty acids to glucose (Tokarska-Schlattner *et al.*, 2006; Tokarska-Schlattner *et al.*, 2005). This is as an adaptive response to decreased ATP output (Tokarska-Schlattner *et al.*, 2006; Tokarska-Schlattner *et al.*, 2005). Fatty acids in the heart are known to be the primary substrate utilized for ATP generation under aerobic conditions. During the early stages of developing cardiac pathologies, there is a decrease in fatty acid oxidation, which is compensated for by an upregulation of glucose utilization. Disrupted fatty acid metabolism has been found in cell culture and animal models as well as in humans following treatment with DXR (Thomas *et al.*, 1994; Tokarska-Schlattner *et al.*, 2005; Wakasugi *et al.*, 1993; Abdel-Aleem *et al.*, 1997; Saito *et al.*, 2000; Kitagawa *et al.*, 2002). Rats treated with DXR showed a significant decrease in fatty acid substrate utilization in comparison with glucose (Vidal *et al.*, 1996). On the other hand, Wakasugi and colleagues (Wakasugi *et al.*, 1993) indicated that DXR-induced cardiomyopathy is associated with a decrease in both fatty acid and glucose utilization.

In addition, decreased oxidation of palmitate, a long-chain fatty acid substrate, was demonstrated in isolated cardiomyocytes acutely treated with DXR (Bordoni *et al.*, 1999), which could possibly have been attributed to the impairment of carnitine palmitoyl transferase 1 (CPT1) and/or depletion of its substrate L-carnitine by DXR. Importantly, reduced oxidation and excessive accumulation of fatty acids not only induces disruptions at the energy substrate level, but also alters the energy-coupling properties of mitochondria (Iliskovic *et al.*, 1998). Furthermore, DXR affects glucose supply and the ability of cells to assimilate glucose. It was demonstrated in another study that DXR inhibited the expression of peroxisome proliferator-activated receptor gamma (PPAR γ), leading to the suppression of adipogenesis and resulting in the impaired import of glucose mediated through glucose transporter type 4 (GLUT4) (Arunachalam *et al.*, 2013). On the other hand, MLT was shown to completely restore the expression of the GLUT4 gene, which was suppressed via reactive oxygen species (ROS)-mediated down-regulation of metabolic genes (Ghosh *et al.*, 2007).

Another factor limiting glycolytic flux in the DXR-challenged heart can be the result of impaired activity of phosphofructokinase (PFK), which is a key regulator of glycolysis. This was observed in studies on cardiomyocytes exposed to DXR, which caused a rapid decrease in mRNA levels of PFK (Bordoni *et al.*, 1999; Iliskovic *et al.*, 1998). These findings clearly demonstrate that DXR challenges the heart to sustain cellular energy production by increasing glycolysis as a way of compensating for the depleted energy stores in the heart. Interestingly, the expression of SIRT3 increases under these adverse cardiac conditions to compensate for the loss of ATP by regulating free fatty acid metabolism to meet the high ATP demand in the heart (Ingwall *et al.*, 2009; Pillai *et al.*, 2010). MLT has been shown to prevent an energetic shift to glycolysis in colonic smooth muscle cells from aged rat (Martin-Cano *et al.*, 2014). However, it remains to be investigated what the effect of MLT is on the changes in metabolic substrate utilization during DXR-induced cardiotoxicity, and whether MLT could favourably modulate SIRT3 activity in this setting, and thus have therapeutic potential. The effects of MLT during DXR-induced bioenergetic failure are summarized in Figure 1.1.

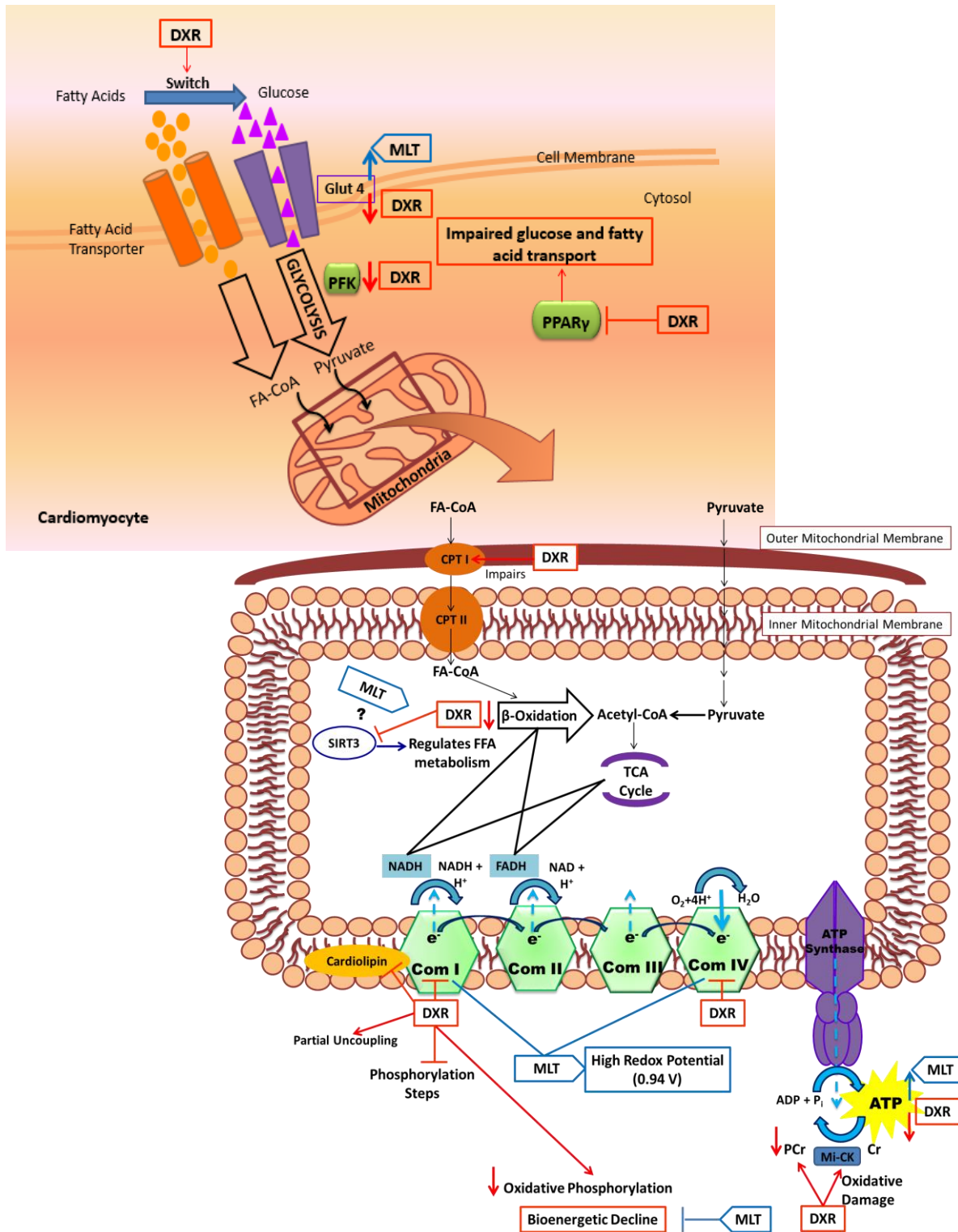


Figure 1.1: The effect of MLT on DXR-induced bioenergetic failure. The figure illustrates the effect of DXR and MLT on mitochondrial respiration, ATP production, as well as glucose and fatty acid metabolism. The question mark (?) represents potential areas that require further investigation. Abbreviations- **MLT**: melatonin; **DXR**: doxorubicin; **Glut 4**: glucose transporter type 4; **PPAR γ** : peroxisome proliferator-activated receptor gamma; **PFK**: phosphofructokinase; **TCA**: tricarboxylic acid; **FA-CoA**: fatty acyl-coenzyme A; **CPT I and II**: carnitine palmitoyltransferase I and II; **ETC**: electron transport chain; Com I, II, II, IV, and V represent mitochondrial electron transport chain complexes; **ATP**: adenosine triphosphate; **ADP**: adenosine diphosphate; **Pi**: inorganic phosphate; **NAD**: nicotinamide adenine dinucleotide; **NADH**: dihydronicotinamide adenine dinucleotide; **FADH**: flavin adenine dinucleotide; **PCr**: phosphocreatine; **Cr**: creatine; Mi-CK: mitochondrial creatine kinase bound to the inner mitochondrial membrane; **SIRT3**: sirtuin 3.

1.4 The role of melatonin in doxorubicin-induced free radical generation

One major and widely investigated hypothesis of DXR-induced cardiotoxicity is based on the generation of free radicals, which induces oxidative stress (Olson *et al.*, 1981). Reports as early as the mid-1970s reported that quinone-containing chemotherapeutic drugs, also known as anthracyclines, such as DXR, produced free radicals. This effect was first observed in rat liver specimens (Bachur *et al.*, 1978). The heart, in particular, is highly susceptible to DXR-induced oxidative damage as it is abundant in mitochondria, which are both sources and targets for ROS (Doroshaw, 1983). Furthermore, the heart has an elevated rate of oxygen consumption and limited antioxidant defense systems when compared to other tissues (Kaiserova *et al.*, 2007; Quiles *et al.*, 2002). It was demonstrated in other studies that cardiomyocytes expressed low levels of catalase and that antioxidant selenium-dependent GSH-peroxidase-1 was inactivated when exposed to DXR, which subsequently decreased cytosolic antioxidant Cu–Zn superoxide dismutase (Doroshaw *et al.*, 1980; Li *et al.*, 2002).

Doxorubicin generates free radicals primarily in two ways: (i) through utilizing cellular oxidoreductases (NADH and NADH dehydrogenase of complex I, NADPH and cytochrome P-450 reductases or endothelial nitric oxide synthase); and (ii) by forming complexes with iron (Tokarska-Schlattner *et al.*, 2006; Doroshaw *et al.*, 1980; Minotti *et al.*, 1999). When DXR reacts with oxidoreductases, it is reduced to a semiquinone (i.e., a free radical). In the presence of oxygen, the semiquinone radical generates superoxide anions which may either give rise to lipids or hydrogen peroxides (Olson *et al.*, 1981). As the heart is abundant in mitochondria, there is an abundance of the enzyme NADH dehydrogenase of mitochondrial complex I, and considering this fact, it has been demonstrated that the main mechanism that leads to ROS formation in the heart is via DXR redox cycling utilizing this enzyme (Wallace, 2003). This type of redox recycling can be detrimental as one molecule of anthracyclines generates many molecules of free radicals (Olson and Mushlin, 1990). Anthracycline free radicals may also form by means of an enzyme-independent mechanism, involving its interaction with iron. Although very little iron is available in myocytes, it has been

reported that DXR has the ability to extract iron from ferritin, a bound form of iron, and thus may also contribute to free radical production (Zweier *et al.*, 1988).

The general clinical approach to combating DXR-induced ROS generation in the heart involves the utilization of various antioxidants. This approach was strengthened by various experiments that yielded positive results when employing antioxidants (Yen *et al.*, 1996; Quiles *et al.*, 2002; Spallarossa *et al.*, 2004). Although antioxidants show promising results, it is apparent that protection against DXR-induced cardiotoxicity in animal models seldom yields the same response in humans. In view of this clinical impediment, ample evidence strongly supports MLT to be one of the essential components to enhance an organism's antioxidant defense system and its antioxidative effect in combating DXR-induced cardiotoxicity (Reiter *et al.*, 2002). The binding of DXR to cardiolipin seems to initiate the disastrous cascade of events leading to free radical generation. This subsequently allows for DXR to inhibit complex I and generate free radicals (Doroshov and Davies, 1986; Davies and Doroshov, 1986). These free radicals induce further lipid peroxidation of cardiolipin and membranes and damage DNA, which can lead to mutations, re-arrangements, and transcriptional errors that impair important mitochondrial components such as that of the mitochondrial respiratory chain. This leads to more oxidative stress, generating a vicious cycle which culminates in cardiomyocyte cell death (Olson and Mushlin, 1990; Minotti *et al.*, 2004; Ogura *et al.*, 1991). As the number of injured mitochondria increase, cardiac functioning is severely compromised.

In addition, DXR reduces or inhibits the activity of the cells antioxidant defense system (Doroshov *et al.*, 1980; Li *et al.*, 2002). MLT can effectively combat these events leading to mitochondrial dysfunction by increasing the expression and activity of the mitochondrial respiration chain complexes (complex I and IV), thereby increasing ATP production (Reiter *et al.*, 2000). It acts as a potent free radical scavenger and possesses antioxidative potential (Reiter *et al.*, 2000; Matuszak *et al.*, 1997; Galano *et al.*, 2011). Hydrogen transfer and electron transfer are known to be the main mechanisms that determine the free radical-scavenging activity of MLT (Galano *et al.*, 2011). MLT reacts intensely with various radicals and prevents the lipid peroxidation of biological membranes (Galano *et al.*, 2011). It has been proposed that MLT prevents lipid peroxidation by scavenging more

reactive species, such as hydroxyl radicals, rather than scavenging peroxy radicals (Galano *et al.*, 2011).

One of the most appealing and unique properties of MLT, which other antioxidants do not possess, is that its metabolites also exhibit antioxidant activity by scavenging ROS and reactive nitrogen species (RNS) (Galano *et al.*, 2011, Galano *et al.*, 2013). MLT and its metabolites generate a free radical scavenging cascade which makes MLT highly effective even at low concentrations and allows for continuous protection against free radical-induced damage (Galano *et al.*, 2013). N1-acetyl-N2-formyl-5-methoxykynuramine (AFMK) is an example of such a metabolite and is formed when MLT scavenges free radicals (Tan *et al.*, 2000; Galano *et al.*, 2011; Galano *et al.*, 2013; Tan *et al.*, 2001; Rozov *et al.*, 2004). Another metabolite, N [1]-acetyl-5-methoxykynuramine (AMK), is formed by deformylation of AFMK. Both these metabolites elicit protective effects against oxidative damage (Galano *et al.*, 2013); AFMK has been found to reduce lipid peroxidation and oxidative DNA damage; it can efficiently scavenge hydroxyl radicals and prevent cellular injury caused by hydrogen peroxide (Tan *et al.*, 2000; Galano *et al.*, 2011; Galano *et al.*, 2013; Tan *et al.*, 2001; Rozov *et al.*, 2004). AMK, on the other hand, is a potent singlet oxygen scavenger, which deactivates a wide variety of ROS and RNS and also other oxidants (Galano *et al.*, 2013).

Another key metabolite, cyclic 3-hydroxymelatonin (C3-HOM), is formed as an immediate product of MLT's interaction with reactive oxygen species (Galano *et al.*, 2014; Tan *et al.*, 2014). This metabolite has been shown to react much faster in aqueous solution than MLT, AMK and AFMK, and is more effective at scavenging peroxy radicals (Tan *et al.*, 2014). This recently identified metabolite of MLT not only reduces oxidative stress via its free radical scavenging cascade, but also plays a critical role in peroxy radical scavenging (Galano *et al.*, 2014). Furthermore, C3-HOM has been shown to protect mitochondrial cytochrome c from free radical-induced damage, and thus, it is likely to inhibit cellular apoptosis induced by the release of oxidized cytochrome c from mitochondria (Tan *et al.*, 2014).

MLT in turn acts to increase an organisms antioxidant defense system as both physiological and pharmacological doses of MLT have resulted in increased gene expression and activities of various

cellular antioxidants (GPx, GRd, SOD and CAT) (Reiter *et al.*, 2000; Antolin *et al.*, 1996; Pablo *et al.*, 1998; Rodriguez *et al.*, 2004; Fischer *et al.*, 2013) and MLT promotes the *de novo* synthesis of glutathione (GSH) by stimulating the activity of its rate-limiting enzyme, g-glut-amyI-cysteine synthetase (Urata *et al.*, 1999). Additionally, an indirect antioxidant action of MLT includes the inhibition of the production of nitric oxide synthase (NOS) at the level of NOS gene transcription (Jimenez-Ortega *et al.*, 2009; Pozo *et al.*, 1997). Furthermore, MLT was also shown to selectively inhibit increased levels of mitochondrial-inducible nitric oxide synthase (i-mtNOS) in cardiac mitochondria, thereby improving cardiac mitochondrial function during sepsis (Ortiz *et al.*, 2014).

MLT's actions successfully stimulate a cascade of antioxidant activity, and this has likely contributed to its success in mitigating DXR-induced free radical generation, thereby preventing lipid peroxidation and improving mitochondrial and cardiac function (Liu *et al.*, 2002; Xua *et al.*, 2001; Balli *et al.*, 2004). Of further value in the context of free radical regeneration is the ability of SIRT3 to prevent a cardiac hypertrophic response by scavenging cellular ROS (Sack, 2011; Scher MB *et al.*, 2007; Sundaresan *et al.*, 2010). Furthermore, SIRT3 transgenic mice had increased levels of both MnSOD and catalase, suggesting that SIRT3 is partly responsible for the increase in antioxidant defense mechanisms in the heart (Scher MB *et al.*, 2007). The use of MLT as a potent antioxidant drug against high levels of oxidative stress during DXR-induced cardiotoxicity has been well established and is greatly beneficial (Reiter *et al.*, 2002). However, considering the role that SIRT3 plays in this context, it would be of further benefit to this field to investigate the effect of MLT on mitochondrial SIRT3. The effects of MLT during DXR-induced free radical generation are summarized in Figure 1.2.

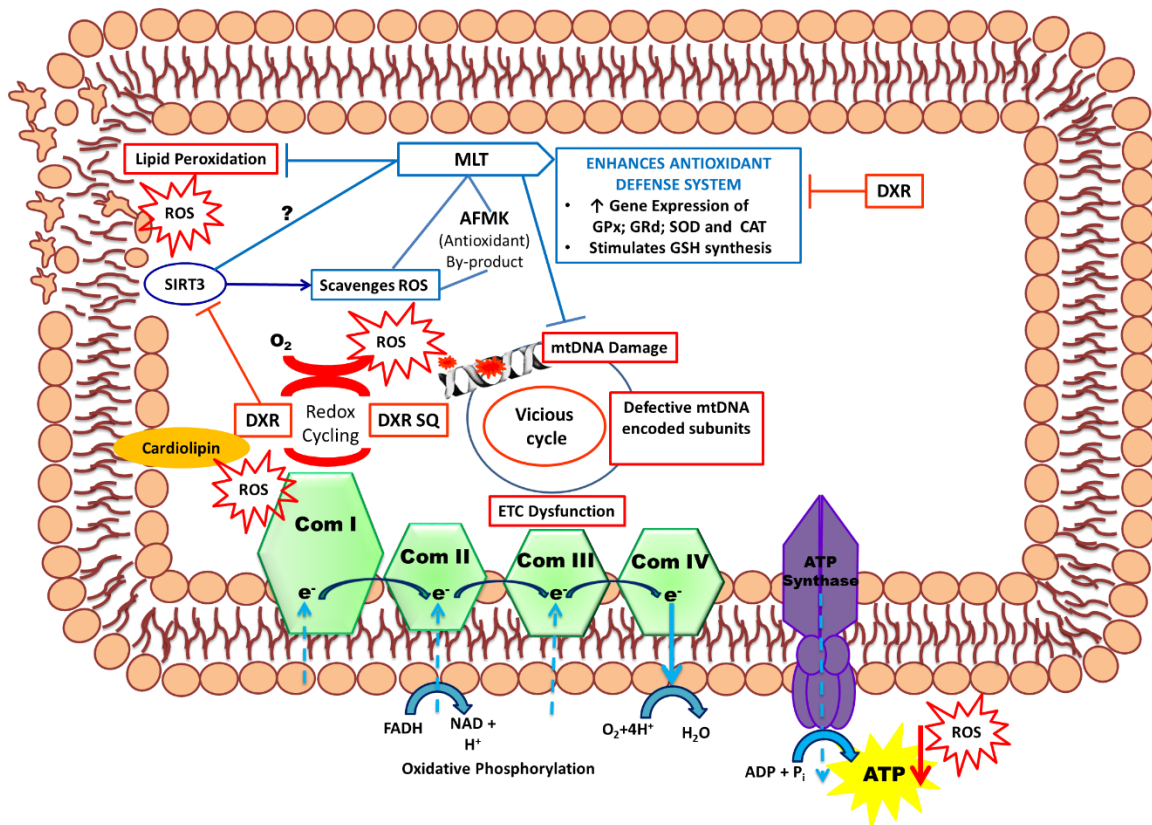


Figure 1.2: The effect of MLT on DXR-induced free radical generation. The figure illustrates how DXR generates ROS, how both ROS and DXR damage mitochondrial DNA, proteins and the ETC, as well as how MLT elicits its beneficial antioxidant effects. The question mark (?) represents potential areas that require further investigation. Abbreviations- **MLT**: melatonin; **DXR**: doxorubicin; **DXR SQ**: doxorubicin-semiquinone; **ROS**: reactive oxygen species; **mtDNA**: mitochondrial deoxyribonucleic acid; **ETC**: electron transport chain; **ATP**: adenosine triphosphate; **ADP**: adenosine diphosphate; **Pi**: inorganic phosphate; **NAD**: nicotinamide adenine dinucleotide; **NADH**: dihydronicotinamide adenine dinucleotide; **FADH**: flavin adenine dinucleotide; **AFMK**: formyl-5-methoxykynuramine; **GPx**: glutathione peroxidase; **GRd**: glutathione reductase; **SOD**: superoxide dismutase; **CAT**: catalase; **SIRT3**: sirtuin 3.

1.5 The role of MLT on doxorubicin-induced cardiomyocyte cell death

The hypothesis that DXR-induced cardiotoxicity terminates in the loss of cardiac myocytes via several cell death pathways has caused this mechanism to be explored at many levels. As cell death is central to this clinical limitation, then the underlying mechanisms involved are worth investigating, as this would result in novel cardioprotective strategies. Mitochondrial dysfunction is indeed a hallmark of DXR-induced cardiotoxicity, and during the last decade, evidence has accumulated to support the critical role of mitochondria in determining the fate of cardiomyocytes. There are three general mechanisms that implicate mitochondria as the central executioners of the intrinsic apoptotic pathway, necrosis and autophagic cell death during DXR-induced cardiotoxicity: (i) disruption of the

ETC, OXPHOS, and ATP production; (ii) release of proteins that trigger the activation of the caspase family of proteases; and (iii) alterations in redox potential (Green *et al.*, 1998; Sainz *et al.*, 2003).

Apoptosis is initiated from two canonical signaling pathways: the extrinsic and intrinsic pathways. The extrinsic pathway involves the binding of death ligands (FasL, TNF- α , TRAIL) to receptors which subsequently recruit and activate caspase 8 and downstream effector caspase 3 (Ashkenazi and Dixit, 1999). The intrinsic pathway is strictly regulated by the Bcl-2 family of proteins namely the anti-apoptotic members Bcl-2, Bcl-xL, the pro-apoptotic members Bax and Bak, and the BH3-only proteins such as Bad, Bid, Nix, and BNIP3 that enhance apoptosis via inhibition of Bcl-2 proteins or activation of pro-apoptotic Bax and Bak. Activation of BH3-only proteins further induces a cascade of events that release cytochrome *c* from the mitochondria, resulting in apoptotic cell death (Kroemer, and Reed, 2000).

Studies investigating the protective role of MLT during DXR-induced cardiotoxicity have yielded positive results, indicating the promising nature of this pineal hormone. Liu and colleagues (2002) found that MLT dramatically improved survival rates in tumor-bearing mice treated with acute high doses of DXR and that MLT was able to attenuate the acute effects of DXR-induced functional changes in mouse hearts. This cardioprotective effect of MLT was attributed in part to the suppression of DXR-induced cardiomyocyte apoptosis via the prevention of DNA fragmentation. It was further demonstrated in this study that MLT exerts its cardioprotective effects without influencing the antitumor activity of DXR (Liu *et al.*, 2002). This is a unique property of MLT when compared to other antioxidants (Sehested *et al.*, 1993; Siveski-Illiskovic *et al.*, 1995; Wahab *et al.*, 2000).

Doxorubicin is known to generate free radicals that are critical inducers of cell death. ROS causes damage to mitochondrial DNA (mtDNA) thus dysregulating transcriptional factors, which lead to the activation of the extrinsic apoptotic pathway (Zhang *et al.*, 2009). In addition, it disturbs calcium homeostasis and induces lipid peroxidation which subsequently decreases mitochondrial redox potential and leads to the opening of the mPTP and the release of cytochrome *c* (Zhang *et al.*, 2009). As a result of the damaging effects of increased ROS production during DXR-induced cardiotoxicity, many researchers have focused on assessing the potential of MLT as an antioxidant to mitigate ROS

production. Indeed, MLT has demonstrated that it exerts a strong anti-apoptotic effect and protects cardiomyocytes from ROS-induced apoptosis (Kim *et al.*, 2005; Sahna *et al.*, 2003; Ahmed *et al.*, 2005; Eser *et al.*, 2006; Matuszak *et al.*, 1997; Galano *et al.*, 2011; Galano *et al.*, 2013; Rozov *et al.*, 2004). Furthermore, in a model of cerebral ischemia, MLT was shown to directly inhibit the opening of the mPTP in a dose-dependent manner, thus preventing apoptotic cell death (Andrabi *et al.*, 2004).

Numerous studies have shown that DXR-induced cardiomyocyte apoptosis is associated with increased expression and activation of the p53 tumor suppressor protein (Liu *et al.*, 2008; L'ecuyer *et al.*, 2006). DNA lesions induced by ROS or directly by DXR-induced activation of ERK1/2, followed by increased phosphorylation of p53, up-regulated genes such as Bax. As a result, the intrinsic apoptosis pathway was activated (Kim *et al.*, 2003). The levels of key stress proteins such as ERK-2, phosphorylated p38, HSP-70, phosphorylated p53, and c-JUN were shown to normalize after MLT pre-treatment in a model of ischemic heart disease (Mukherjee *et al.*, 2012). As there is strong evidence supporting the role of MLT in antagonizing the mitochondrial pathway of apoptosis, it is suggested that further studies be conducted to fully explore its effects in models of DXR-induced apoptosis.

The mPTP opening is a critical feature of DXR-induced cell death: not only can it lead to apoptotic cell death but if the opening of this pore is prolonged, ATP levels become totally depleted leading to necrotic cell death. Necrosis has been thought to be apparent at the end stages of cardiotoxicity, but recent findings suggest the occurrence of necroptosis, which shares common features with both apoptotic and necrotic cell death (Christofferson and Yuan, 2010).

Necroptosis is caused by poly (ADP-ribose)-polymerase (PARP) hyperactivation and subsequent energy depletion (Yu *et al.*, 2002) in response to extensive DNA damage and increased ROS production induced by DXR, and it is a caspase-independent form of cell death (Xu *et al.*, 2010). Necrostatin-1 (Nec-1), a potent inhibitor of necroptosis (Degterev *et al.*, 2005) in combination with an apoptotic inhibitor, has been shown to protect the heart against ischemic injury. However, such research remains to be explored in the context of DXR-induced cardiotoxicity. Further investigations

are required to determine the effects of MLT in combination with Nec-1 to mitigate necroptosis in the DXR-challenged heart.

In addition, mitochondrial dynamics have been found to play an essential role in cellular function and apoptosis (Suen *et al.*, 2008). This robust regulatory potential of mitochondrial structural dynamism is essential in ensuring that mitochondria maintain their integrity and efficiency and it is achieved by sustaining a balance between mitochondrial fission and fusion. These well-orchestrated processes lead to heterogeneous mitochondrial morphology ranging from small, roundish individual elements to highly connected networks and are ever changing allowing for mitochondria to adapt according to the changes in their cellular environment (Rambold *et al.*, 2011).

During optimal cellular conditions or if successful adaption to a stressful environment is achieved, mitochondria tend to become tubulated and form extensive networks that are characteristic of mitochondrial fusion (Rambold *et al.*, 2011). This process involves the activity of fusion proteins such as mitofusin (Mfn) 1 and 2 and the optic atrophic protein 1 (OPA1) (Rambold *et al.*, 2011). In contrast, during conditions of stress, mitochondria become small, roundish fragments that are characteristic of fission (Frank *et al.*, 2001; Karbowski and Youle, 2003). Previous studies have demonstrated that upon induction of oxidative stress, dynamin-related protein 1 (Drp1), a protein involved in mitochondrial fission, translocates from the cytosol to the mitochondria to execute the mitochondrial division process (Frank *et al.*, 2001). This involves hydrolyzing GTP (Karbowski and Youle, 2003), which dysregulates the balance between mitochondrial fusion and fission. Mitochondrial fission leads to cytochrome *c* release and activation of caspases, which can ultimately lead to cell death (Frank *et al.*, 2001).

Further supporting the relationship between mitochondrial fission and apoptosis, it was demonstrated that DXR-induced mitochondrial fission is associated with the upregulation of the proteins p-Akt, p-Erk 1/2, p-Drp1, and p-p53 (Gharanei *et al.*, 2013). However, co-administration of DXR with mdivi-1, a mitochondrial fission inhibitor, prevented detrimental effects of DXR via reduced expression of p-Drp1 and also prevented an increase in the levels of both p53 and Erk 1/2, thus suggesting a role for fission inhibitors in cardioprotection. Remarkably, MLT demonstrated multiple

mitochondrial protective effects in a study on Alzheimer's disease by significantly reducing ROS-mediated mitochondrial fission, mitochondrial membrane potential depolarization, and retardation of mitochondrial movement to stabilize cardiolipin; thereby preventing enhanced mitochondrial-mediated cell death (Hsiao *et al.*, 2013). In contrast to DXR-mediated mitochondrial fission, SIRT3-dependent activation of OPA1 contributed to the preservation of mitochondrial networking by favoring mitochondrial fusion and thus protected cardiomyocytes from DXR-induced cell death (Scher MB *et al.*, 2007).

Mitochondrial fission as well as the oxidative challenge posed by DXR on the heart has also been correlated with an increase in autophagy. Autophagy is a catabolic cellular self-degradation process, which is responsible for the removal of damaged organelles and proteins, and maintains energy homeostasis through intracellular recycling during periods of stress (Rabinowitz and White, 2010). Characteristic of this process is the formation of a double-membrane structure called an autophagosome (Xie and Klionsky, 2007; Wang and Klionsky, 2011; Yorimitsu and Klionsky, 2005). When mitochondria are damaged, autophagy facilitates their degradation and engulfs the mitochondrial fragments into autophagosomes; this selective process is referred to as mitophagy (Kim *et al.*, 2007). The elimination of damaged or malfunctioning mitochondria by mitophagy is essential to maintain cellular homeostasis therefore autophagy may be acting as a form of protection in this scenario. DXR exposure can also disrupt the clearance of damaged mitochondria by upregulation of p53 (Hoshino *et al.*, 2012). High cytosolic p53 levels inhibit the translocation of PARKIN to the mitochondrial outer membrane (Geisler *et al.*, 2010). The highest levels of PARKIN protein that function to tag defective mitochondria for autophagic degradation are found in the heart (Geisler *et al.*, 2010). Thus, DXR induces autophagy but simultaneously impairs mitochondrial clearance by mitophagy (Geisler *et al.*, 2010).

However, autophagy serves as a double-edged sword in the heart under conditions of stress: on the one hand, it serves as a significant renewal and pro-survival mechanism of cellular organelles and, on the other hand, if autophagy persists beyond a certain threshold, it may lead to cellular demise (de Meyer *et al.*, 2009; Gustafsson *et al.*, 2009; Terman and Brunk, 2005). Autophagy has been shown to be upregulated in the myocardium in response to ischemia/reperfusion (Matsui *et al.*, 2007)

as well as in DXR-induced cardiotoxicity, and this finding was strongly correlated with decreased cell death (Sishi *et al.*, 2013), suggesting that autophagy was protective under these conditions. In contrast, in a rat model of chronic DXR cardiotoxicity, it was demonstrated that increased autophagy contributed to a loss of cardiac myocytes and increased the pathogenesis of cardiomyopathy (Lu *et al.*, 2009). It was found in this study that treatment with 3-methyladenine (3-MA), an autophagic inhibitor, reduced autophagy and improved cardiac function, suggesting that autophagy is detrimental in the case of chronic DXR-induced cardiotoxicity.

The controversy surrounding autophagic cell death in many studies arises from the evidence which is lacking for a causative role of autophagy in cell death (i.e., there is cell death with autophagy but not by autophagy) (Liu *et al.*, 2013). A recent study conducted by Liu and colleagues (2013) highlighted that selective overactivation of autophagy can cause cell death with unique morphological features distinct from apoptosis and necrosis. These authors coined the term 'autosis' to describe this unique form of autophagic cell death. Based on the study, they proposed that autosis should meet two essential criteria put forth by the Nomenclature Committee on Cell Death: (i) the suppression by inhibition of the autophagic pathway and (ii) the lack of features of apoptosis and necrosis.

In addition, it was demonstrated that autosis can be characterized by the classical morphological criteria of autophagic cell death (increased autolysosomes in dying cells lacking features of apoptosis and necrosis), death induced in starved adherent cells and by autophagy-inducing peptides that is accompanied by endoplasmic reticulum (ER) dilation and stereotypic nuclear changes, involving an early convoluted appearance, the formation of focal concave regions of the nucleus with surrounding focal swelling of the perinuclear space, and the accumulation of structures within this space at early stages of the process (Liu *et al.*, 2013). Moreover, autosis but not apoptosis or necrosis was shown to be selectively inhibited by cardiac glycosides (Liu *et al.*, 2013). In light of the above information, it would be of interest to evaluate the extent to which autophagic cell death by autosis contributes to cardiomyocyte cell loss in the context of DXR-induced cardiotoxicity as the criteria to distinguish this form of cell death from others are now available.

Although the role of MLT in the regulation of autophagy and mitophagy was highlighted in a recent review (Coto-Montes *et al.*, 2012), the effect of MLT on autophagy and mitophagy during DXR-induced cardiotoxicity remains to be elucidated. Only recently Kang *et al.* (2014) demonstrated, using a model of liver ischemia/reperfusion (I/R) injury, that autophagic flux was increased in response to I/R injury, but this was attenuated by MLT via inhibiting mammalian target of rapamycin (mTOR)-dependent autophagy (Kang *et al.*, 2014). However, it is unclear to what extent MLT activates mTOR-dependent or mTOR-independent pathways. The suppression of autophagy by MLT suggested its protective role during I/R injury (Kang *et al.*, 2014). It seems possible that MLT could also potentially suppress the increase in autophagic flux observed during DXR-induced cardiotoxicity; however, this aspect would have to be investigated. The effects of MLT and DXR on apoptosis, necrosis, necroptosis, autophagy, mitophagy, and mitochondrial fission and fusion during DXR-induced cardiotoxicity are summarized in Figure 1.3.

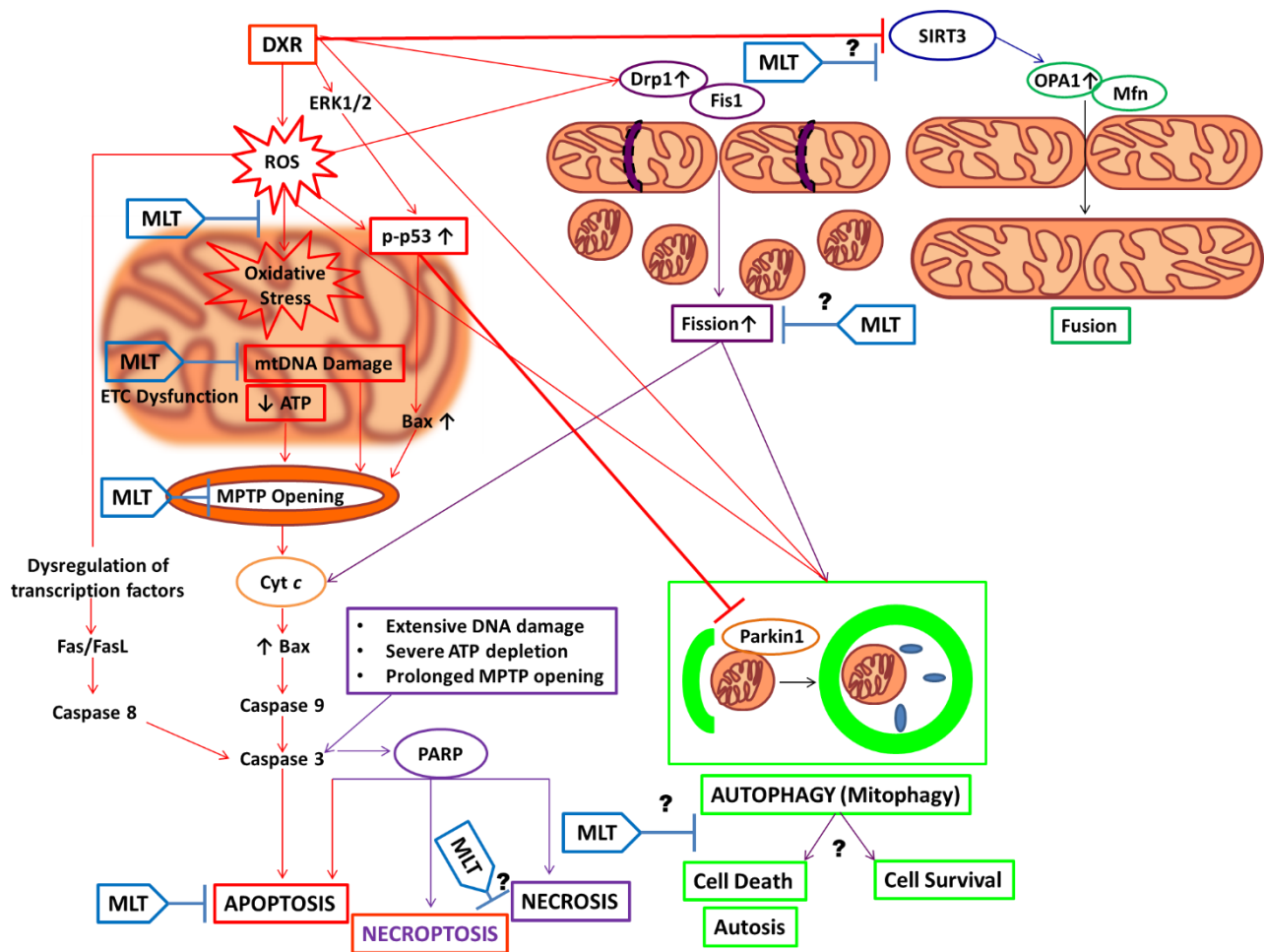


Figure 1.3: The effect of MLT and DXR on cardiomyocyte cell death. Mechanisms of cell death include apoptosis, necroptosis, necrosis, and autophagy. The question mark (?) represents potential areas that require further investigation. Abbreviations: **MLT**: melatonin; **DXR**: doxorubicin; **ROS**: reactive oxygen species; **mtDNA**: mitochondrial deoxyribonucleic acid; **MPTP**: mitochondrial permeability transition pore; **PARP**: poly [ADP-ribose] polymerase; **cyt c**: cytochrome complex; **ERK1/2**: extracellular signal-regulated kinases 1/2; **p-p53**: phospho-tumor protein 53; **Drp1**: dynamin-related protein 1; **Fis1**: mitochondrial fission 1 protein; **OPA1**: optic atrophy protein 1; **Mfn**: mitofusin; **BAX**: apoptosis regulator protein/B-cell lymphoma 2-like protein 4; **Fas/FasL**: apoptosis-stimulating fragment/apoptosis-stimulating fragment ligand; **SIRT3**: sirtuin 3.

1.6 Motivation

Despite advances in medical technology, surgical approaches and the discovery of novel drugs in the current era, chemotherapy remains a major breakthrough in combating cancer and has been shown to significantly increase the survival rate of cancer patients. Doxorubicin (DXR) is one of the most effective and generally prescribed chemotherapeutic drugs for the treatment of various cancers. Regrettably, the eminent use of this antineoplastic agent is limited due to detrimental side effects such as cardiotoxicity. Abnormal mitochondrial function, damaged mitochondrial DNA,

decreased respiratory complex activity, increased ROS production, and augmented electron leakage and mPTP opening have all been shown to play crucial roles in the pathophysiology of DXR-induced cardiotoxicity. Mitochondrial changes are not only observed at the level of respiratory complex dysfunction and oxidative damage, but also in the disturbed balance between mitochondrial fusion and fission and defective clearance of these organelles by mitophagy, with the consequence of compromised cardiac function and contractility. It is therefore crucial to equally assess other mitochondrial parameters such as fission and fusion, mitophagy, and mitochondrial sirtuin activity. The key role of mitochondria in DXR-induced cardiotoxicity indicates that supporting the integrity and functioning of these organelles should be given priority, thereby reducing cardiomyocyte death.

Cardiotoxicity poses a major clinical challenge to the collaborative field of cardio-oncology and a compelling need for novel or adjuvant therapeutic agents is needed. Melatonin (MLT), a hormone primarily secreted from the pineal gland may serve as such an agent. Its administration during or prior to chemotherapy shows great promise in this therapeutic avenue as demonstrated in various studies owing to its dually oncostatic and cardioprotective nature. The beneficial effects of MLT administration against DXR-induced cardiotoxicity are in part due to its direct free radical scavenger activity and its indirect antioxidant properties. An increased reporting of the effect of MLT on mitochondrial bioenergetics, mitochondrial fission and fusion, its action on mitochondrial sirtuin activity, its role in autophagy and mitophagy and in cell death will undoubtedly provide insights that deepen our understanding of MLT's protective mechanisms during DXR-induced cardiotoxicity.

Therefore this study aimed to investigate the effect of pre-treatment with MLT during DXR-induced cardiotoxicity on: cell death and autophagy/mitophagy, mitochondrial ROS production, mitochondrial membrane potential, mitochondrial morphology, mitochondrial fission and fusion, mitochondrial bioenergetics and biogenesis and, sirtuin activity. We further aimed to investigate the effect of daily MLT administration on cardiac function and tumor growth in an in vivo tumor-bearing rat model of acute DXR-induced cardiotoxicity. We hypothesize that pre-treatment with MLT will stabilize mitochondrial function during DXR-induced cardiotoxicity which will subsequently increase cardiomyocyte survival and improve cardiac function whilst inhibiting tumor growth.

Chapter 2

Materials and methods

2.1 *In vitro* Study design – Phase 1

In phase 1 of this study, the *in vitro* model of acute doxorubicin-induced cardiotoxicity is described. H9c2 rat embryonic heart-derived ventricular cells were employed and five treatment groups were established: (i) control; (ii) vehicle control; (iii) doxorubicin; (iv) melatonin and; (v) pre-treatment with melatonin followed by doxorubicin exposure. The following cellular and mitochondrial parameters were assessed: Cell viability and apoptosis, autophagy and mitophagy, ROS generation, mitochondrial membrane potential, mitochondrial morphology, mitochondrial fission and fusion, mitochondrial bioenergetics and biogenesis, and sirtuin activity. The methods used to assess the above parameters are illustrated in Figure 2.1.

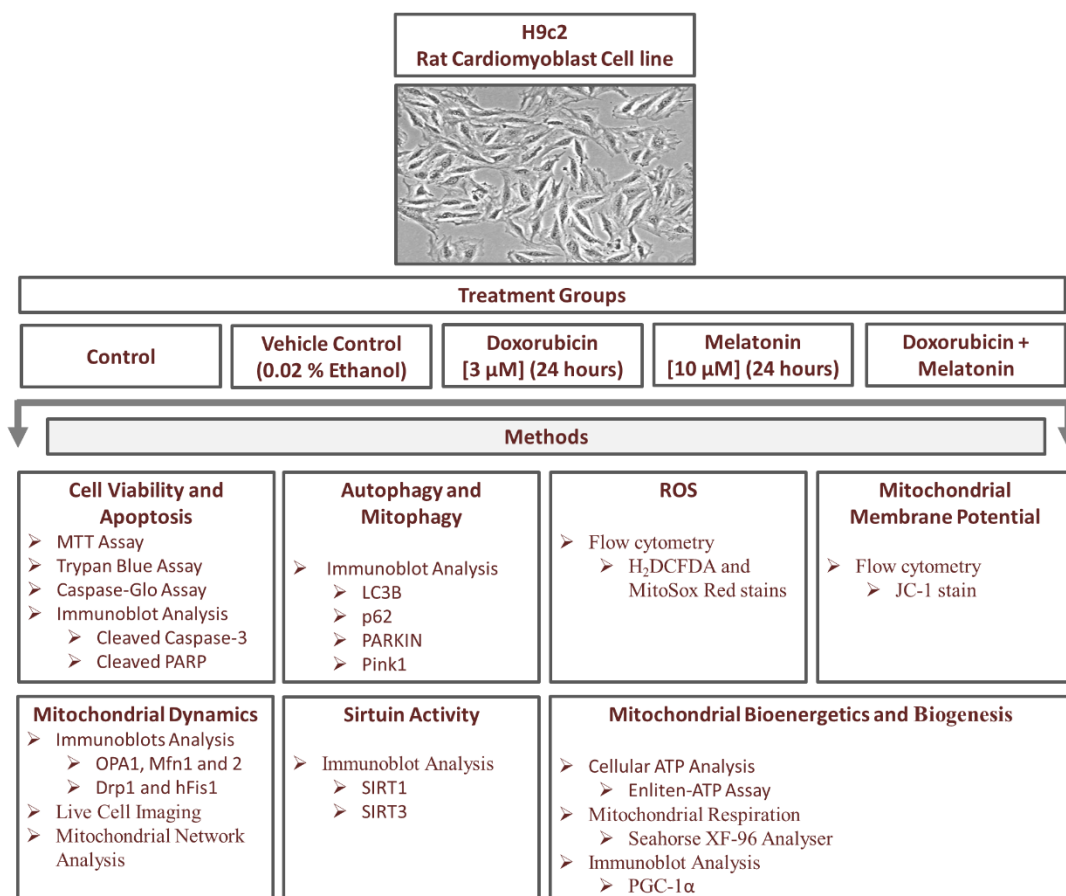


Figure 2.1: Schematic representation of the *in vitro* study design. H9c2 cells were treated as indicated above, and were used to assess various mitochondrial and cellular parameters.

2.1.2 Cell culture and maintenance of H9c2 cell line

H9c2 rat embryonic heart-derived ventricular cells were originally obtained from the European Collection of Cell Cultures (ECACC No. 8809294). Cells were maintained in a monolayer at 37°C and in a 21% O₂, 5% CO₂, humidified air atmosphere of 95% and were cultured in Dulbecco's modified Eagle's medium (DMEM, Invitrogen Gibco), supplemented with 10% fetal bovine serum (Invitrogen, Gibco) and 1% penicillin/streptomycin solution (Invitrogen, Gibco). Cells were allowed to proliferate in T75 flasks (75 cm² flasks, Nest Scientific, USA) and the growth medium was refreshed every 48 hours. When cultures reached 80% confluency they were sub-cultured (splitting of cell cultures were achieved) by washing the cell monolayer with warm (37°C) media (DMEM) followed by trypsinization using 0.25% Trypsin-ethylene-diaminetetra-acetic acid (trypsin-EDTA) (Invitrogen Gibco). Cells were gently agitated to ensure complete detachment from the flask and were transferred to a sterile tube for centrifugation at 1500 rpm for 3 minutes. Cell pellets were re-suspended in fresh warm growth medium and a hemocytometer was used to count the cells. Cells were then seeded at the appropriate density in fresh warm growth medium for experiments or further passaging. Cells between passages 10 and 17 were used in all experiments.

2.1.3 Cell culture treatments

Upon treatment, growth medium was removed and replaced with fresh growth medium containing respective treatments. Additionally, cells were washed twice with warm DMEM to ensure the removal of debris and non-viable cells. Initially, a pilot study was performed to determine a clinically relevant concentration of DXR that would induce DXR-induced cardiotoxicity (Figure 3.1.1). H9c2 cardiac myoblasts were treated with 1, 2, 3, 4 and 5 µM of DXR for 24 hours and cell viability was assessed. Based on the results (Figure 3.1.1), cells treated with DXR at a concentration of 3 µM for 24 hours was used in all *in vitro* experiments. Additionally, a dose and time response study was performed to determine a concentration of MLT that would reduce the toxicity in H9c2 cells treated with DXR (3 µM). Cells were pre-treated with MLT at concentrations of 10, 20 and 50 µM for either 1 or 24 hours, the cell culture medium was removed and thereafter cells were treated with DXR (3 µM) for 24 hours.

Based on the results, cells pre-treated with MLT at a concentration of 10 μM for 24 hours followed by DXR treatment (3 μM) for 24 hours was used in all *in vitro* experiments. Once the dose and time responses for treatments were established, five treatment groups were used for the *in vitro* model of this study as mentioned in section 2.1 (study design).

2.1.3.1 Doxorubicin (DXR) treatment

A stock solution of DXR (Sigma Chemical Co., St Louis, MO, US) at a concentration of 3.4 mM was prepared by dissolving the compound in DMEM. Upon treatment, DXR was added to fresh warm growth medium to achieve a final concentration of 3 μM . Flasks containing DXR treated cells were covered in aluminum foil as DXR is a light sensitive compound. Flasks were then incubated for 24 hours.

2.1.3.2 Melatonin (MLT) treatment

A stock solution of MLT (Sigma Chemical Co., St Louis, MO, US) at a concentration of 21.5 mM was prepared by dissolving the compound in ethanol. Absolute ethanol (95%) was diluted with sterile deionized water (dH_2O) to 50% prior to being used to dissolve the MLT. Upon treatment, the MLT stock solution was freshly prepared and was added to fresh warm growth medium to achieve a final concentration of 10 μM . Flasks containing MLT treated cells were covered in aluminum foil as MLT is a light sensitive compound. Flasks were then incubated for 24 hours. Since the MLT was dissolved in ethanol, a vehicle control group was initially included in cell viability experiments to assess if ethanol had an effect on cell viability (Figure 3.1.2). The vehicle control group was treated with 0.02% of ethanol.

2.1.4 Cell Viability Assays

2.1.4.1 MTT Cell Viability Assay

The MTT cell viability assay is based on the principal of MTT (3-(4, 5-Dimethylthiazol-2-yl)-2, 5-diphenyltetrazolium bromide, a tetrazole) (Sigma Chemical Co., St Louis, MO, US), a yellow salt,

which is reduced to purple formazan crystals by enzymes in the cytoplasm and in the mitochondria of viable cells. This reductive capacity is dependent on active mitochondrial reductase enzymes (dehydrogenases), thus the conversion can be directly correlated with the number of viable cells when assessed spectrophotometrically. Mitochondrial dehydrogenases of viable cells cleave the tetrazolium ring, yielding purple MTT formazan crystals which are insoluble in aqueous solutions. Acidified solutions such as the Isopropanol/Triton X solution can be used to dissolve the purple crystals.

After the termination of the treatment, growth medium was removed from each well of a 6 well plate (Nest Scientific, USA) and cells were washed with warm (37°C) sterile phosphate buffered saline (PBS). A solution of PBS and MTT (0.01 g/ml) was added to each well. The plate was covered in aluminum foil and incubated at 37°C for 1 hour. Next, if cells were detached, the contents of each well was transferred to brown microtubes and centrifuged at 1000 rpm for 2 minutes. The supernatant was decanted and 2 ml of hydrogen chloride-isopropanol/Triton (1% HCl in isopropanol; 0.1% Triton X-100; 50:1) solution was added to each pellet and re-suspended. Some cells remained attached to the well, thus the re-suspension was added back into the wells, the plates were covered with aluminum foil and gently agitated at 37°C for 5 minutes to dissolve the purple crystals formed. The contents of each well was then transferred to a 2 ml cuvette. The optical density (OD) was determined spectrophotometrically (Cecil-CE 2021-2000 Series, Lasec) at a wavelength of 540 nm, using the HCl-isopropanol/Triton X solution as a blank. All values obtained from the treated groups were expressed as a percentage of the control values. All MTT assays were performed in triplicate for each group and three independent experiments were done.

2.1.4.2 Trypan blue cell exclusion technique

Trypan Blue cell exclusion technique is based upon the unique properties of the chromophores present in this vital dye. The chromophores are negatively charged, thus only interact with cells that have damaged membranes (staining blue). Thus, all cells which are viable exclude the dye.

H9c2 cells were grown and treated as previously described (section 2.1.3). At the termination of treatment, growth medium was removed and cells were washed with warm (37°C) sterile PBS,

trypsinised and centrifuged at 1500 rpm for 3 minutes. The supernatant was removed and the pellet re-suspended in 1 ml PBS. From this cell suspension 10 µl were removed and added to 10 µl of a 0.3% Trypan Blue dye (Invitrogen, USA) and gently agitated. Of this solution, 10 µl were added to a two chambered cell counting slide (Invitrogen, USA). The slide was then inserted into the Countess® Automated Cell Counter (Invitrogen, USA) and the number of trypan blue positive and negative cells, and the absolute total cell number of the suspension was automatically calculated by the instrument. All values obtained from treated groups were expressed as a percentage of the control values. All assays were performed in triplicate for each group and three independent experiments were done.

2.1.5 Apoptosis assay

2.1.5.1 Caspase-Glo® 3/7 Assay

The Caspase-Glo® 3/7 assay kit (Promega, G8091) provides a reagent containing a luminogenic caspase-3/7 substrate, which is optimized for caspase and luciferase activity. Addition of the reagent to the cells result in caspase mediated cleavage of the substrate, followed by the release of amino-luciferin (a substrate for luciferase) which generates a luminescent signal. Luminescence is proportional to the amount of caspase activity present in the sample.

H9c2 cells were grown and treated, as previously stated (section 2.1.3) in a 96-well white plate. Caspase-3/7 reagent was added to each well (100 µl) and incubated for 1 hour at room temperature. Immediately after incubation, luminescence was measured using a luminometer (GloMax® 96 microplate Luminometer, Promega). All values obtained from treated groups were expressed as a percentage of the control values. Three independent experiments were done with 12 replicates for each group for each independent experiment.

2.1.6 ROS generation

ROS generation was assessed using the 2', 7'-dichlorodihydrofluorescein diacetate (H₂DCFDA, Molecular Probes, D399) and MitoSOX Red (Molecular Probes, M7514) respectively. H₂DCFDA is a versatile fluorescent probe since it is able to detect hydrogen peroxide (H₂O₂), nitrogen dioxide, hydroxyl radicals, and carbonate radicals in intact cells. H₂DCFDA is hydrolyzed in the cytosol and forms a DCFH carboxylate anion. Oxidation of the DCFH carboxylate anion yields a fluorescent product of DCF, which is excited at 495 nm and emits fluorescence at 520 nm. MitoSOX Red is a fluorescent probe used to measure superoxide production in the mitochondrial matrix. Due to its cationic properties, MitoSOX Red is able to rapidly target the mitochondria, where it is oxidized by superoxide. Oxidation of MitoSOX Red yields a fluorescent product known as 2-hydroxymitoethidium, which is excited at 510 nm and emits fluorescence at 580 nm.

H9c2 cells were grown and treated as previously described in T25 flasks (25 cm² flasks, Nest Scientific, USA). A positive control treated with H₂O₂ (100 µmol/L) was included. At the termination of treatment, growth medium was removed and cells were washed with warm (37°C) sterile PBS. Cells were then trypsinized using 0.25% trypsin-EDTA and centrifuged in a 15 ml tube at 1500 rpm for 3 minutes. The supernatant was discarded and cells were resuspended in 500 µl warm PBS. DCF (50 µmol/L) and MitoSOX Red (5 µM) were added to the cell suspension and cells were gently resuspended to ensure an even distribution of the fluorescent probes. The cells were incubated at 37°C for 15 minutes and analysed on the FACS Aria I flow cytometer (Becton Dickinson Biosciences, USA). A 488 nm laser was used for laser-induced fluorescence and the fluorescent emission was collected between wavelength regions 510-580 nm, a minimum of 10 000 events were analyzed. Fluorescent intensity signal was measured using the geometric mean on the intensity histogram. Due to the inherent fluorescent properties of DXR which are similar to MitoSOX Red, the fluorescent intensity of DXR was measured and subtracted from cells treated with DXR and stained with MitoSOX Red. All values obtained from treated groups were expressed as a percentage of the control values. At least three independent experiments were done with duplicates for each group for each independent experiment.

2.1.7 Mitochondrial Membrane Potential Analysis

Differences in mitochondrial membrane potential were detected by using 5, 5', 6, 6',-tetrachloro-1, 1', 3, 3',-tetraethylbenzimidazolylcarbocyanine (JC-1) (Invitrogen, T3168). JC-1 is a ratiometric (red/green), cationic, lipophilic fluorescence probe. Due to its cationic nature, JC-1 easily enters the mitochondria and forms aggregates (J-aggregates) that emit red fluorescence in the phycoerythrin (PE - red) channel. However, in cells with decreased mitochondrial membrane potential or depolarized mitochondria, JC-1 remains in the cytoplasm in its monomeric form, which emits green fluorescence in the fluorescein (FITC - green) channel. Since the monomers and aggregates of JC-1 have different emission spectra, changes in mitochondrial membrane potential can be assessed by comparing the ratio of PE to FITC (red/green). Therefore, the ratio of red/green decreases as the mitochondrial membrane potential decreases.

H9c2 cells were grown and treated as previously described in T25 flasks (25 cm² flasks, Nest Scientific, USA). A positive control treated with Carbonyl cyanide m-chlorophenyl hydrazone (CCCP) (1 µM) was also included. At the termination of treatment, growth medium was removed and cells were washed with warm (37°C) sterile PBS. Cells were then trypsinized using 0.25% trypsin-EDTA and then centrifuged in 15 ml tube at 1500 rpm for 3 minutes. The supernatant was discarded and the cells were resuspended in 500 µl of warm PBS. JC-1 (5 µM) was added to the cell suspension and cells were gently resuspended to ensure an even distribution of the fluorescent probe. The cells were incubated at 37°C for 20 minutes and analysed on the FACSAria I flow cytometer (Becton Dickinson Biosciences, USA). A 488 nm laser was used for laser-induced fluorescence and the fluorescence emission was collected between wavelength regions 515-545 nm and 575-625 nm, a minimum of 10 000 events were analyzed. The fluorescence intensity signal was measured using the geometric mean on the intensity histogram. All values obtained from treated groups were expressed as a percentage of the control values. At least three independent experiments were done with duplicates for each group for each independent experiment.

2.1.8 Mitochondrial Network Analysis

2.1.8.1 Live Cell Imaging

Assessment of the mitochondrial network was performed using live cell imaging. H9c2 cells were seeded at a density of 20×10^3 cells in eight-well chamber coverglass slides (Nunc, Denmark) and treated as previously described. At the termination of treatment, growth medium was removed and warm fresh growth medium containing Tetramethylrhodamine, Ethyl Ester, Perchlorate (TMRE) (1:1000, Molecular Probes, T669) and Hoechst 33342 (1:200, ThermoScientific, 62249) was added to each well to stain for the mitochondrial network (red) and the nucleus (blue) respectively. The Olympus Cell[®] system attached to an IX 81 inverted fluorescence microscope fitted with an F-view-II cooled CCD camera (Soft Imaging Systems) was used to observe cells which were maintained at 37°C during the imaging process. Images were acquired through an Olympus Plan Apo N60x/1.4 Oil objective lens. The mitochondrial network was imaged through excitation of TMRE using a 572 nm excitation filter and the nucleus was imaged through excitation of Hoechst 33342 using a 360 nm excitation filter. Emission was collected using a UBG triple bandpass emission filter. Cell[^]R software was then used to process the acquired images.

2.1.8.2 Mitochondrial Network and Morphology assessment

A morphometric network assessment of the mitochondria was conducted on processed images as previously described by Mortiboys *et al.* (2008), using ImageJ (version 1.42) software. The mitochondrial parameters assessed included the mitochondrial aspect ratio and the form factor. The mitochondrial aspect ratio is the ratio between the major and minor axes of the ellipse equivalent to each mitochondrion and, the form factor or degree of branching is defined by the equation $Pm^2/4\pi Am$, where Pm is the perimeter or length of the mitochondrial outline and Am is the area of the mitochondrion. Four independent experiments were conducted and a minimum of 50 images were processed for each experimental group.

2.1.9 Mitochondrial Bioenergetics

2.1.9.1 Cellular ATP Analysis

Cellular ATP levels were quantified using the Enliten ATP assay kit (Promega, FF2000). H9c2 cells were grown and treated as previously described (section 2.1.3) in T25 flasks (25 cm² flasks, Nest Scientific, USA). At the termination of treatment, growth medium was transferred to sterile 2 ml microtubes and centrifuged at 1500 rpm for 3 minutes to ensure that detached cells were also included for ATP analysis. Adherent cells were then trypsinized using 0.25% trypsin-EDTA and then centrifuged in 2 ml microtubes at 1500 rpm for 3 minutes. The supernatant was discarded and cells were resuspended in growth medium (DMEM). The cells were then centrifuged at 10 000 rpm for 3 minutes at 4°C, the supernatant was discarded and the pellet was resuspended in 50 µl ice cold lysis buffer (pH 7.75) containing 2-Amino-2-(hydroxymethyl)-1,3-propanediol hydrochloride (Tris-HCl, 100 mM) and Ethylenediaminetetraacetic acid (EDTA, 4 mM) as previously described (Essman *et al.*, 2003). The lysis buffer was boiled and added (150 µl) to the cell suspension which was maintained at 99°C for 2 minutes in a water bath. The cells were then centrifuged at 10 000 rpm for 3 minutes at 4°C. The supernatant containing cellular ATP was collected in 2 ml sterile microtubes and stored at -80 °C until further analysis. Samples were obtained from four independent experiments. The samples (50 µl) and rL/L reagent (50 µl, Enliten ATP assay, Promega, FF2000) were added to a 96-well luminometer white plate. In addition, a standard curve was produced according to the manufacturer's protocol that was later used to calculate the concentration of cellular ATP contained in each sample which was normalized to the amount of protein present in each sample and expressed as nM of ATP per µg of protein. Luminescence was measured using a luminometer (GloMax® 96 microplate Luminometer, Promega).

2.1.9.2 Mitochondrial Respiration Analysis

Mitochondrial respiration was measured in intact H9c2 cells using the Seahorse XF96 Cell Mito Stress Test Kit (Seahorse Biosciences, USA), according to the manufacturer's instructions. Cells were seeded into a 96-well XF Analyser Cell Culture Plate at an optimized density of 7x10³ cells per well and were incubated overnight at 37°C. Cells were then treated as previously described. At

termination of treatment, cells were washed and refreshed with 175 μ l of XF Assay Medium (DMEM containing 2 mM of L-glutamine supplemented with 5 mM glucose and 1 mM sodium pyruvate), and placed into a CO₂ - free incubator at 37°C for 1 h. Thereafter, the oxygen consumption rate (OCR) was measured in each well using the Seahorse XFe 96 Extracellular Flux Analyzer (Seahorse Biosciences, USA) and the XFe Wave software (Seahorse Biosciences, USA).

The Seahorse assay is based upon the fluorimetric detection of O₂ and H⁺ levels by using probes on a sensor cartridge which is attached to the a 96-well XF Analyser Cell Culture Plate. After each recorded measurement, the sensor cartridge rises which allows for the re-oxygenation of media through mechanical mixing thus making it possible for repeated O₂ and pH measurements to be recorded in real time. The sensor cartridge is equipped with four drug-delivery injection ports which were loaded with 25 μ l of: oligomycin (a complex V inhibitor), carbonyl cyanide p-trifluoromethoxyphenyl hydrazine (FCCP, a protonophore which collapses the inner membrane gradient, causing the ETC to function at its maximal rate), rotenone and antimycin A (complex I and III inhibitors respectively which are used to shut down the ETC completely). Three cycles of OCR measurements were performed for each well, consisting of basal OCR measurements, OCR measurements following the injection of 1 μ M oligomycin, OCR measurements following the injection of 1 μ M carbonyl cyanide p-trifluoromethoxyphenyl hydrazine (FCCP), and OCR measurements following the simultaneous injection of 1 μ M rotenone and 1 μ M antimycin A. Each cycle consisted of a 3 minute recorded measurement following 3 minutes of re-oxygenation of media through mechanical mixing. Non-mitochondrial respiration was assessed by measuring OCR after complete inhibition of the ETC with rotenone and antimycin A and this rate was subtracted from all other measurements in order to obtain the OCR by the mitochondria.

Four parameters of OCR were calculated as follows: (i) Basal Respiration Rate (BRR) was calculated by subtracting non-mitochondrial respiration from the baseline OCR, (ii) ATP- linked respiration which was calculated by subtracting the oligomycin OCR rate from the BRR, (iii) Electron Transport System Capacity (ETS) was calculated by subtracting non-mitochondrial respiration from the FCCP OCR, (iv) Mitochondrial Spare Respiratory Capacity (MSRC) was calculated by subtracting the BRR

from the MRC. All OCR measurements were expressed as pmol O₂ per minute and normalized to cell number using the CyQUANT Cell proliferation kit (Invitrogen, USA). The CyQUANT assay is based on a fluorochrome binding to nucleic acids and therefore measures the relative DNA content in each well of the plate. The fluorescence was measured in a microplate luminometer with an excitation wavelength of 485 nm and an emission wavelength of 530 nm. Respiration parameters were calculated during one independent experiment based on an average of each replicate per measurement (no. of replicates=12). Measurements were performed three times for each replicate.

2.1.10 Immunoblot Analysis

2.1.10.1 Whole Cell Protein Extraction

H9c2 cells were grown and treated as previously described in T25 flasks (25 cm² flasks, Nest Scientific, USA). At the termination of treatment, growth medium was removed and cells were washed with cold PBS (4°C). Proteins were extracted from cells by adding 500 µl of cold Radioimmunoprecipitation assay (RIPA) buffer, pH 7.4, containing: Tris-HCL (2.5 mM), EDTA (1 mM), Sodium Fluoride (NaF, 50 mM), Sodium orthovanadate (Na₃VO₄, 1 mM), soybean trypsin inhibitor (SBTI, 4 µg/ml), phenyl-methyl-sulphonyl fluoride (PMSF, 0.1 mM), Leupeptin (10 mg/ml), Benzamidin (1 mM), Nonidet-P40 (NP-40, 1%) and, Sodium Deoxycholate (NADC, 0.5%). Cells were then gently scraped from the bottom of culture flasks using a sterile cell scraper whilst maintained on ice. The contents of each flask was then transferred to pre-chilled 2 ml Eppendorf tube followed by sonication at 15% amplitude for 10 seconds using the Misonic Ultrasound Liquid Processor (Qsonica, USA). Sonication of cells was performed to ensure the release of cellular proteins by lysing the cell membrane. Cell lysates were then centrifuged at 8000 rpm for 10 minutes at 4°C, the supernatant was transferred into pre-chilled microtubes and stored at -80°C until further use. Protein lysates were obtained for each group from four independent experiments.

2.1.10.2 Mitochondrial Isolation from cells and Protein Extraction

Mitochondrial isolation from cultured cells was performed using the Mitochondrial Isolation Kit for Cultured cells (Abcam, ab110170) according to the manufacturer's instructions. H9c2 cells were grown and treated as previously described in T25 flasks (25 cm² flasks, Nest Scientific, USA). At the termination of treatment, growth medium was removed and cells were washed with cold PBS (4°C). Proteins were extracted from cells by adding 500 µl of cold Radioimmunoprecipitation assay (RIPA) buffer. Cells were then gently scrapped from the bottom of culture flasks using a sterile cell scraper whilst maintained on ice. The contents of each flask was then transferred to pre-chilled 2 ml microtubes and was stored at -80°C overnight. Samples were then thawed in order to weaken the cell membranes and resuspended in 5 mg/ml of Reagent A (Abcam, ab110170) followed by incubation on ice for 10 minutes. Cells were transferred to a pre-cooled Dounce Homogenizer and mechanically homogenized using 30 dounce strokes with a pestle. The homogenate was then transferred to 2 ml microtubes and centrifuged at 2000 rpm for 10 minutes at 4°C. The supernatant #1 was transferred to a pre-cooled 2 ml Eppendorf tube and maintained on ice and the pellet was resuspended in 5 mg/ml of Reagent B (Abcam, ab110170). The homogenization and centrifugation at 2000 rpm for 10 minutes at 4°C was then repeated and supernatant #2 was combined with supernatant #1, the pellet was discarded. The combined supernatants (#1 and #2) were then mixed thoroughly and centrifuged at 8000 rpm for 15 minutes at 4°C. The supernatant was discarded and the pellet was resuspended in 500 µl of Reagent C (Abcam, ab110170) supplemented with protease inhibitors. The mitochondrial lysates were then stored at -80°C until further use. Mitochondrial lysates were obtained for each group from four independent experiments.

2.1.10.3 Protein Determination and Sample Preparation

Cellular and mitochondrial protein content was quantified using the Direct Detect® FTIR Spectrometer (Merck Millipore, USA). The Direct Detect® protein quantification method is based on the principal of using Infrared Spectroscopy where infrared light interacts with a molecule that absorbs radiation at specific frequencies depending on its structure. Mitochondrial, protein lysates and RIPA buffer that was used to extract proteins, were thawed whilst maintained on ice. Cartridge

cards containing four slots were then loaded with 2 µl of each sample (slots 2 - 4), 2 µl of RIPA buffer was added to the first slot on each new card as it served as the blank. The card was then inserted into the instrument, which then initiated an automated drying cycle of the samples. The protein content was measured in each sample in µg/ml. Protein samples at a concentration of 20 µg/ml were prepared using a combination of β-Mercaptoethanol (150 µl) and Laemmli sample buffer (850 µl). Samples were then stored at - 80°C until further use.

2.1.10.4 Sodium Dodecyl-Sulphate Polyacrylamide Gel Electrophoresis (SDS-PAGE) and Electrotransfer

Proteins were loaded and separated using gradient polyacrylamide gels with a 4% stacking gel (4 – 20% Mini-PROTEAN® TGX Stain-Free™ Protein Gels, Bio-Rad). A BLUeye pre-stained protein ladder (GeneDirex, PM007-0500) was loaded in the first lane on each gel for determination of molecular weights of specific bands. Protein samples were boiled for 5 min at 95°C and briefly centrifuged before loading each sample (20 µg/ml) into the remaining gel lanes. Proteins were separated by SDS-PAGE (Criterion-PROTEAN® Tetra cell, Bio-Rad) at a constant voltage of 100 V and current of 400 mA for 10 minutes and thereafter at a constant voltage of 150 V for 60 minutes (Power Pac 1000, Bio-Rad). Following SDS-PAGE, the stain-free gels were imaged using the ChemiDoc™ XRS + System (Bio-Rad) to ensure equal loading. The proteins were then transferred to a polyvinylidene fluoride (PVDF) membrane (Trans-Blot® midi transfer pack, Bio-Rad) at a constant voltage of 12 V for 12 minutes using the Trans-Blot Turbo System (Bio-Rad). The PVDF membranes were imaged using the ChemiDoc™ XRS + System (Bio-Rad).

2.1.10.5 Immuno-detection

Non-specific binding sites were blocked with 5% fat-free milk in TRIS-buffered saline-Tween (TBS-T) for 2 hours and membranes were incubated overnight at 4°C with the primary antibodies diluted in TBS-T. The following proteins were detected using the cellular protein lysates: cleaved caspase-3, cleaved Poly (ADP-ribose) polymerase (cleaved PARP), Microtubule-associated proteins 1B light chain 3 (LC3), Sequestosome 1 (SQSTM1/p62), Sirtuin 1 (SIRT1), Peroxisome proliferator-activated

receptor gamma coactivator 1-alpha (PGC-1 α) and Beta-actin (β -actin). The mitochondrial protein lysates were used to detect the following proteins: Dynamin-related protein 1 (Drp1), Fission 1 protein (hFis1), Optic Atrophy 1 (OPA1), Mitofusin 1 (Mfn1), Mitofusin 2 (Mfn2), PTEN-induced putative kinase 1 (Pink1), Parkinson protein (PARKIN), Sirtuin 3 (SIRT3) and Translocase of outer mitochondrial membrane 20 (TOM20). Following overnight incubation, membranes were washed in TBS-T (3 x 5 minutes) and the primary antibody was conjugated by the addition of a diluted horseradish peroxidase-labeled secondary antibody for 1 hour at room temperature. Thereafter, membranes were thoroughly washed before being incubated with Clarity™ Western ECL Substrate (Bio-Rad). Membranes were then exposed with the ChemiDoc™ XRS + System (Bio-Rad). Protein bands were quantified using Image Lab™ Software (Bio-Rad).

2.1.11 Statistical Analysis

Values are expressed as mean \pm standard error of the mean (SEM). Analysis of data was conducted using GraphPad Prism, version 5.0 (GraphPad Inc.). One-way Analysis of Variance (ANOVA) with Bonferroni's Multiple Comparison as a post-hoc test was used to assess the statistical significance between treatment groups. Values of $p < 0.05$ were considered significant.

2.2 *In vivo* Study design – Phase 2

Phase 2 of this study, describes an *in vivo* tumor-bearing rat model of acute doxorubicin-induced cardiotoxicity. Female Sprague Dawley rats were randomly allocated to the following groups: (i): control (CTRL); (ii): tumor control (T CTRL); (iii): vehicle control (V CTRL); (iv): doxorubicin (DXR); (v): melatonin (MLT) and; (vi): doxorubicin and melatonin (DXR+MLT). Briefly, at the age of sixteen weeks, all rats, except the control group, were inoculated with LA7 rat tumor cells. The DXR group received 4 mg/kg of DXR on days 4, 8 and 12, the MLT group received 6 mg/kg of MLT in their drinking water daily and, the DXR+MLT group received both DXR and MLT. The study was terminated after 14 days and rat hearts were rapidly excised to perform isolated rat heart perfusions. The perfused heart tissues were then used for immunoblot analysis. A schematic representation of the study design is provided in Figure 2.2.

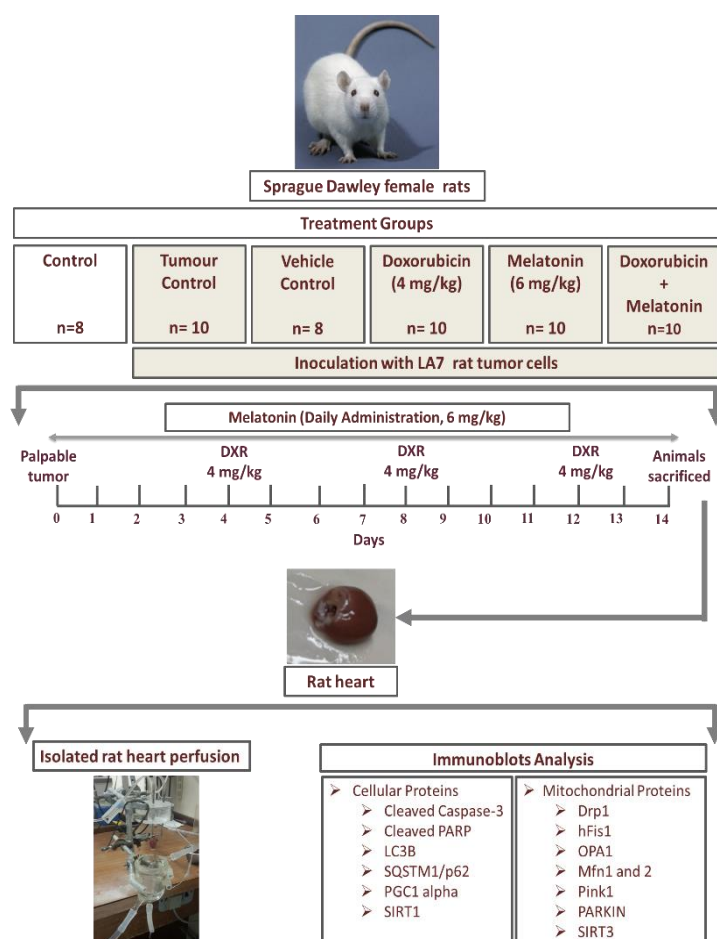


Figure 2.2: Schematic representation of *in vivo* study design. Female Sprague Dawley rats were inoculated with LA7 rat tumor cells. Animals were treated with 4 mg/kg of DXR and daily with 6 mg/kg of MLT. Rat hearts were used to conduct isolated heart perfusions whereafter, rat heart tissues were freeze-clamped and stored at -80°C until further analysis.

2.2.1 Animal care and grouping

Female Sprague Dawley rats were obtained from the University of Stellenbosch Central Research Facility. Upon receiving animals between 8 – 10 weeks of age, animals were randomly grouped in cages. Animals were allowed to acclimatize to the environment for \pm 6 weeks prior to the commencement of this study and were housed with free access to water and food, a 12-h dark/light cycle (light from 6:00 a.m. to 6:00 p.m.) with temperature and humidity kept constant at 22°C and 40%, respectively. The experimental procedures were conducted according to the guidelines for the care and use of laboratory animals implemented at Stellenbosch University and were approved by the Committee for Ethical Animal Research of the Faculty of Health Sciences, University of Stellenbosch (Ethical clearance: SU-ACUM13-00015).

2.2.2 Cell culture and maintenance of LA7 cell line

LA7 rat mammary adenocarcinoma-derived tumor cells (ATCC No CRL2283) were a kind gift from Dr Annadie Krygsman (Stellenbosch University, SA). Cells were maintained in a monolayer at 37°C and in a 21% O₂, 5% CO₂, humidified air atmosphere of 95% and were cultured in Dulbecco's modified Eagle's medium (DMEM, Invitrogen Gibco): Ham's F12 nutrient mixture at a ratio of 1:1, supplemented with 10% fetal bovine serum (Invitrogen, Gibco) and 1% penicillin/streptomycin solution (Invitrogen, Gibco), 0.005 mg/ml insulin (Stelkor Pharmacy, Stellenbosch, SA), 50 nM hydrocortisone (Sigma Chemical Co., St Louis, MO, US) and 20 mM HEPES (Sigma Chemical Co., St Louis, MO, US). Cells were allowed to proliferate in T175 flasks (175 cm² flasks). When cultures reached 80% confluency they were sub-cultured by washing the cell monolayer with warm (37°C) media (DMEM) followed by trypsinization using 0.25% Trypsin-ethylene-diaminetetra-acetic acid (trypsin-EDTA) (Invitrogen Gibco). Cells were gently agitated to ensure complete detachment from the flask followed by centrifugation at 1500 rpm for 3 minutes. Cell pellets were re-suspended in fresh warm growth medium and a hemocytometer was used to count the cells. Cells were

resuspended at a density of 16×10^6 in 300 μ l of Hank's Balanced Salt Solution (HBSS, Invitrogen Gibco). All harvested cells were used within 1 hour of preparation.

2.2.3 Mammary tumor induction

Mammary tumor induction was performed as previously described by Abbasalipourkabar *et al.* (2010). Rats were anesthetized by inhalation of 3% Isoflorane® (USP, Abbott Laboratories, USA) coupled with an oxygen regulator. Animals were orientated in a supine position. The injection site was cleaned and sterilized with ethanol. The cell suspension was aspirated using 1-cc (1-ml) TB syringes without needles to minimize cell lysis. A 26 gauge needle was then attached to the TB syringe and the cell suspension was subcutaneously inoculated into the mammary fat pad (right flank) of the animal. The needle was inserted through the skin approximately 2 mm anterior and 3 mm lateral to the mammary and then inserted 5 mm into the mammary fat pad. The 300 μ l cell suspension was injected slowly over five minutes.

All animals were monitored daily for mammary tumor development. Tumors were palpable 3 days post-inoculation. Tumor diameters and animal weight were measured daily. The tumor mass was measured horizontally and vertically, parallel to the ventricular surface of the rats, using a digital caliper. The volume of the tumor (V) was calculated according to Carlsson *et al.* (1983): $V=(ab^2)/2$, where 'a' and 'b' is the longest and shortest diameter of the tumor, respectively.

2.2.4 Doxorubicin treatment

DXR (Sigma Chemical Co., St Louis, MO, US) was prepared by dissolving the compound in Hank's Balanced Salt Solution (HBSS, Invitrogen Gibco). The amount of DXR to be injected was calculated according to the average body weight of animals. A 22 gauge needle was used to administer 200 μ l of DXR solution through the intraperitoneal injection. The DXR and DXR+MLT groups received a total of three intraperitoneal injections of DXR (4 mg/ kg) at three day intervals with an accumulative dose of 12 mg/kg.

2.2.5 Melatonin treatment

Melatonin (MLT) (Sigma, St. Louis, MO) was orally administered to Sprague Dawley via the drinking water at a dose of 6 mg/rat/day. The amount of drinking water consumed by the group of animals per cage was monitored and recorded for one week prior to the commencement of the study and thus the average volume of drinking water consumed per animal was calculated. On the basis of the pre-determined water consumption of 50 ml/rat/day, MLT was dissolved in 700 ml of drinking water at a final concentration of 30 µg/ml. The water bottles were covered with aluminum foil as melatonin is a light sensitive compound; clean bottles with fresh solutions were prepared daily. The dosage of 6 mg/kg/day was regularly adjusted according to the body weight gain of the animals which was measured daily. Animals drank water and MLT (6 mg/kg/day) *ad libitum*. Since a small volume of MLT was used in this study, it was completely dissolvable in the large volume of drinking water provided, therefore it was not necessary to dissolve the MLT in ethanol prior to adding it to the drinking water.

2.2.6 Isolated rat heart perfusions

Hearts were perfused with a modified Krebs-Henseleit bicarbonate buffer (KHB) containing: sodium chloride (NaCl, 119 mM), sodium bicarbonate (NaHCO₃, 24.9 mM), potassium chloride (KCl, 4.7 mM), potassium monophosphate (KH₂PO₄, 1.2 mM), magnesium sulphate heptahydrate (MgSO₄·7H₂O, 0.59 mM), sodium sulphate (Na₂SO₄, 0.59 mM), calcium chloride dihydrate (CaCl₂·2H₂O, 1.25 mM) and glucose (10 mM). The KHB was kept at a constant of pH 7.4; oxygenation was achieved by gassing the perfusate with 95% O₂ and 5% CO₂ at 37°C.

2.2.6.1 Perfusion technique of isolated perfused rat heart

Upon termination of the experimental protocol, rats were anaesthetized using sodium pentobarbitone (160 mg/kg) via intraperitoneal injection, and body weights were recorded. The hearts were rapidly excised and immediately arrested in ice-cold (4°C) Krebs-Henseleit bicarbonate buffer (KHB). Thereafter, hearts were mounted onto the aortic cannula via the aorta. After cannulation, stabilization of the heart was achieved by perfusing the hearts retrogradely (Langendorff mode), in a non-recirculating manner at constant hydrostatic pressure (100 cm H₂O) for 15 minutes. During this time, the left atrium was cannulated via the pulmonary vein to allow atrial perfusion (atrial pressure 15 cm H₂O). The left ventricle ejected against a hydrostatic pressure of 100 cm H₂O. After 15 minutes of retrograde perfusion, the perfusion mode was switched to the working heart mode maintaining a preload of 15 cm H₂O and an afterload of 100 cm H₂O for 15 minutes. Myocardial temperature was maintained at 37°C and thermostatically controlled as well as continuously monitored by inserting a temperature probe into the pulmonary artery. At the end of the perfusion protocol, hearts were weighed and immediately freeze-clamped with Wollenberger tongs and submerged in liquid nitrogen. The heart tissue samples were stored at - 80°C until further use.

2.2.6.2 Determination of cardiac function

Coronary (Q_e) and aortic (Q_a) flow rates in ml/minute were measured manually. The aortic pressure (mmHg) and heart rate was recorded using a Viggo-Spectramed pressure transducer which was connected to a computer and attached to the side-arm of the aortic cannula. The peak systolic pressure (PSP) was obtained from the recordings. The following parameters were calculated to assess cardiac function: Cardiac output (CO) (ml/min) = (Aortic flow rate + Coronary flow rate), Stroke volume (SV) (ml/min) = (Cardiac output/Heart rate) and, Total Work performance (TW, mWatts) which is the mean external power produced by the left ventricle was calculated using a formula previously described by Kannengieser *et al.* (1979): $0.002222 (PAO - 11.25) (CO)$ where PAO = aortic pressure, CO = cardiac output.

2.2.7 Immunoblot Analysis

2.2.7.1 Tissue Protein Extraction

Heart tissues were retrieved from the -80 °C freezer and immediately placed in liquid nitrogen. Small pieces of tissue were cut, weighed, ground to powder by gently tapping it with a pre-cooled pestle and, homogenized in 1 ml of cold Radioimmunoprecipitation assay (RIPA) buffer using a Polytron PT10 homogenizer. The RIPA buffer, pH 7.4, contained: Tris-HCL (2.5 mM), EDTA (1 mM), Sodium Fluoride (NaF, 50 mM), Sodium orthovanadate (Na_3VO_4 , 1 mM), soybean trypsin inhibitor (SBTI, 4 $\mu\text{g}/\text{ml}$), phenyl-methyl-sulphonyl fluoride (PMSF, 0.1 mM), Leupeptin (10 mg/ml), Benzamidine (1 mM), Nonidet-P40 (NP-40, 1%) and Sodium Deoxycholate (NADC, 0.5%). Samples were then centrifuged at 12 000 rpm for 15 minutes at -4°C, the supernatant was transferred into pre-chilled microtubes and stored at -80°C until further use.

2.2.7.2 Mitochondrial Isolation from Tissue and Protein Extraction

Mitochondrial isolation was performed using the Mitochondrial Isolation Kit for Tissue (Abcam, ab110168) according to the manufacturer's instructions. Frozen heart tissue was weighed (0.4 g as recommended to yield 1- 2 mg of isolated mitochondria). The sample tissue was washed twice with 1.5 ml of Wash Buffer (Abcam, ab110168). The tissue was minced and homogenized using a pre-chilled Dounce Homogenizer (40 dounce strokes as recommended) in 2 ml of Isolation Buffer (Abcam, ab110168). The homogenate was transferred to 2 ml microtubes, filled to a volume of 2 ml with Isolation buffer and centrifuged at 2000 rpm for 10 minutes at 4°C. The supernatant was separated into equal volumes using two microtubes and filled to a volume of 2 ml with Isolation buffer. Both samples of the supernatant were centrifuged at 8000 rpm for 15 minutes at 4°C. Both pellets were resuspended in 1 ml of isolation buffer supplemented with 10 μl of protease inhibitor cocktail (ABCAM, ab65621) and centrifuged at 8000 rpm for 15 minutes at 4°C and this step was repeated twice. The pellets were then combined and resuspended in 500 μl of Isolation Buffer and supplemented with 0.5 μl of protease inhibitor cocktail. The samples were then stored at -80°C until use.

2.2.7.3 Protein Determination, Sample Preparation, SDS-PAGE, Electrotransfer and Immuno-detection

The methodology was similar as previously described in sections 2.1.10.3 - 2.1.10.5. Protein expression was normalized to the corresponding total protein per sample.

2.2.8 Statistical Analyses

Values are expressed as mean \pm standard error of the mean (SEM). Analysis of data was conducted using GraphPad Prism, version 5.0 (GraphPad Inc.). One-way Analysis of Variance (ANOVA) with Bonferroni's Multiple Comparison as a post-hoc test was used to assess the statistical significance between treatment groups. Two-way repeated measures ANOVA with Fisher's LSD as a post-hoc test was used to assess the statistical significance between treatment groups and day on tumor volume or animal weight. Values of $p < 0.05$ were considered significant.

Chapter 3

Results

3.1 Pilot study

A dose and time response study was initially conducted to determine clinically relevant doxorubicin (DXR) and melatonin (MLT) concentrations and treatment durations for the main study.

3.1.1 The effect of various Doxorubicin (DXR) concentrations on cell viability

In order to determine a treatment concentration of DXR, H9c2 cardiac myoblasts were incubated with 1, 2, 3, 4, and 5 μM of DXR for 24 hours and cell viability was assessed using the MTT assay. Cells treated with DXR at a concentration of 3 μM and 5 μM for 24 hours significantly decreased cell viability when compared to the CTRL ($39.67 \pm 7.688\%$ vs 100% , $p < 0.001$; $38.67 \pm 8.413\%$ vs 100% , $p < 0.001$, respectively) (Figure 3.1.1). The lower concentration of 3 μM of DXR was chosen for this study as it is within the clinically relevant range for DXR treatment.

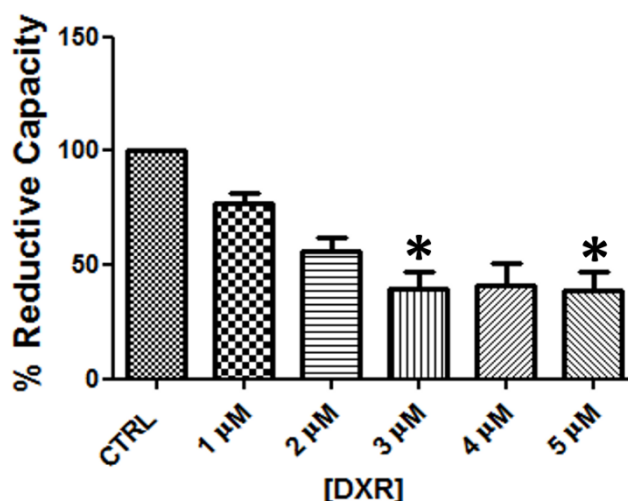


Figure 3.1.1: The effect of various DXR concentrations on the cell viability of H9c2 cardiac myoblasts. Cells were treated with increasing concentrations of DXR for 24 hours. Cell viability was assessed using the MTT Assay. Values are expressed as a percentage of the control and presented as means \pm SEM ($n=3$), * $p < 0.001$ vs CTRL. Abbreviations- **CTRL**: control; **DXR**: doxorubicin.

3.1.2 The effect of various melatonin (MLT) concentrations on cell viability

In order to determine a treatment concentration of MLT, H9c2 cardiac myoblasts were incubated with 10, 20, and 50 μM of MLT for 24 hours and cell viability was assessed using the MTT assay. Cells treated with MLT at a concentration of 50 μM for 24 hours significantly decreased cell viability when compared to the CTRL ($68.33 \pm 6.741\%$ vs 100% , $p < 0.05$). A concentration of 10 μM of MLT was chosen for this study, as there was no significant change in cell viability in comparison to the CTRL (Figure 3.1.2).

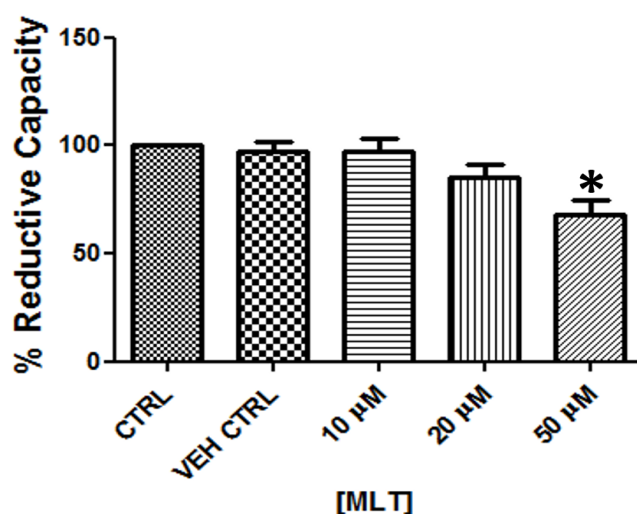


Figure 3.1.2: The effect of various MLT concentrations on the cell viability of H9c2 cardiac myoblasts. Cells were treated with increasing concentrations of MLT for 24 hours. Cell viability was assessed using the MTT Assay. Values are expressed as a percentage of the control and presented as means \pm SEM ($n=3$), * $p < 0.05$ vs CTRL. Abbreviations- **CTRL**: control; **VEH CTRL**: vehicle control; **MLT**: melatonin.

3.1.3 The effect of MLT pre-treatment on cell viability and doxorubicin-induced cell death

In order to determine a treatment duration for MLT, H9c2 cardiac myoblasts were pre-treated with 10 μM of MLT for 1 hour and 24 hours followed by incubation with DXR (3 μM) for 24 hours. Cell viability was assessed using the MTT assay. No significant changes in cell viability were demonstrated when cells were pre-treated with MLT for 1 hour followed by DXR treatment in comparison to the DXR treated group only. However, the viability of H9c2 cells pre-treated with MLT for 24 hours followed by DXR treatment significantly increased in comparison to the DXR treated group ($76.33 \pm 6.642\%$ vs 35.67 ± 6.566 , $p < 0.001$) (Figure 3.1.3).

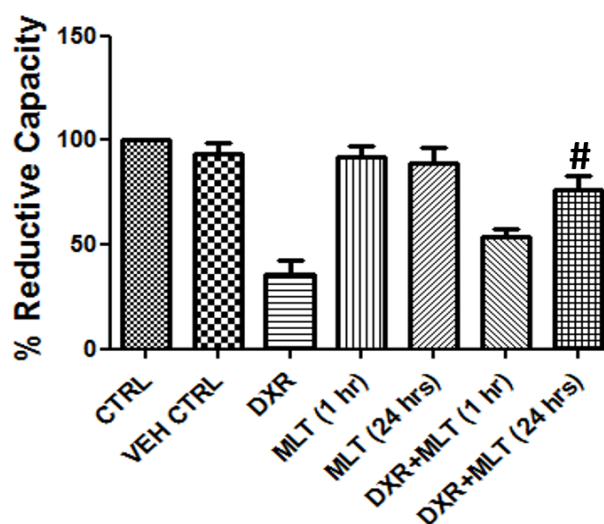


Figure 3.1.3: The effect of MLT pre-treatment on the cell viability and DXR-induced cell death. Cells were treated with 10 μM MLT for 1 hour and 24 hours followed by incubation with 3 μM DXR for 24 hours. Cell viability was assessed using the MTT Assay. Values are expressed as a percentage of the control and presented as means \pm SEM (n=3), [#]p < 0.001 vs DXR. Abbreviations- **CTRL**: control; **VEH CTRL**: vehicle control; **DXR**: doxorubicin; **MLT**: melatonin; **hr**: hour.

Based on the results obtained in the pilot study, pre-treatment with MLT at a concentration of 10 μM for 24 hours was chosen for future *in vitro* experiments as it induced a protective effect against DXR-induced cell death. Therefore, the following five treatment groups were used in this study: (i) control (CTRL); (ii) vehicle control (VEH CTRL, 0.02% EtOH); (iii) doxorubicin (DXR) at 3 μM for 24 hours; (iv) melatonin (MLT) at 10 μM for 24 hours and (v) pre-treatment with melatonin followed by doxorubicin exposure (DXR+MLT).

3.2 The effect of MLT on cell viability and apoptosis during DXR-induced cardiotoxicity

3.2.1 Trypan blue assay

To further confirm the results of the MTT assay, cell viability was additionally assessed using the trypan blue assay. Cell viability significantly decreased in the DXR treated group in comparison to the CTRL ($36.67 \pm 4.806\%$ vs 100%, p < 0.001). However, pre-treatment with MLT for 24 hours significantly increased the amount of viable cells in comparison to DXR treated group ($75.67 \pm 7.535\%$ vs $36.67 \pm 4.806\%$) (Figure 3.2.1).

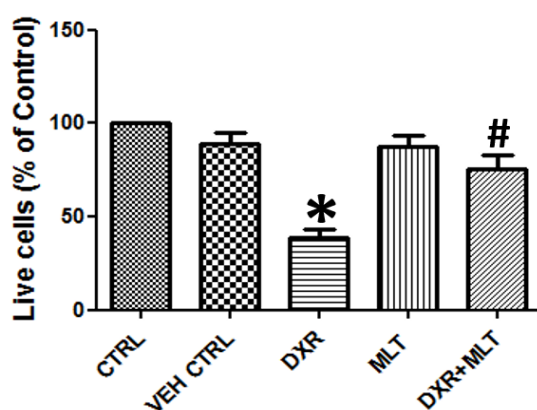


Figure 3.2.1: The effect of MLT on the cell viability during DXR-induced cardiotoxicity. Cells were treated with 10 μ M MLT for 24 hours followed by incubation with 3 μ M DXR for 24 hours. Cell viability was assessed using the Trypan blue assay. Values are expressed as a percentage of the control and presented as means \pm SEM (n=3), *p < 0.001 vs CTRL, #p < 0.01 vs DXR. Abbreviations- **CTRL**: control; **VEH CTRL**: vehicle control; **DXR**: doxorubicin; **MLT**: melatonin.

3.2.2 Caspase 3/7 activity assessment

H9c2 cells displayed a significant increase in caspase 3/7 activity in response to DXR treatment when compared to the CTRL (2.393 \pm 0.093 fold vs 1.000 \pm 0.000 fold, p < 0.001) (Figure 3.2.2). However, a significant decrease in caspase 3/7 activity was detected when cells were pre-treated with MLT for 24 hours followed by treatment with DXR for 24 hours when compared to the DXR treated group only (1.710 \pm 0.076 fold vs \pm 2.393 \pm 0.093 fold, p < 0.001) (Figure 3.2.2).

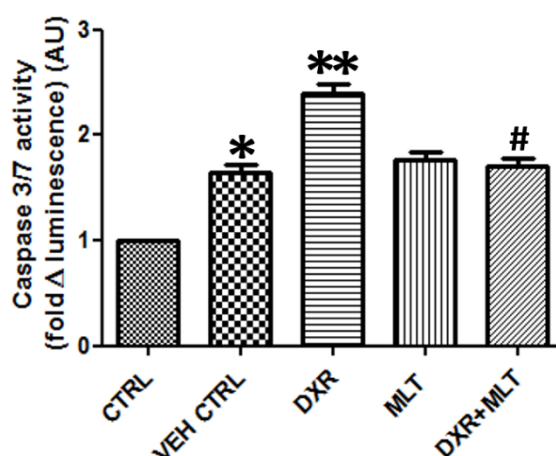


Figure 3.2.2: The effect of MLT on the caspase 3/7 activity during DXR-induced cell death. Cells were treated with 10 μ M MLT for 24 hours followed by incubation with 3 μ M DXR for 24 hours. Cell viability was assessed using the Caspase-Glo® 3/7 Assay. Caspase 3/7 activity was taken to be proportionate to the produced luminescence intensity per sample. Results represent the fold change in luminescence and are presented as means \pm SEM (n=3), *p < 0.001 vs CTRL, **p < 0.001 vs CTRL, #p < 0.001 vs DXR. Abbreviations- **CTRL**: control; **VEH CTRL**: vehicle control; **DXR**: doxorubicin; **MLT**: melatonin; **AU**: arbitrary units.

The VEH CTRL (0.02% EtOH) shows a significant increase in caspase activity in comparison to the CTRL (1.647 ± 0.067 fold vs 1.000 ± 0.000 fold, $p < 0.001$), however this discrepancy may be attributed to the reaction of ethanol with the reagents supplied in the Caspase-Glo Promega Kit as no change in cell viability was demonstrated when the MTT assay and trypan blue cell viability assays were conducted.

3.2.3 Immunoblot analysis of cleaved caspase-3 and cleaved PARP protein levels

To further assess programmed cell death and confirm that the vehicle control (0.02% EtOH) is not inducing cell death in our model, immunoblot analysis for apoptotic proteins cleaved caspase-3 and cleaved PARP were performed. Caspase-3 cleavage significantly increased in response to DXR treatment when compared to the CTRL ($237.7 \pm 16.56\%$ vs 100% , $p < 0.001$) (Figure 3.2.3 A). Cells pre-treated with MLT were able to mitigate this effect and significantly decreased caspase-3 cleavage in comparison to the DXR treated group ($126.6 \pm 10.52\%$ vs $237.7 \pm 16.56\%$, $p < 0.001$) (Figure 3.2.3 A).

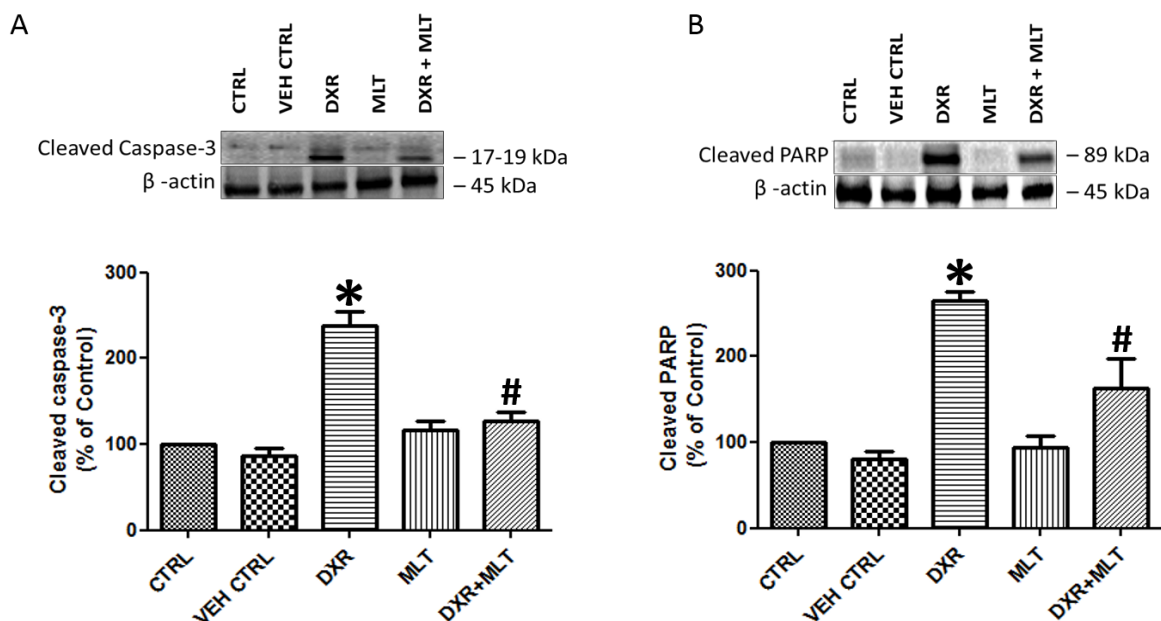


Figure 3.2.3: The effect of MLT on cleaved caspase-3 and PARP cleavage during DXR-induced cell death. Cells were treated with 10 μ M MLT for 24 hours followed by incubation with 3 μ M DXR for 24 hours. Apoptotic cell death was assessed using immunoblot analysis. Bar graphs show: **A.** Cleaved caspase-3 and **B.** Cleaved-PARP protein levels (normalized to β -actin vs control). Values are expressed as a percentage of the control and presented as means \pm SEM (n=3), **A:** * $p < 0.001$ vs CTRL, # $p < 0.001$ vs DXR. **B:** * $p < 0.001$ vs CTRL, # $p < 0.05$ vs DXR. Abbreviations- **CTRL:** control; **VEH CTRL:** vehicle control; **DXR:** doxorubicin; **MLT:** melatonin.

Similar results were observed in response to PARP cleavage. The DXR treated group significantly increased PARP cleavage in comparison to the CTRL ($264.9 \pm 11.26\%$ vs 100% , $p < 0.001$) and pre-treatment with MLT significantly decreased PARP cleavage in comparison to the DXR group ($162.8 \pm 35.38\%$ vs $264.9 \pm 11.26\%$, $p < 0.001$) (Figure 3.2.3 B). Since the VEH CTRL (0.02% EtOH) showed no significant changes in caspase-3 and PARP cleavage in comparison to the CTRL, the VEH CTRL was not included in further analyses as we were confident that it had no effect.

3.3 The effect of MLT on autophagy during DXR-induced cardiotoxicity

3.3.1 Immunoblot analysis of autophagy proteins LC3 II and SQSTM1/p62

To assess autophagic flux, four additional treatment groups were included in this analysis. H9c2 cells were treated as previously described and at the end of each treatment, cells were treated additionally with an autophagic inhibitor bafilomycin A1 (BAF) at a concentration of 10 nM for 4 hours. Immunoblot analysis was conducted to assess the protein levels of LC3 II and p62.

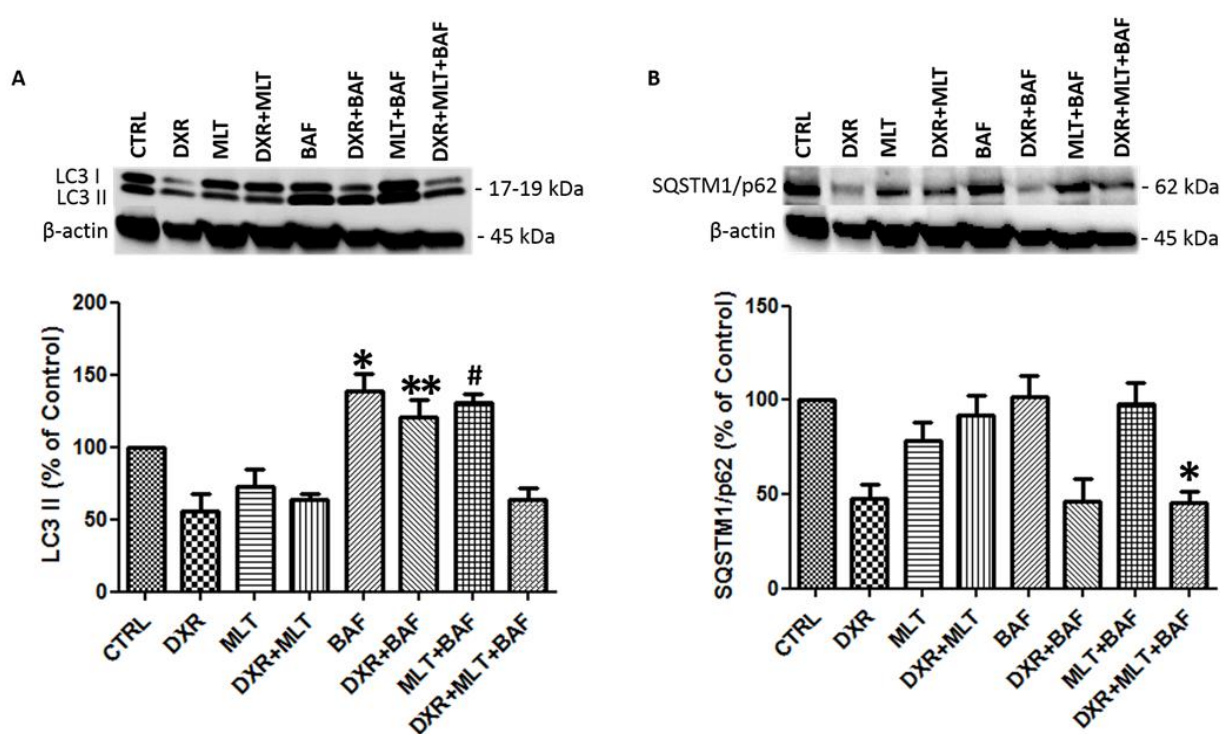


Figure 3.3.1: The effect of MLT on autophagy during DXR-induced cardiotoxicity. Cells were treated with 10 μ M MLT for 24 hours followed by incubation with 3 μ M DXR for 24 hours and thereafter treated with 10 nM BAF for 4 hours. Autophagic flux was assessed using immunoblot analysis. Bar graphs show: **A.** LC3 II and **B.** SQSTM1/p62 protein levels (normalized to β -actin vs control). Values are expressed as a percentage of the control and presented as means \pm SEM (n=4), **A:** *p < 0.05 vs CTRL, **p < 0.01 vs DXR, #p < 0.05 vs MLT. **B:** *p < 0.05 vs DXR+MLT. Abbreviations- **CTRL:** control; **DXR:** doxorubicin; **MLT:** melatonin; **BAF:** Bafilomycin A1.

There was a significant increase in LC3 II levels when cells were treated with BAF in comparison to the CTRL ($149 \pm 7.90\%$ vs 100% , $p < 0.05$). Cells treated with DXR+BAF significantly increased LC3 II levels in comparison to the DXR treated group ($120.8 \pm 11.43\%$ vs $56.16 \pm 11.92\%$, $p < 0.01$). Similarly, MLT+BAF increased LC3 II levels significantly in comparison to the MLT group ($131 \pm$

6.137% vs $73.02 \pm 12.05\%$, $p < 0.05$) (Figure 3.3.1 A). Interestingly, no significant changes in LC3 II levels occurred with the DXR+MLT treated group in comparison to the DXR+MLT+BAF group.

Furthermore, no significant changes in p62 levels occurred when cells were treated with BAF in comparison to the CTRL. However, cells treated with DXR+MLT+BAF significantly decreased p62 levels in comparison to the DXR+MLT treated group ($45.16 \pm 6.57\%$ vs $92.29 \pm 10.49\%$, $p < 0.05$) (Figure 3.3.1 B).

3.3.2 Immunoblot assessment of Pink1 and PARKIN protein levels

Pink1 and PARKIN proteins are associated with mitophagy. To assess Pink1 and PARKIN protein levels, cells were treated with MLT at $10 \mu\text{M}$ for 24 hours followed by incubation with DXR at $3 \mu\text{M}$ for 24 hours and the mitochondria were isolated at the end of treatment from each group. Pink1 which is an indicator of mitochondrial damage, significantly increased in response to DXR treatment in comparison to the CTRL ($274.9 \pm 36.58\%$ vs 100% , $p < 0.01$) (Figure 3.3.2 A).

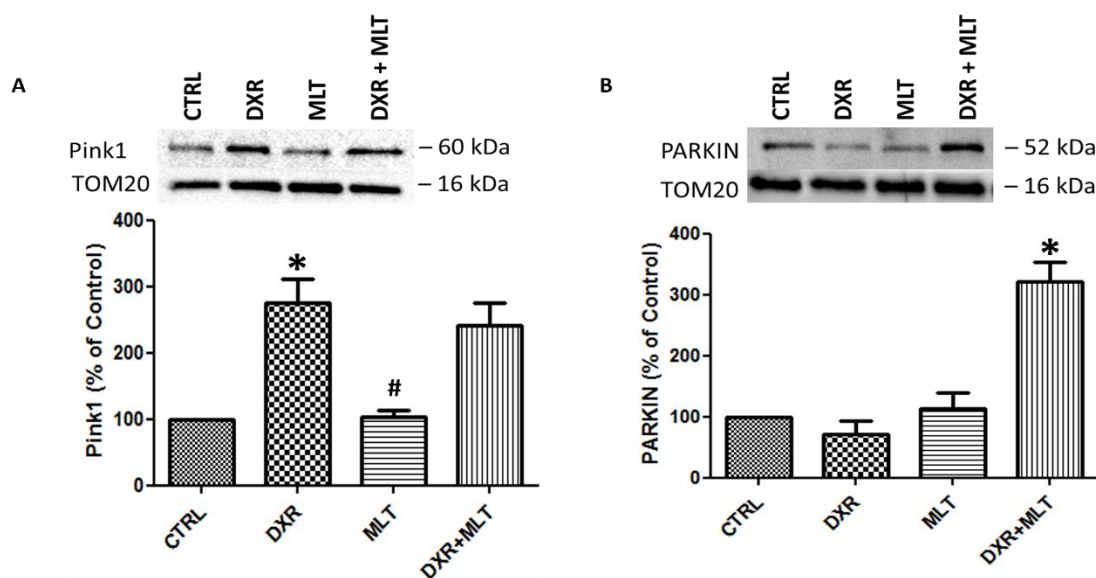


Figure 3.3.2: The effect of MLT on Pink1 and PARKIN during DXR-induced cardiotoxicity. Cells were treated with $10 \mu\text{M}$ MLT for 24 hours followed by incubation with $3 \mu\text{M}$ DXR for 24 hours. Mitochondria were isolated from treated cells and Pink1 and PARKIN were assessed using immunoblot analyses. Bar graphs show: **A.** Pink1 and **B.** PARKIN protein levels (normalized to TOM20 vs control). Values are expressed as a percentage of the control and presented as means \pm SEM ($n=3$), **A:** * $p < 0.01$ vs CTRL, # $p < 0.01$ vs DXR. **B:** * $p < 0.001$ vs DXR. Abbreviations- **CTRL:** control; **DXR:** doxorubicin; **MLT:** melatonin.

Pink1 levels were significantly decreased in the MLT treated group in comparison to the DXR group ($103 \pm 11.26\%$ vs $274.9 \pm 36.58\%$, $p < 0.01$) (Figure 3.3.2 A). However, no significant changes in protein levels of Pink1 occurred between DXR+MLT and the DXR group. Furthermore, DXR+MLT treatment significantly increased PARKIN protein levels in comparison to the DXR treated group only ($320.7 \pm 31.78\%$ vs $72.06 \pm 21.18\%$, $p < 0.001$) (Figure 3.3.2 B).

3.4 The effect of MLT on ROS and mitochondrial ROS generation during DXR-induced cardiotoxicity

3.4.1 Flow cytometry analysis of ROS generation with H₂DCFDA and MitoSox Red staining

H9c2 cells were treated as previously described and stained with H₂DCFDA and MitoSox Red to quantify ROS and mitochondrial ROS generation, respectively. The mean fluorescent intensity was measured using flow cytometry analysis.

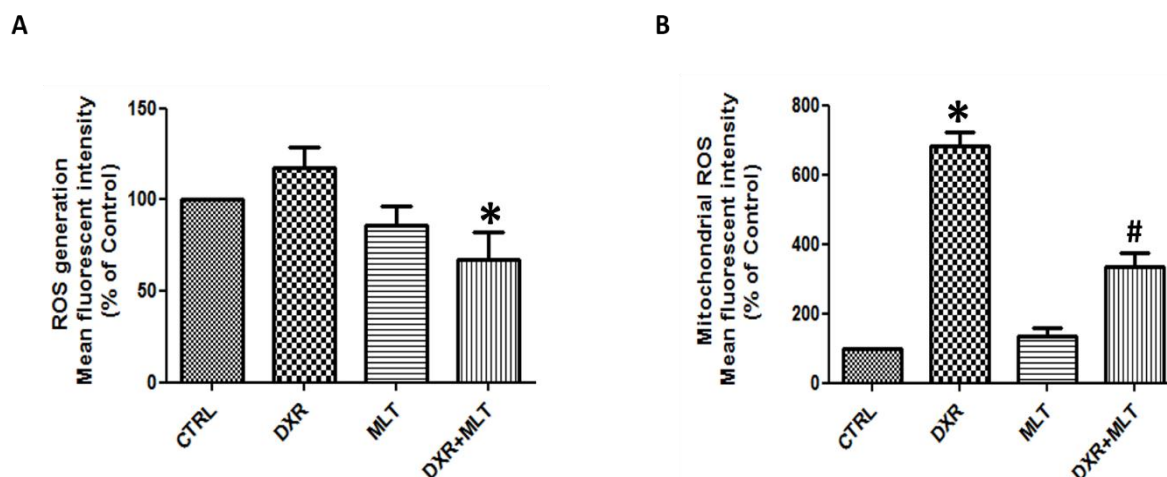


Figure 3.4.1: The effect of MLT on ROS and mitochondrial ROS generation during DXR-induced cardiotoxicity. Cells were treated with 10 μ M MLT for 24 hours followed by incubation with 3 μ M DXR for 24 hours. Cells were then stained with H₂DCFDA and MitoSox Red and analyzed using flow cytometry to measure ROS and mitochondrial ROS, respectively. Bar graphs show: **A.** ROS generation and **B.** Mitochondrial ROS. Values are expressed as a percentage of the control and presented as means \pm SEM ($n=4$), **A:** * $p < 0.05$ vs DXR, **B:** * $p < 0.001$ vs CTRL, # $p < 0.001$ vs DXR. Abbreviations- **CTRL:** control; **DXR:** doxorubicin; **MLT:** melatonin.

ROS generation significantly decreased when cells were pre-treated with MLT for 24 hours in comparison to the DXR treated group only ($67.27 \pm 14.70\%$ vs $117.3 \pm 11.45\%$, $p < 0.05$) (Figure

3.4.1 A). However, the increase in ROS generation induced by DXR treatment was not significant in comparison to the CTRL (Figure 3.4.1 A).

DXR treatment significantly increased mitochondrial ROS production in comparison to the CTRL ($681.8 \pm 42.58\%$ vs 100% , $p < 0.001$) (Figure 3.4.1 B). Pre-treatment with MLT significantly decreased mitochondrial ROS generation induced by the DXR ($335.0 \pm 40.08\%$ vs $681.8 \pm 42.58\%$, $p < 0.001$) (Figure 3.4.1 B).

3.5 The effect of MLT on mitochondrial membrane potential during DXR-induced cardiotoxicity

3.5.1 Flow cytometry analysis of mitochondrial membrane potential with JC-1 staining

H9c2 cells were treated as previously described and stained with JC-1 to assess mitochondrial membrane potential. JC-1 is a ratio metric dye and therefore the PE/FITC (red/green) mean fluorescent intensity was measured using flow cytometry analysis

Treatment with $3 \mu\text{M}$ DXR for 24 hours significantly decreased mitochondrial membrane potential in comparison to the CTRL ($63.80 \pm 10.97\%$ vs 100% , $p < 0.05$) (Figure 3.5.1). Interestingly, treatment with MLT significantly increased mitochondrial membrane potential in comparison to the CTRL ($143.8 \pm 8.866\%$ vs 100% , $p < 0.01$). In addition, cells pre-treated with MLT significantly increased mitochondrial membrane potential when compared to the DXR group ($105.3 \pm 5.105\%$ vs $63.80 \pm 10.97\%$, $p < 0.05$) (Figure 3.5.1).

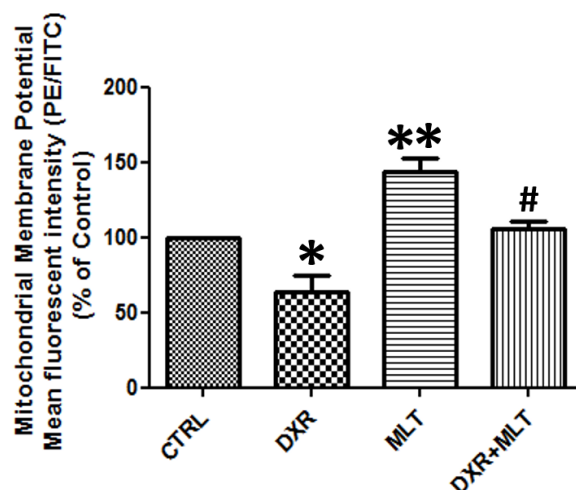


Figure 3.5.1: The effect of MLT on mitochondrial membrane potential during DXR-induced cardiotoxicity. Cells were treated with 10 μ M MLT for 24 hours followed by incubation with 3 μ M DXR for 24 hours. Cells were then stained with JC-1 and analyzed using flow cytometry to measure the mean fluorescent intensity (PE/FITC). Values are expressed as a percentage of the control and presented as means \pm SEM (n=4), *p < 0.05 vs CTRL, **p < 0.01 vs CTRL, #p < 0.05 vs DXR. Abbreviations- **CTRL**: control; **DXR**: doxorubicin; **MLT**: melatonin.

3.6 The effect of MLT on mitochondrial dynamics during DXR-induced cardiotoxicity

3.6.1 Mitochondrial Morphometric Network Assessment

In order to assess the mitochondrial network, H9c2 cells were treated and stained with Hoechst and TMRE. Live cell imaging was performed. A morphometric assessment of the mitochondrial network was conducted on the processed images as previously described by Mortiboys *et al.* (2008), using ImageJ (version 1.42) software (see section 2.1.8).

A high degree of mitochondrial fission (round-shaped mitochondria) following DXR treatment occurred in comparison to the CTRL group which maintained a healthy fused mitochondrial network (long, elongated mitochondria) (Figure 3.6.1.1). Pre-treatment with melatonin followed by DXR treatment decreased the degree of mitochondrial fission in comparison to the DXR treated group (Figure 3.6.1.1).

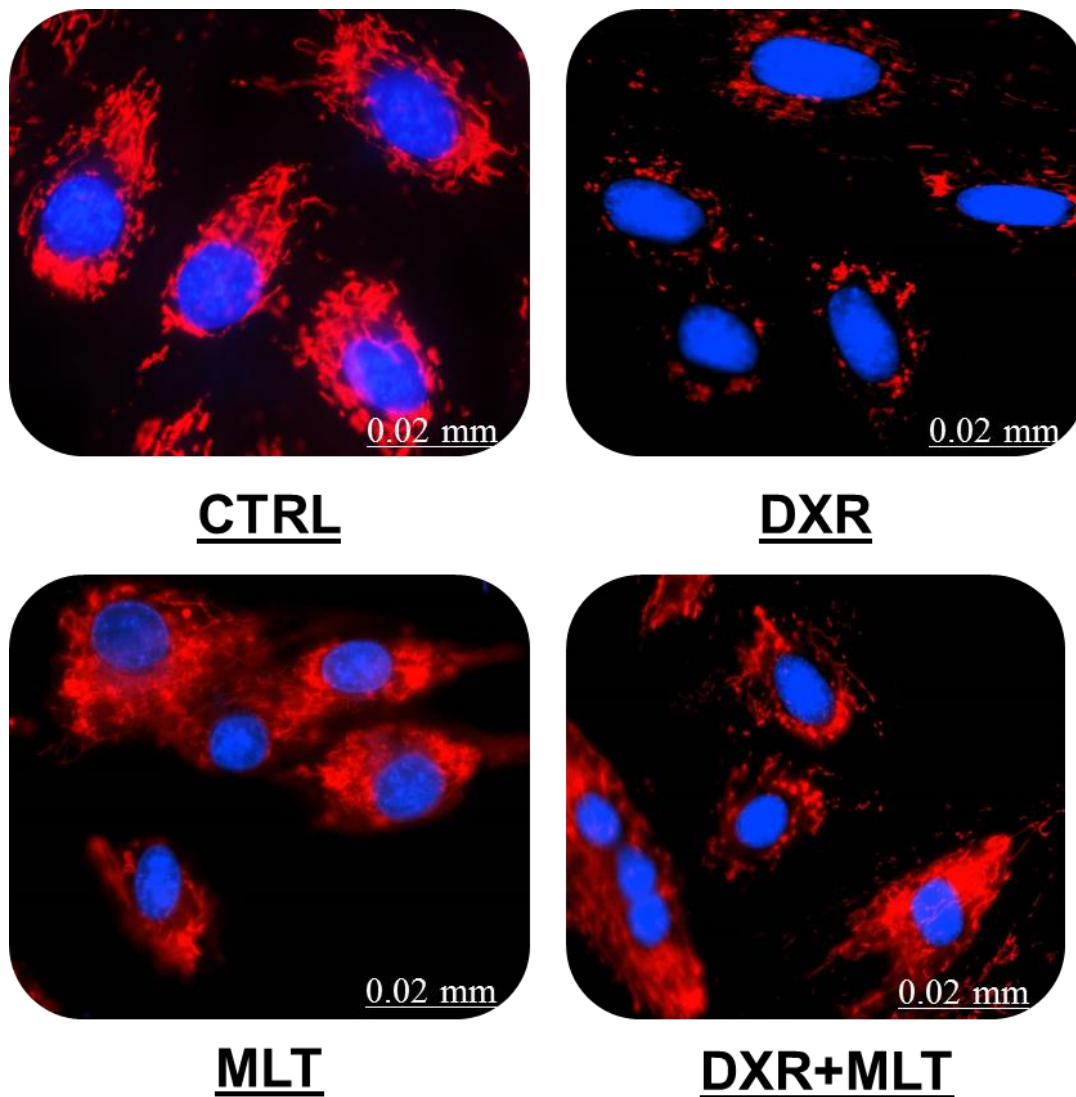


Figure 3.6.1.1: Fluorescence microscopy images of H9c2 cells which were treated and stained with Hoechst (blue) and TMRE (red) to visualize the cell nucleus and mitochondrial network, respectively. Abbreviations- **CTRL**: control; **DXR**: doxorubicin; **MLT**: melatonin.

Cells treated with DXR for 24 hours significantly decreased the mitochondrial major/minor aspect ratio in comparison to the CTRL (1.162 ± 0.1279 vs 3.834 ± 0.2689 , $p < 0.001$) (Figure 3.6.1.2 A). However, pre-treatment with MLT significantly increased the major/minor aspect ratio of mitochondria when compared to the DXR group (3.174 ± 0.5138 vs 1.162 ± 0.1279 , $p < 0.05$) (Figure 3.6.1.2 A). Similarly, treatment with DXR significantly decreased the degree of mitochondrial branching in comparison to the CTRL (1.867 ± 0.4055 vs 4.190 ± 0.3934 , $p < 0.05$) (Figures 3.6.1.1 and 3.6.1.2 B). Pre-treatment with MLT significantly increased the degree of branching in comparison to the DXR group (4.317 ± 0.5800 vs 1.867 ± 0.4055 , $p < 0.05$) (Figure 3.6.1.2 B).

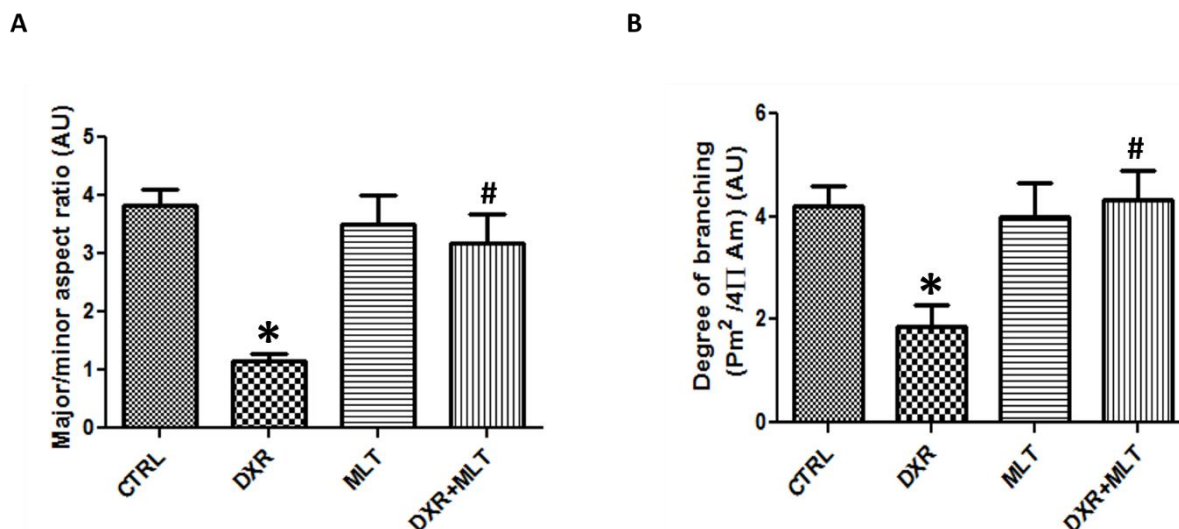


Figure 3.6.1.2: The effect of MLT on the mitochondrial network during DXR-induced cardiotoxicity. A morphological and network assessment of the mitochondria was conducted on the processed images. Bar graphs show: **A.** Major/minor aspect ratio and **B.** Degree of branching. Values are presented as means \pm SEM (n=4), **A:** *p < 0.001 vs CTRL, #p < 0.05 vs DXR, **B:** *p < 0.05 vs CTRL, #p < 0.05 vs DXR. Abbreviations- **CTRL:** control; **DXR:** doxorubicin; **MLT:** melatonin; **AU:** arbitrary units.

3.6.2 Immunoblot analysis of mitochondrial fission and fusion proteins

To confirm the results of the mitochondrial network assessment, immunoblot analysis for key mitochondrial fusion proteins (Mfn1, Mfn2 and OPA1) and fission proteins (Drp1 and hFis1) were conducted.

DXR treatment significantly decreased the protein level of Mfn1 in comparison to the CTRL ($54.78 \pm 11.75\%$ vs 100% , $p < 0.001$) (Figure 3.6.2.1 A). Pre-treatment with MLT followed by DXR treatment resulted in a significant increase in Mfn1 protein level ($85.39 \pm 13.15\%$ vs $54.78 \pm 11.75\%$, $p < 0.01$) (Figure 3.6.2.1 A). Similarly, Mfn2 protein level significantly decreased in response to DXR treated cells in comparison to the CTRL ($42.68 \pm 9.992\%$ vs 100% , $p < 0.001$) (Figure 3.6.2.1 B), whereas MLT pre-treatment significant increased the protein level of Mfn2 in comparison to the DXR group ($86.61 \pm 6.278\%$ vs $42.68 \pm 9.992\%$, $p < 0.01$) (Figure 3.6.2.1 B). Interestingly, no significant changes in the Long-form of OPA1 (L-OPA1) expression was observed among the all treatment groups (Figure 3.6.2.2). L-OPA1 was quantified as it the pre-dominant isoform of OPA1.

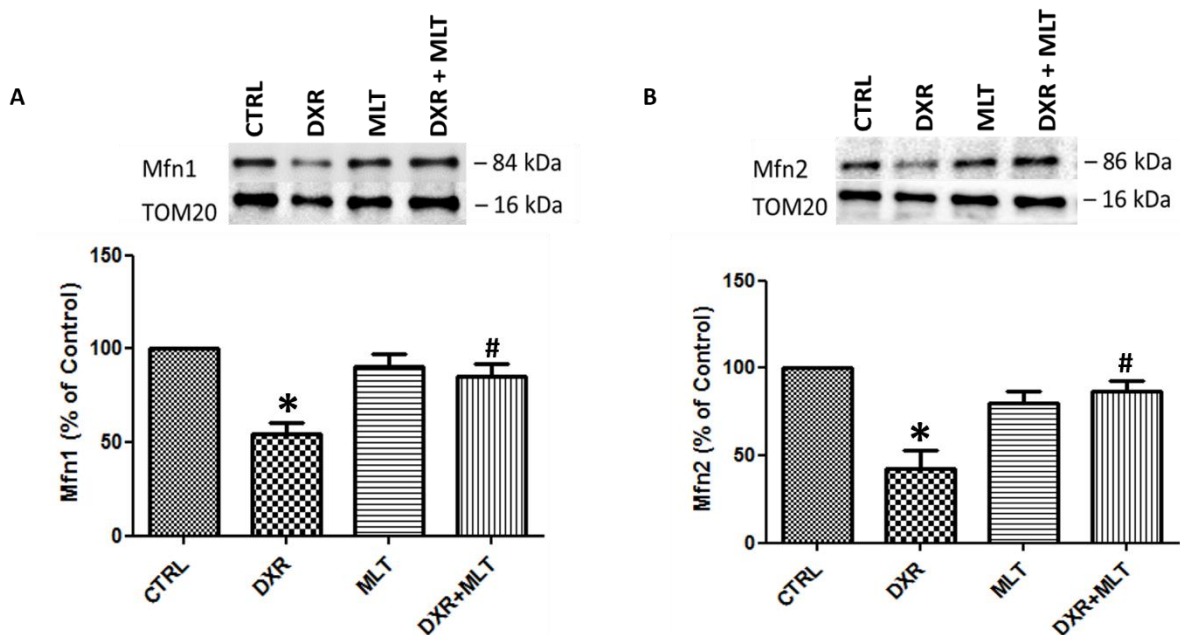


Figure 3.6.2.1: The effect of MLT on mitochondrial fusion proteins Mfn1 and Mfn2 during DXR-induced cardiotoxicity. Cells were treated with 10 μ M MLT for 24 hours followed by incubation with 3 μ M DXR for 24 hours. Mitochondria were isolated from treated cells and fusion protein levels were assessed using immunoblot analysis. Bar graphs show: **A.** Mfn1 and **B.** Mfn2 protein levels (normalized to TOM20 vs control). Values are expressed as a percentage of the control and presented as means \pm SEM (n=4), **A:** * p < 0.001 vs CTRL, # p < 0.01 vs DXR. **B:** * p < 0.001 vs CTRL, # p < 0.01 vs DXR. Abbreviations- **CTRL:** control; **DXR:** doxorubicin; **MLT:** melatonin.

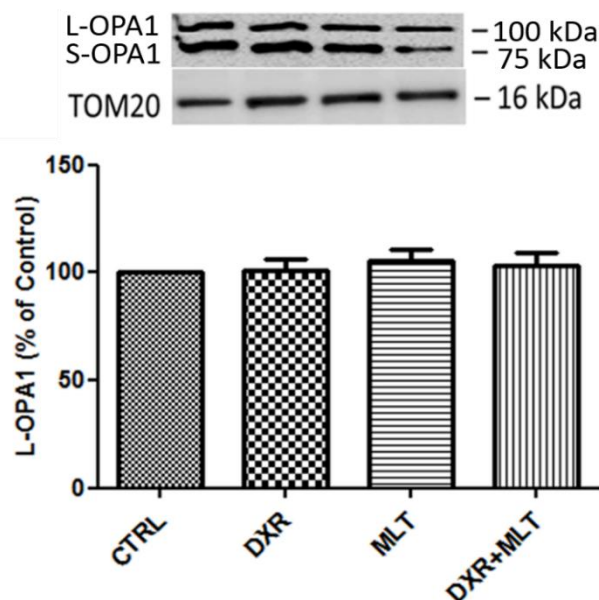


Figure 3.6.2.2: The effect of MLT on mitochondrial fusion protein OPA1 during DXR-induced cardiotoxicity. Cells were treated with MLT at 10 μ M for 24 hours followed by incubation with DXR at 3 μ M for 24 hours. Mitochondria were isolated from treated cells and fusion protein levels of OPA1 was assessed using immunoblot analysis. Bar graph illustrates L-OPA1 protein levels (normalized to TOM20 vs control). Values are expressed as a percentage of the control and presented as means \pm SEM (n=4), no significant changes occurred. Abbreviations- **CTRL:** control; **DXR:** doxorubicin; **MLT:** melatonin.

Mitochondrial fission protein Drp1 levels significantly increased in response to DXR treatment in comparison to the CTRL group ($330.7 \pm 26.45\%$ vs 100% , $p < 0.001$) (Figure 3.6.2.3 A). No significant changes in Drp1 protein levels occurred with the MLT treated group in comparison to the CTRL. However, Drp1 protein levels significantly decreased when cells were pre-treated with MLT in comparison to the DXR treated group ($87.13 \pm 20.45\%$ vs $330.7 \pm 26.45\%$, $p < 0.001$) (Figure 3.6.2.3 A).

A similar trend was observed with hFis1 protein expression levels. hFis1 protein levels significantly increased in the DXR treated group in comparison to the CTRL ($438.1 \pm 17.31\%$ vs 100% , $p < 0.001$) and a significant decrease in hFis1 protein levels occurred when cells were pre-treated with MLT ($306.9 \pm 32.79\%$ vs $438.1 \pm 17.31\%$, $p < 0.001$) (Figure 3.6.2.3 B).

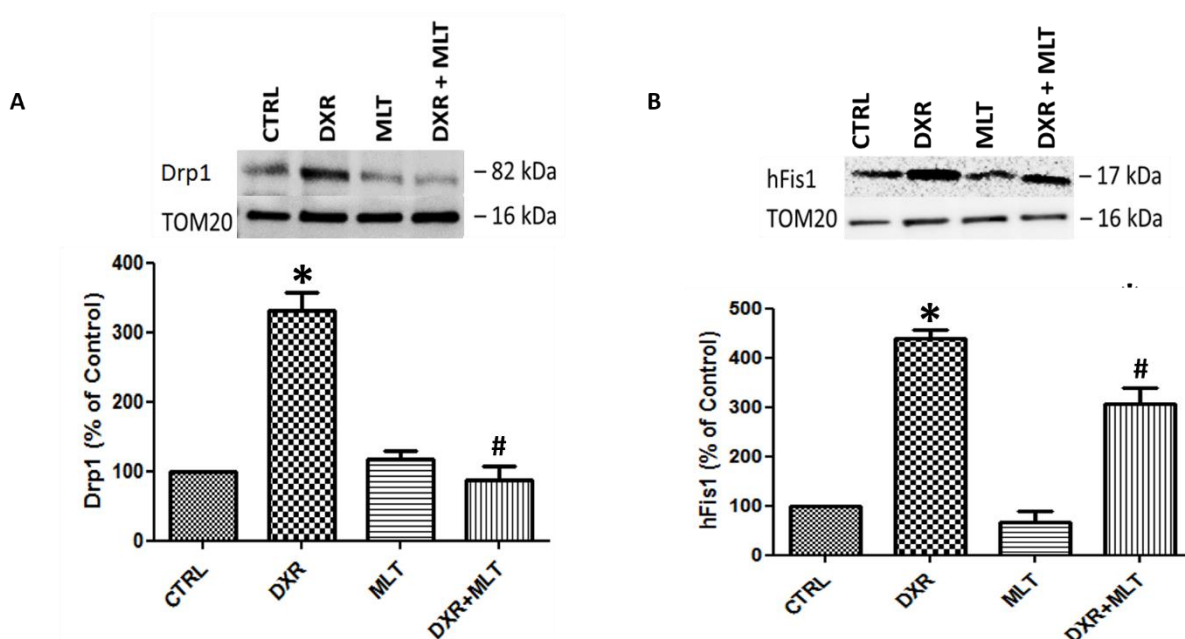


Figure 3.6.2.3: The effect of MLT on mitochondrial fission proteins Drp1 and hFis1 during DXR-induced cardiotoxicity. Cells were treated with $10 \mu\text{M}$ MLT for 24 hours followed by incubation with $3 \mu\text{M}$ DXR for 24 hours. Mitochondria were isolated from treated cells and fission protein levels were assessed using immunoblot analysis. Bar graphs show: **A.** Drp1 and **B.** hFis1 protein levels (normalized to TOM20 vs control). Values are expressed as a percentage of the control and presented as means \pm SEM ($n=4$), **A:** * $p < 0.001$ vs CTRL, # $p < 0.001$ vs DXR. **B:** * $p < 0.001$ vs CTRL, # $p < 0.01$ vs DXR. Abbreviations- **CTRL:** control; **DXR:** doxorubicin; **MLT:** melatonin.

3.7 The effect of MLT on mitochondrial bioenergetics and biogenesis during DXR-induced cardiotoxicity

3.7.1 Mitochondrial respiration

Mitochondrial respiration was assessed using the Seahorse XFe 96 Extracellular Flux Analyzer. H9c2 cells were treated as previously described and the oxygen consumption rate (OCR) was measured in real time at the end of treatments. The basal respiration rate (BRR), ATP-linked respiration, electron transport system capacity (ETS) and Mitochondrial Spare Respiratory Capacity (MSRC) (see section 2.1.9.2) were measured.

There were no significant changes in the basal oxygen consumption rate among the treated groups. Interestingly, no significant changes in ATP-linked respiration occurred as well. However, MLT pre-treatment significantly increased the ETS capacity in comparison to DXR treated group ($125.6 \pm 3.784\%$ vs $99.06 \pm 5.825\%$, $p < 0.01$) (Figure 3.7.1.1 C). A similar trend was observed as MLT pre-treatment significantly increased MSRC in comparison to DXR treated group ($155.2 \pm 5.879\%$ vs $105.1 \pm 13.02\%$, $p < 0.05$) (Figure 3.7.1.1 D).

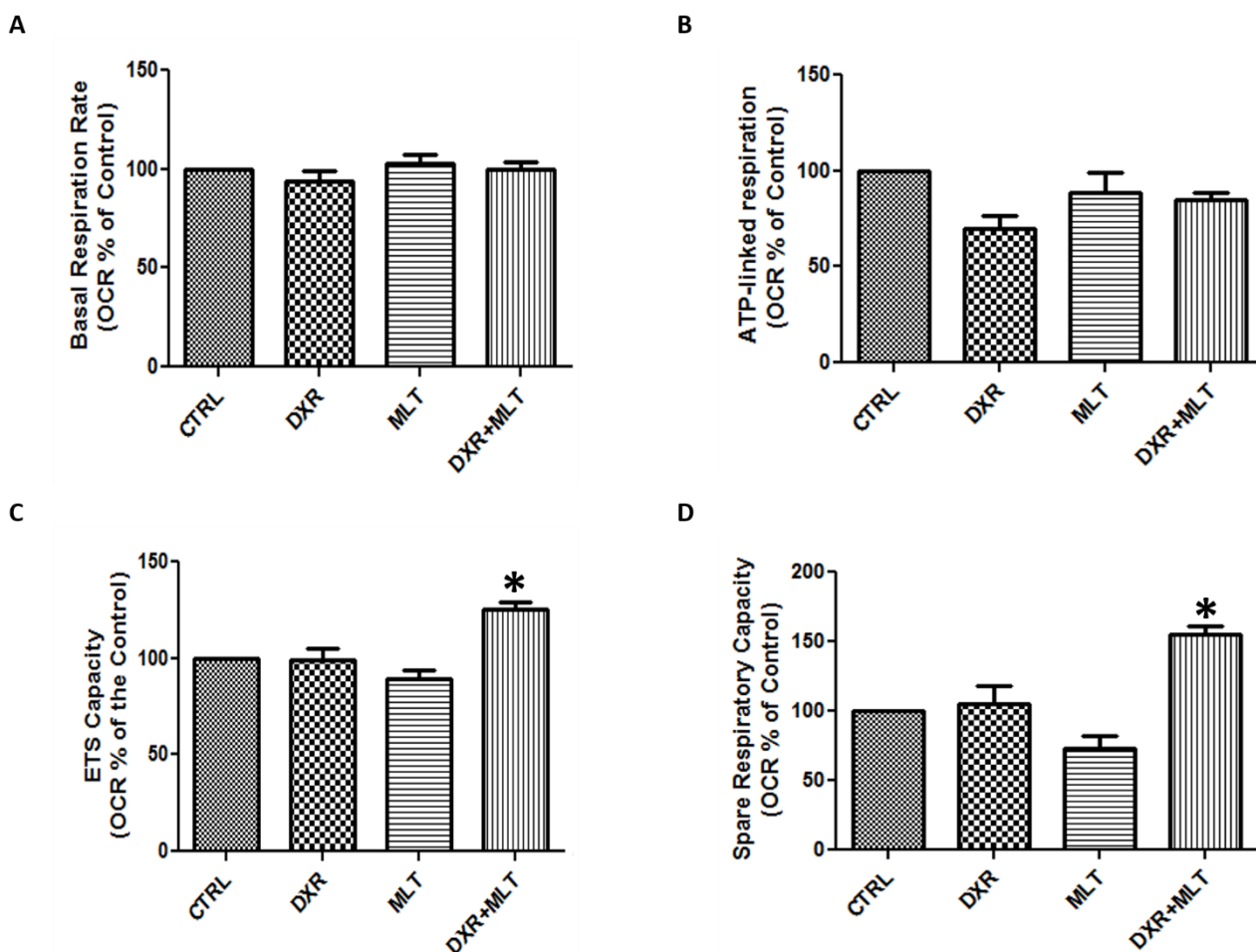


Figure 3.7.1.1: The effect of MLT on mitochondrial respiration during DXR-induced cardiotoxicity. Cells were treated with 10 μ M MLT for 24 hours followed by incubation with 3 μ M DXR for 24 hours. Oxygen consumption rate was measured using the Seahorse XFe 96 Extracellular Flux Analyzer. Bar graphs show: **A.** Basal Respiration Rate, **B.** ATP-linked respiration, **C.** Electron transport system capacity and **D.** Mitochondrial Spare Respiratory Capacity. Values are expressed as a percentage of the control and presented as means \pm SEM (n=12 replicates/group), **C:** *p < 0.01 vs DXR, **D:** *p < 0.05 vs DXR. Abbreviations- **CTRL:** control; **DXR:** doxorubicin; **MLT:** melatonin.

3.7.2 ATP Analysis

In addition to measuring mitochondrial respiration an ATP assay was used to quantify cellular ATP content after cells were treated. The ATP concentration significantly decreased in response to DXR treatment in comparison to the CTRL (42.91 ± 5.049 nM/ μ g of protein vs 67.75 ± 4.392 nM/ μ g of protein, $p < 0.05$) (Figure 3.7.2.1). Pre-treatment with MLT significantly increased ATP concentration in comparison to the DXR treated group (75.91 ± 6.355 nM/ μ g of protein vs 42.91 ± 5.049 nM/ μ g of protein, $p < 0.01$) (Figure 3.7.2.1).

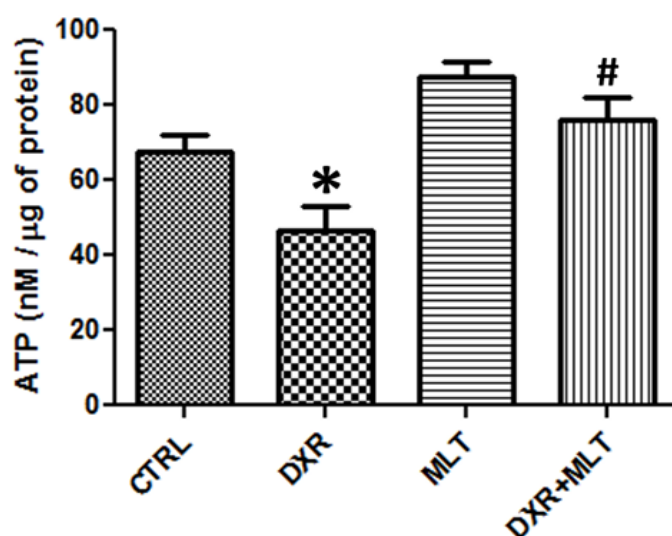


Figure 3.7.2.1: The effect of MLT on cellular ATP levels during DXR-induced cardiotoxicity. Cells were treated with MLT at $10 \mu\text{M}$ for 24 hours followed by incubation with DXR at $3 \mu\text{M}$ for 24 hours. Cellular ATP levels were quantified using an ATP assay. Values are normalized to the amount of protein present in each sample and presented as means \pm SEM ($n=4$), * $p < 0.05$ vs CTRL, # $p < 0.01$ vs DXR. Abbreviations- **CTRL**: control; **DXR**: doxorubicin; **MLT**: melatonin.

3.7.3 Immunoblot analysis of Peroxisome proliferator-activated receptor gamma coactivator 1-alpha (PGC-1 α)

Immunoblot analysis was conducted to measure the protein expression levels of PGC-1 α , a key regulator of mitochondrial biogenesis. DXR treatment significantly decreased PGC-1 α protein levels in comparison to the CTRL ($11.41 \pm 4.167\%$ vs 100% , $p < 0.001$) (Figure 3.7.3.1). No significant changes in PGC-1 α protein levels occurred with the MLT treated group in comparison to the CTRL.

However, MLT pre-treatment significantly increased PGC-1 α protein levels in comparison to the DXR treated group (90.67 ± 12.23 % vs 11.41 ± 4.167 %, $p < 0.001$) (Figure 3.7.3.1).

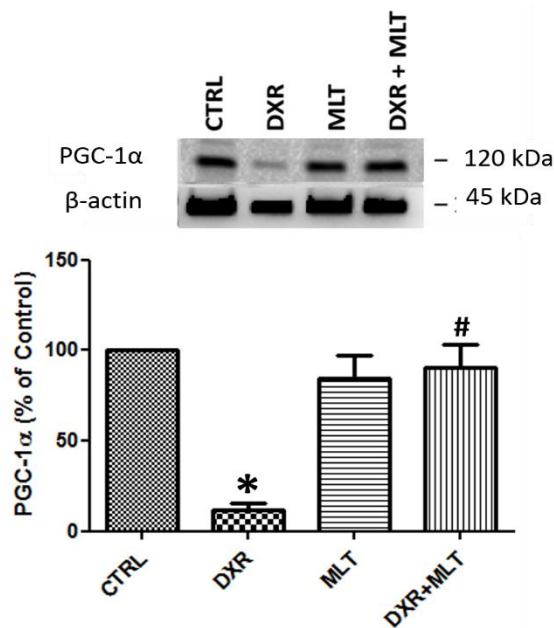


Figure 3.7.3.1: The effect of MLT on PGC-1 α during DXR-induced cardiotoxicity. Cells were treated with 10 μ M MLT for 24 hours followed by incubation with 3 μ M DXR for 24 hours. Protein levels of PGC-1 α was assessed using immunoblot analysis. Bar graph illustrates PGC-1 α protein levels (normalized to β -actin vs control). Values are expressed as a percentage of the control and presented as means \pm SEM (n=4), * $p < 0.001$ vs CTRL, # $p < 0.001$ vs DXR. Abbreviations- **CTRL**: control; **DXR**: doxorubicin; **MLT**: melatonin.

3.8 The effect of MLT on sirtuin activity during DXR-induced cardiotoxicity

3.8.1 Immunoblot analysis of SIRT1 and SIRT3

Immunoblot analysis was conducted to measure the protein levels of SIRT1 and SIRT3. DXR treatment significantly decreased SIRT1 protein levels in comparison to the CTRL (44.5 ± 4.505 % vs 100%, $p < 0.001$) and a significant decrease also occurred with MLT treatment in comparison to the CTRL (42.03 ± 6.847 % vs 100%, $p < 0.001$) (Figure 3.8.1.1 A). Interestingly, pre-treatment with MLT increased SIRT1 protein levels in comparison to the DXR treated group (87.84 ± 6.373 % vs 44.5 ± 4.505 %, $p < 0.001$) (Figure 3.8.1.1 A).

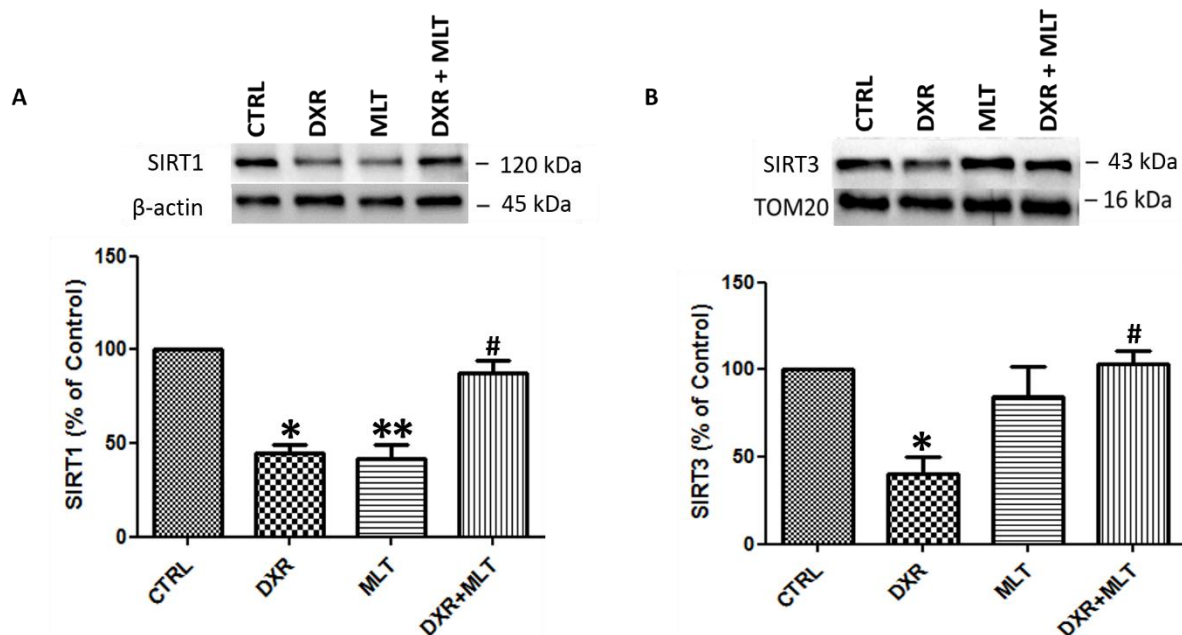


Figure 3.8.1.1: The effect of MLT on sirtuin activity during DXR-induced cardiotoxicity. Cells were treated with 10 μ M MLT for 24 hours followed by incubation with 3 μ M DXR for 24 hours. Sirtuin activity was assessed using immunoblot analysis. Bar graphs show: **A.** SIRT1 and **B.** SIRT3 protein levels (normalized to β -actin or TOM20 vs control). Values are expressed as a percentage of the control and presented as means \pm SEM (n=4), **A:** *p < 0.001 vs CTRL, **p < 0.001 vs CTRL, #p < 0.001 vs DXR. **B:** *p < 0.05 vs CTRL, #p < 0.05 vs DXR. Abbreviations- **CTRL:** control; **DXR:** doxorubicin; **MLT:** melatonin.

Furthermore, SIRT3 protein levels significantly decreased in response to DXR treatment in comparison to the CTRL ($40.24 \pm 9.404\%$ vs 100% , $p < 0.05$) (Figure 3.8.1.1 B). However, MLT pre-treatment significantly increased SIRT3 protein levels in comparison to the DXR group ($103.0 \pm 7.605\%$ vs $40.24 \pm 9.404\%$, $p < 0.05$) (Figure 3.8.1.1 B).

3.9 *In vivo* Study

3.9.1 The effect of daily MLT administration on rat body weight during DXR- induced cardiotoxicity

Female Sprague Dawley rats aged between 16-18 weeks were divided into six groups and treated as previously described (section 2.2 study design). A significant decrease in body weight was observed in DXR-treated rats in comparison to the V CTRL on day 10 (228.23 ± 6.75 g vs 263.43 ± 1.25 g, $p < 0.01$). By day 14, the body weight of DXR-treated rats were significantly reduced in comparison to: T CTRL (222.22 ± 6.47 g vs 277.61 ± 7.90 g, $p < 0.0001$), the V CTRL (222.22 ± 6.47 g vs 266.66 ± 7.68 g, $p < 0.01$), MLT-treated rats (222.22 ± 6.47 g vs 271.15 ± 8.98 g, $p < 0.0001$), and DXR+MLT-treated rats (222.22 ± 6.47 g vs 284.07 ± 6.53 g, $p < 0.0001$).

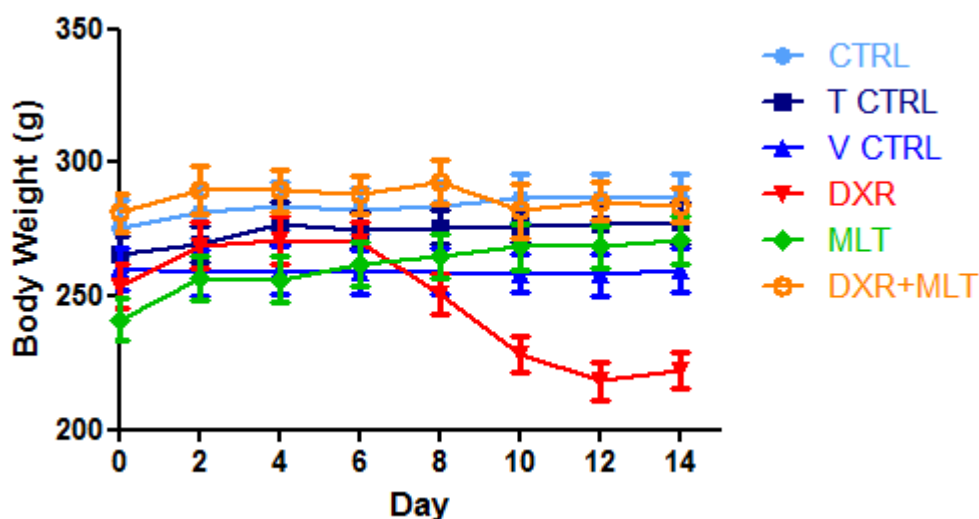


Figure 3.9.1: The effect of daily MLT administration on rat body weight during DXR-induced cardiotoxicity. Rats were either treated with MLT (6 mg/kg) or DXR (4 mg/kg) or both MLT and DXR. The animal weights were recorded daily. CTRL (n=8); T CTRL (n=10); V CTRL (n=8); DXR (n=10); MLT (n=10); DXR+MLT (n=10). Abbreviations- **CTRL**: control; **T CTRL**: tumor control; **V CTRL**: vehicle control; **DXR**: doxorubicin; **MLT**: melatonin.

3.9.2 The effect of daily MLT administration on tumor growth during DXR-induced cardiotoxicity

Animals were inoculated with LA7 rat tumor cells and treated as previously described (section 2.2.3). Tumors were palpable 3 days post-inoculation. Tumor volumes based on digital caliper measurements were calculated using the formula: $V=(ab^2)/2$. Tumor volumes were significantly reduced in DXR+MLT-treated rats on day 8 in comparison to the DXR-treated rats ($1668.10 \pm 9.34 \text{ mm}^3$ vs $7332.74 \pm 2038.04 \text{ mm}^3$, $p < 0.05$). By day 10, tumors were significantly reduced in DXR-treated rats in comparison to the V CTRL ($3661.98 \pm 1421.97 \text{ mm}^3$ vs $14386.11 \pm 3220.527 \text{ mm}^3$, $p < 0.01$), in MLT-treated rats in comparison to the T CTRL ($1427.35 \pm 774.89 \text{ mm}^3$ vs $10506.66 \pm 1306.77 \text{ mm}^3$, $p < 0.001$) and in DXR+MLT-treated rats in comparison to the T CTRL ($150.27 \pm 150.27 \text{ mm}^3$ vs $10506.66 \pm 1306.77 \text{ mm}^3$, $p < 0.0001$).

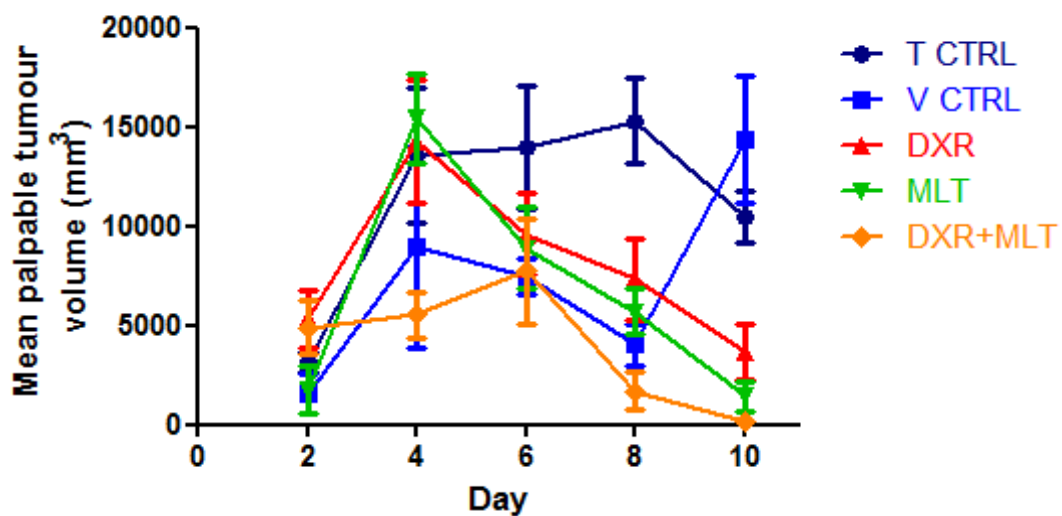


Figure 3.9.2: The effect of daily MLT administration on rat tumor volume during DXR-induced cardiotoxicity. Rats were either treated with MLT (6 mg/kg) or DXR (4 mg/kg) or both MLT and DXR. Tumors were measured daily and tumor volumes calculated ($V=ab^2/2$). CTRL (n=8); T CTRL (n=10); V CTRL (n=8); DXR (n=10); MLT (n=10); DXR+MLT (n=10). Abbreviations- **CTRL**: control; **T CTRL**: tumor control; **V CTRL**: vehicle control; **DXR**: doxorubicin; **MLT**: melatonin.

3.9.3 The effect of daily MLT administration on rat heart weight during DXR-induced cardiotoxicity

Upon termination of the experimental protocol, rats were anaesthetized and rat heart weights were recorded. Rat heart weights significantly decreased in DXR-treated rats in comparison to the V CTRL group (1.117 ± 0.02802 g vs 0.9635 ± 0.02807 g, $p < 0.001$). However, the heart weights of rats treated with DXR+MLT significantly increased in comparison to the DXR-treated rats (1.161 ± 0.03454 g vs 0.9635 ± 0.02807 g, $p < 0.001$) (Figure 3.9.3).

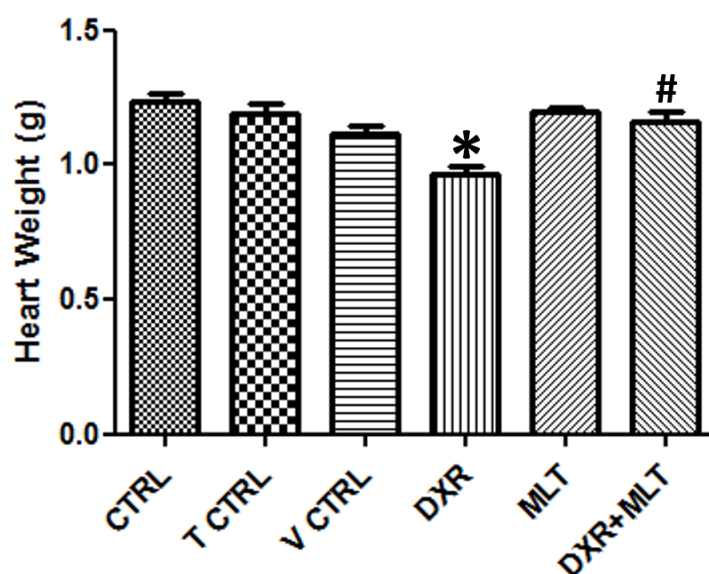


Figure 3.9.3: The effect of daily MLT administration on rat heart weight during DXR-induced cardiotoxicity. Rats were either treated with MLT (6 mg/kg) or DXR (4 mg/kg) or both MLT and DXR. The heart weights were recorded at the end of the study. Values are expressed as a percentage of the control and presented as means \pm SEM (n=minimum of 8), A: * $p < 0.01$ vs V CTRL, # $p < 0.001$ vs DXR. Abbreviations- CTRL: control; T CTRL: tumor control; V CTRL: vehicle control; DXR: doxorubicin; MLT: melatonin.

3.9.4 The effect of daily MLT administration on cardiac function during DXR-induced cardiotoxicity

Upon termination of the experimental protocol, rats were anaesthetized and hearts were rapidly excised to conduct isolated rat heart perfusions. The following parameters were assessed: cardiac output (ml/min), total work performance (mWatts), heart rate (beats/min), stroke volume (ml/beat) (section 2.2.6.2).

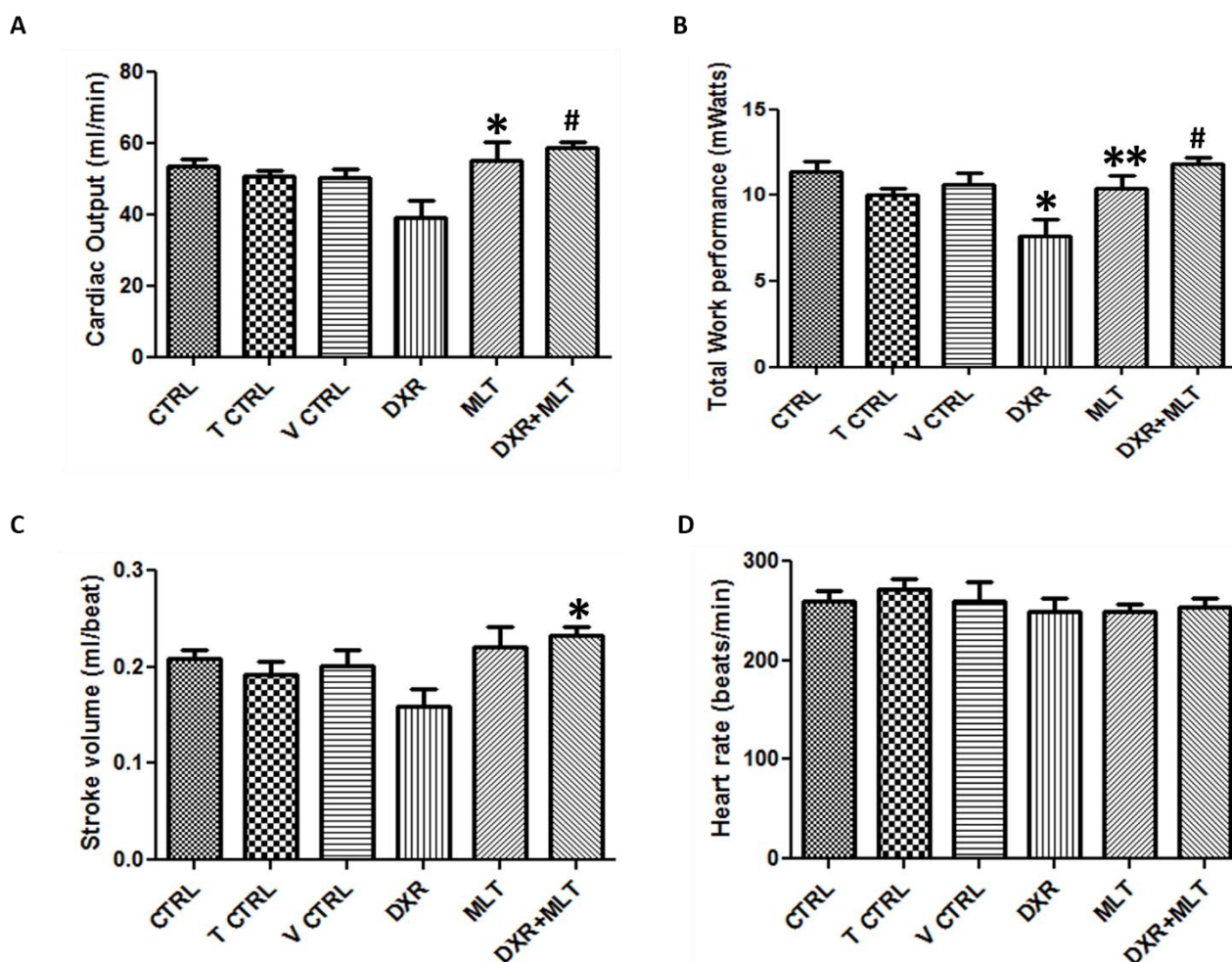


Figure 3.9.4: The effect of daily MLT administration on cardiac function during DXR-induced cardiotoxicity. Rats were either treated with MLT (6 mg/kg) or DXR (4 mg/kg) or both MLT and DXR. Isolated rat heart perfusions were conducted to assess cardiac function. Bar graphs indicate: **A.** Cardiac output, **B.** Total work performance, **C.** Stroke volume and **D.** Heart rate. Values are expressed as means \pm SEM (n =minimum of 8), **A:** * p < 0.05 vs DXR, # p < 0.01 vs DXR. **B:** * p < 0.01 vs CTRL, ** p < 0.05 vs DXR, # p < 0.001 vs DXR. **C:** * p < 0.05 vs DXR. **D:** no significant changes. Abbreviations- **CTRL:** control; **T CTRL:** tumor control; **V CTRL:** vehicle control; **DXR:** doxorubicin; **MLT:** melatonin.

The cardiac output significantly increased in MLT-treated rats in comparison to the DXR-treated rats (55.15 ± 5.202 ml/min vs 39.25 ± 4.586 ml/min, $p < 0.05$). Cardiac output was significantly increased in DXR+MLT-treated rats in comparison to the DXR-treated rats (58.75 ± 1.633 ml/min vs 39.25 ± 4.586 ml/min, $p < 0.01$) (Figure 3.9.4 A).

A similar trend was observed when the total work performance was assessed. The total work performance of isolated rat hearts significantly decreased in DXR-treated rats in comparison to the CTRL (11.40 ± 0.5789 mWatts vs 7.661 ± 0.9279 mWatts, $p < 0.01$). The total work performance of isolated rat hearts significantly increased in MLT-treated rats in comparison to the DXR-treated rats (10.40 ± 0.7339 mWatts vs 7.661 ± 0.9279 mWatts, $p < 0.05$). The total work performance significantly increased in DXR+MLT-treated rats in comparison to the DXR-treated rats (11.86 ± 0.3423 mWatts vs 7.661 ± 0.9279 mWatts, $p < 0.001$) (Figure 3.9.4 B).

Furthermore, the stroke volume of rats treated with DXR+MLT significantly increased in comparison to DXR-treated rats (10.40 ± 0.7339 mWatts vs 7.661 ± 0.9279 mWatts, $p < 0.05$) (Figure 3.9.4 C). However, no significant differences in heart rate occurred among the treated groups (Figure 3.9.4 D).

3.9.5 The effect of daily MLT administration on apoptosis during DXR-induced cardiotoxicity

3.9.5.1 Immunoblot assessment of cleaved caspase-3 and cleaved PARP protein levels

To provide further insight into programmed cell death, heart tissue from the various treated groups were analyzed using cleaved caspase-3 and cleaved-PARP as markers for apoptotic cell death. The presence of these markers in the treated groups were quantified using immunoblot analysis. Cleaved caspase-3 protein levels in the hearts of DXR-treated rats were significantly increased in comparison

to the V CTRL ($383.1 \pm 56.86\%$ vs $149 \pm 23.60\%$, $p < 0.01$). Cleaved caspase-3 significantly decreased in MLT-treated rats in comparison to DXR-treated rats ($146.3 \pm 36.36\%$ vs $383.1 \pm 56.86\%$, $p < 0.01$). Furthermore, a significant decrease in cleaved caspase-3 protein levels occurred in DXR+MLT-treated rats in comparison to the DXR-treated group ($152.8 \pm 9.264\%$ vs $383.1 \pm 56.86\%$, $p < 0.01$) (Figure 3.9.5.1 A).

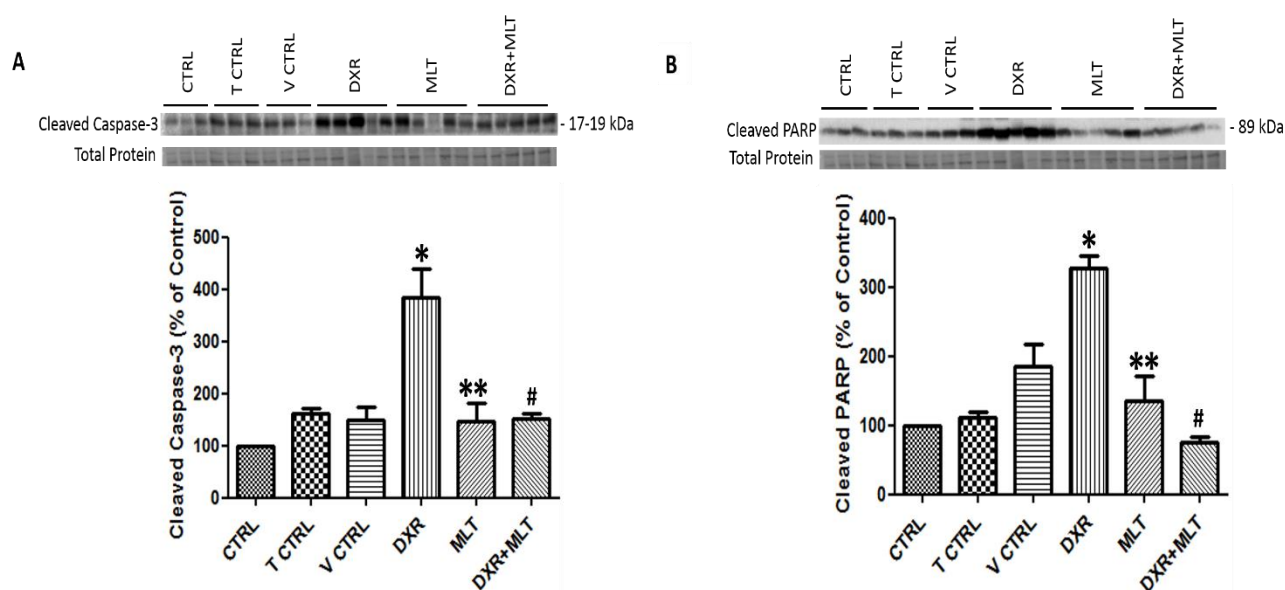


Figure 3.9.5.1: The effect of daily MLT administration on cleaved caspase-3 and PARP cleavage during DXR-induced cell death. Rats were either treated with MLT (6 mg/kg) or DXR (4 mg/kg) or both MLT and DXR. Apoptotic cell death was assessed in rat hearts using immunoblot analysis. Bar graphs show: **A.** Cleaved caspase-3 and **B.** Cleaved-PARP protein levels (normalized to total protein vs control). Values are expressed as a percentage of the control and presented as means \pm SEM (n =minimum of 3), **A:** * $p < 0.01$ vs V CTRL, ** $p < 0.01$ vs DXR, # $p < 0.01$ vs DXR. **B:** * $p < 0.01$ vs V CTRL, ** $p < 0.001$ vs DXR, # $p < 0.001$ vs DXR. Abbreviations- **CTRL:** control; **T CTRL:** tumor control; **V CTRL:** vehicle control; **DXR:** doxorubicin; **MLT:** melatonin.

Similarly, PARP cleavage was significantly increased in DXR-treated rats in comparison to the V CTRL ($328.3 \pm 16.25\%$ vs $185.0 \pm 32.32\%$, $p < 0.01$). PARP cleavage in MLT-treated rats significantly decreased in comparison to the DXR-treated rats ($135.2 \pm 36.59\%$ vs $328.3 \pm 16.25\%$, $p < 0.001$). Additionally, a significant decrease in PARP cleavage occurred in DXR+MLT-treated rats in comparison to the DXR-treated group ($75.83 \pm 7.984\%$ vs $328.3 \pm 16.25\%$, $p < 0.001$) (Figure 3.9.5.1 B).

3.9.6 The effect of daily MLT administration on autophagy during DXR-induced cardiotoxicity

3.9.6.1 Immunoblot assessment of autophagy proteins LC3 II and SQSTM1/p62

Heart tissue from the various treated groups were analyzed using LC3 II and SQSTM1/p62 as markers for autophagy. The presence of these markers in the treated groups were quantified using immunoblot analysis. A significant increase in LC3 II protein levels was observed in the heart tissue of DXR-treated rats in comparison to the V CTRL ($151.9 \pm 5.454\%$ vs $100.9 \pm 77.85\%$, $p < 0.05$). LC3 II protein levels were significantly increased in MLT-treated rats in comparison to the T CTRL ($166.9 \pm 7.842\%$ vs $82.73 \pm 6.395\%$, $p < 0.001$). Furthermore, LC3 II protein levels were significantly increased in DXR+MLT-treated rats in comparison to DXR-treated rats ($205.0 \pm 12.15\%$ vs $151.9 \pm 5.454\%$, $p < 0.01$) (Figure 3.9.6.1 A).

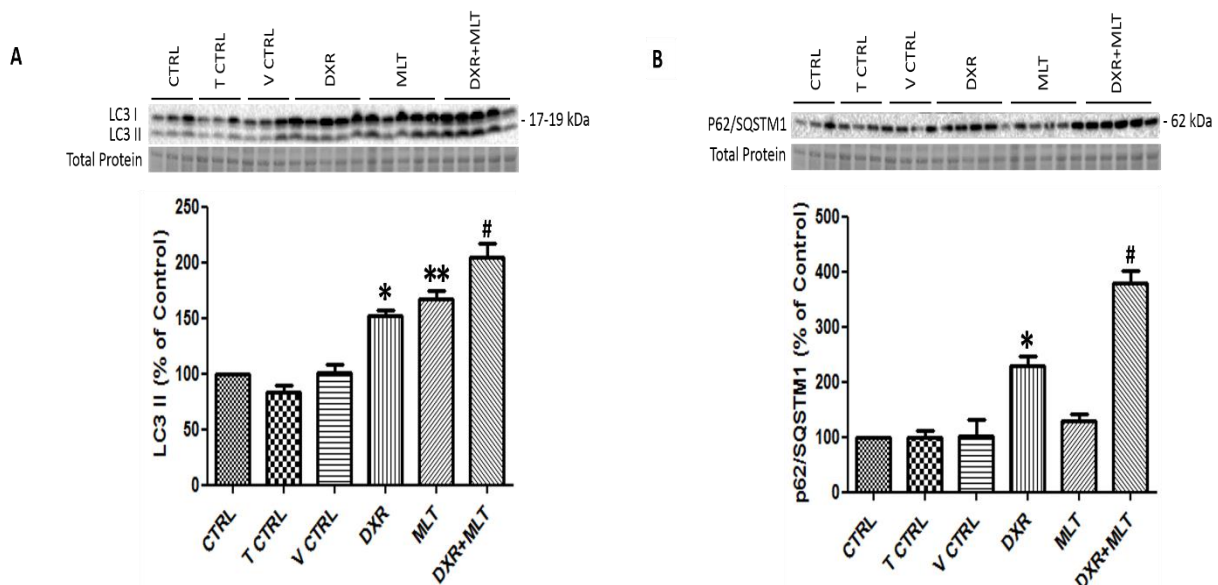


Figure 3.9.6.1: The effect of daily MLT administration on LC3 II and p62/SQSTM1 protein levels during DXR-induced cardiotoxicity. Rats were either treated with MLT (6 mg/kg) or DXR (4 mg/kg) or both MLT and DXR. LC3 II and p62/SQSTM1 protein levels were assessed in rat hearts using immunoblot analysis. Bar graphs show: **A.** LC3 II and **B.** p62/SQSTM1 protein levels (normalized to total protein vs control). Values are expressed as a percentage of the control and presented as means \pm SEM (n =minimum of 3), **A:** * $p < 0.05$ vs V CTRL, ** $p < 0.001$ vs T CTRL, # $p < 0.01$ vs DXR. **B:** * $p < 0.01$ vs V CTRL, # $p < 0.001$ vs DXR. Abbreviations- CTRL: control; T CTRL: tumor control; V CTRL: vehicle control; DXR: doxorubicin; MLT: melatonin.

A significant increase in p62 protein levels was observed in the heart tissue of DXR-treated rats in comparison to the V CTRL ($230.4 \pm 17.39\%$ vs $102.4 \pm 28.74\%$, $p < 0.01$). A significant increase in LC3 II protein levels was also observed in DXR+MLT-treated rats in comparison to the DXR-treated group ($378.5 \pm 23.75\%$ vs $230.4 \pm 17.39\%$, $p < 0.001$) (Figure 3.6.9.1 B).

3.9.6.2 Immunoblot analysis of Pink1 and PARKIN protein levels

Pink1 and PARKIN proteins are associated with mitophagy. Mitochondria were isolated from rat heart tissue to assess the presence of these markers in the treated groups. Pink1 and PARKIN protein levels were quantified using immunoblot analysis. Pink1 protein levels were significantly increased in DXR-treated rats in comparison to the V CTRL ($417.6 \pm 24.12\%$ vs $139.6 \pm 36.79\%$, $p < 0.001$). However, a significant decrease in Pink1 protein levels occurred in DXR+MLT-treated rats in comparison to DXR-treated rats ($103.3 \pm 16.21\%$ vs $417.6 \pm 24.12\%$, $p < 0.001$) (Figure 3.9.6.2 A).

Similarly, PARKIN protein levels significantly increased in DXR-treated rats in comparison to the V CTRL ($237.1 \pm 32.22\%$ vs $116.5 \pm 27.27\%$, $p < 0.05$) (Figure 3.9.6.2 B). However, no significant changes in PARKIN protein levels occurred in DXR+MLT-treated rats in comparison to DXR-treated rats.

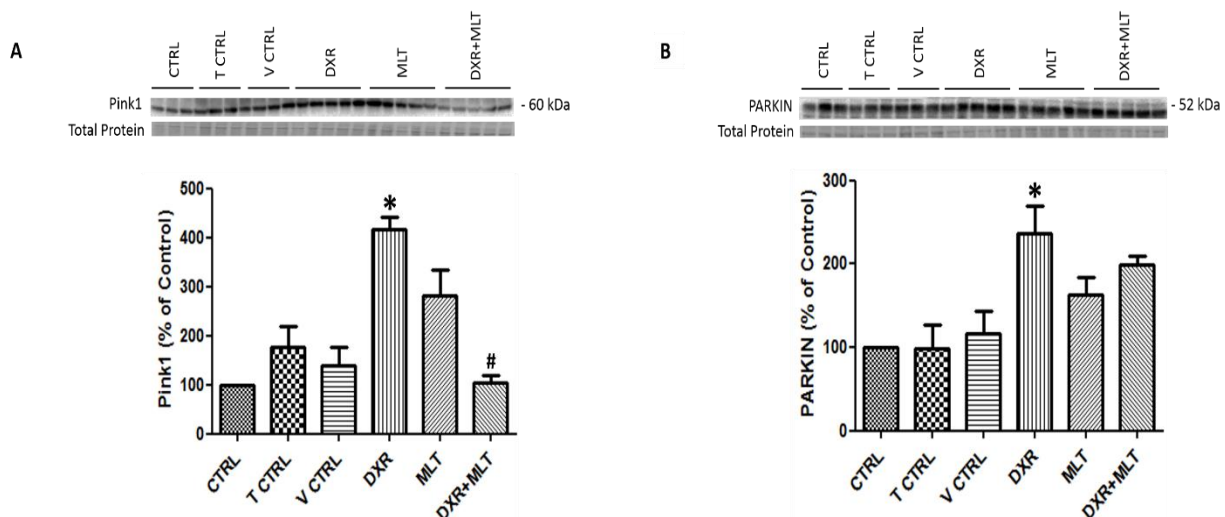


Figure 3.9.6.2: The effect of daily MLT administration on Pink1 and PARKIN protein levels during DXR-induced cardiotoxicity. Rats were either treated with MLT (6 mg/kg) or DXR (4 mg/kg) or both MLT and DXR. Pink1 and PARKIN protein levels were assessed in rat hearts using immunoblot analysis. Bar graphs show: **A.** Pink1 and **B.** PARKIN protein levels (normalized to total protein vs control). Values are expressed as a percentage of the control and presented as means \pm SEM (n =minimum of 3), **A:** * $p < 0.001$ vs V CTRL, # $p < 0.001$ vs DXR. **B:** * $p < 0.05$ vs V CTRL. Abbreviations- **CTRL:** control; **T CTRL:** tumor control; **V CTRL:** vehicle control; **DXR:** doxorubicin; **MLT:** melatonin.

3.9.7 The effect of daily MLT administration on mitochondrial fusion and fission during DXR-induced cardiotoxicity

3.9.7.1 Immunoblot analysis of mitochondrial fusion proteins

Mitochondria were isolated from rat heart tissue and the protein levels of key mitochondrial fusion proteins (Mfn1, Mfn2 and OPA1) were assessed using immunoblot analysis. Mfn1 protein levels were significantly increased in DXR+MLT-treated rats in comparison to DXR-treated rats ($109.8 \pm 12.49\%$ vs $62.48 \pm 7.752\%$, $p < 0.05$) (Figure 3.9.7.1 A).

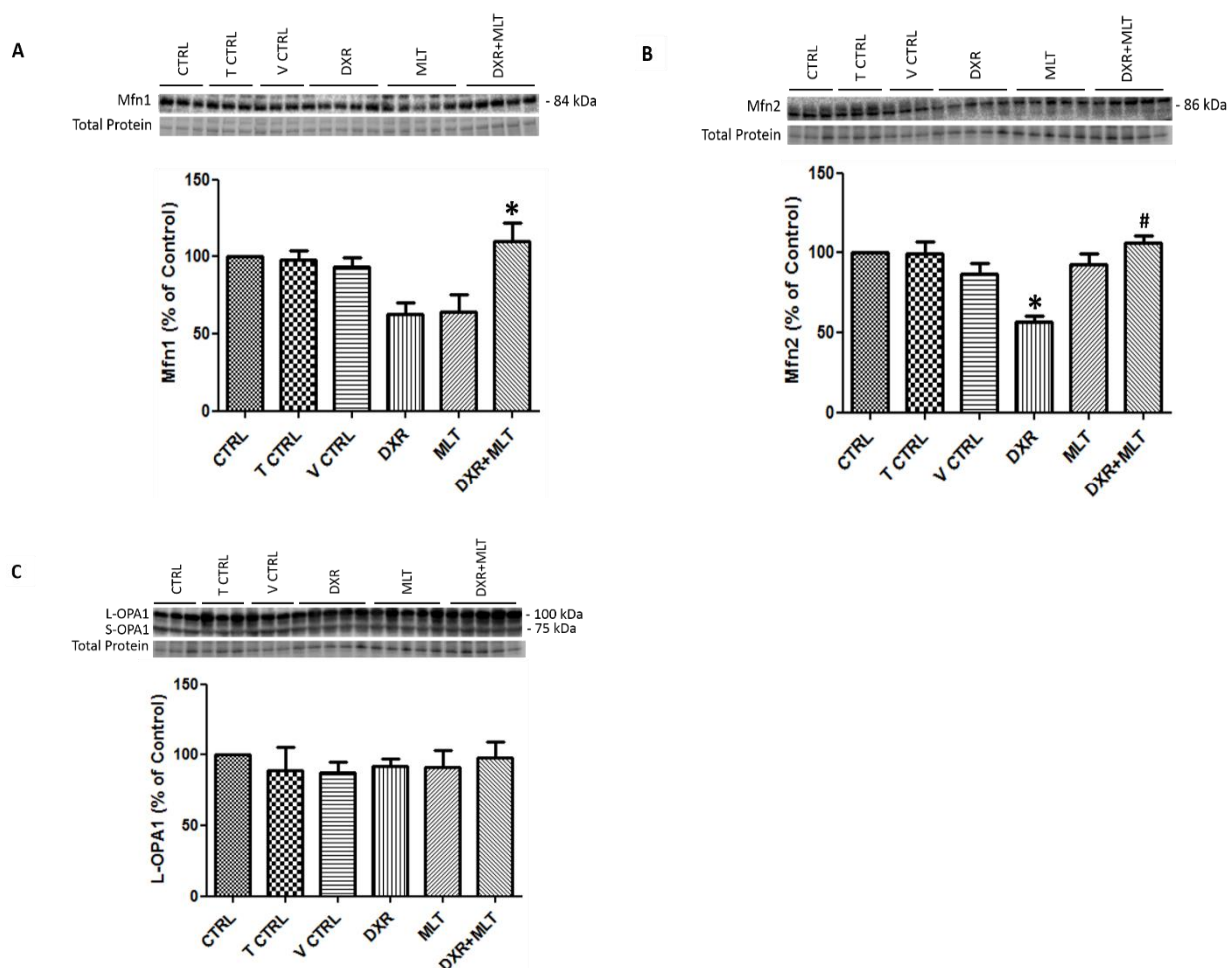


Figure 3.9.7.1: The effect of daily MLT administration on Mfn1, Mfn2 and OPA1 protein levels during DXR-induced cardiotoxicity. Rats were either treated with MLT (6 mg/kg) or DXR (4 mg/kg) or both MLT and DXR. Mfn1, Mfn2 and OPA1 protein levels were assessed in rat hearts using immunoblot analysis. Bar graphs show: **A.** Mfn1, **B.** Mfn2 and **C.** L-OPA1 protein levels (normalized to total protein vs control). Values are expressed as a percentage of the control and presented as means \pm SEM (n =minimum of 3), **A:** * $p < 0.05$ vs DXR. **B:** * $p < 0.05$ vs V CTRL, # $p < 0.001$ vs DXR. **C:** no significant changes. Abbreviations- **CTRL:** control; **T CTRL:** tumor control; **V CTRL:** vehicle control; **DXR:** doxorubicin; **MLT:** melatonin.

Mfn2 protein levels were significantly decreased in DXR-treated rats in comparison to the V CTRL group ($56.92 \pm 3.393\%$ vs $86.71 \pm 12.09\%$, $p < 0.05$). Furthermore, a significant increase in Mfn2 protein levels occurred in DXR+MLT-treated rats in comparison to DXR-treated rats ($106.5 \pm 4.142\%$ vs $56.92 \pm 3.393\%$, $p < 0.001$) (Figure 3.9.7.1 B). However, no significant changes in L-OPA1 levels were observed among the treated groups (Figure 3.9.7.1 C).

3.9.7.2 Immunoblot analysis of mitochondrial fission proteins

Protein levels of mitochondrial fission proteins (Drp1 and hFis1) were assessed using immunoblot analysis. Drp1 protein levels were significantly increased in DXR-treated rats in comparison to the CTRL ($194.5 \pm 15.53\%$ vs 100% , $p < 0.01$). Drp1 protein levels were significantly decreased in DXR+MLT-treated rats in comparison to DXR-treated rats ($74.13 \pm 12.80\%$ vs $194.5 \pm 15.53\%$, $p < 0.001$) (Figure 3.9.7.2 A). A similar trend was observed in hFis1 protein levels as hFis1 protein levels were significantly increased in DXR-treated rats in comparison to the CTRL ($251.7 \pm 29.66\%$ vs 100% , $p < 0.01$). However, hFis1 protein levels were significantly decreased in DXR+MLT-treated rats in comparison to DXR-treated rats ($144.6 \pm 14.52\%$ vs $251.7 \pm 29.66\%$, $p < 0.05$) (Figure 3.9.7.2 B).

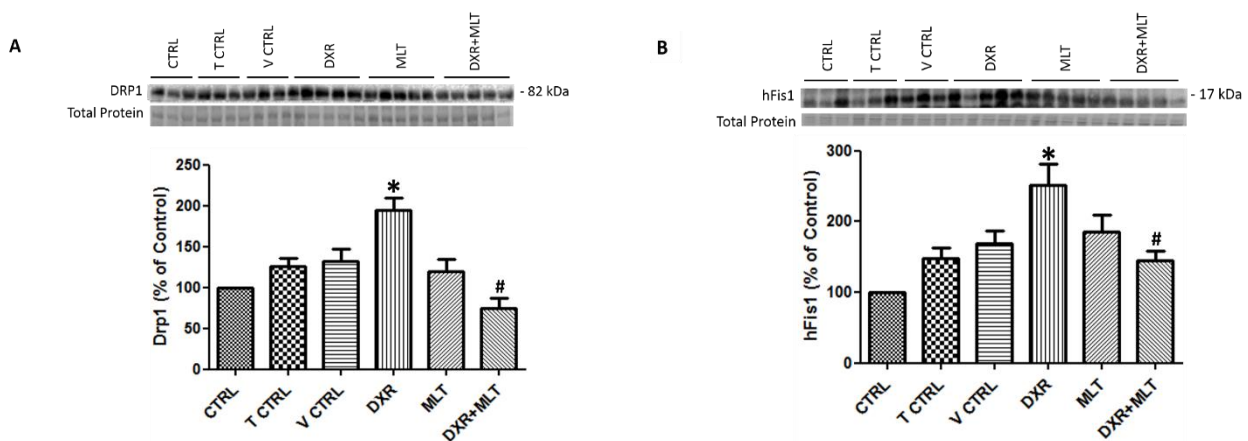


Figure 3.9.7.2: The effect of daily MLT administration on Drp1 and hFis1 protein levels during DXR-induced cardiotoxicity. Rats were either treated with MLT (6 mg/kg) or DXR (4 mg/kg) or both MLT and DXR. Drp1 and hFis1 protein levels were assessed in rat hearts using immunoblot analysis. Bar graphs show: **A:** Drp1 and **B:** hFis1 protein levels (normalized to total protein vs control). Values are expressed as a percentage of the control and presented as means \pm SEM (n =minimum of 3), **A:** * $p < 0.01$ vs CTRL, # $p < 0.001$ vs DXR. **B:** * $p < 0.01$ vs CTRL, # $p < 0.05$ vs DXR. Abbreviations- **CTRL:** control; **T CTRL:** tumor control; **V CTRL:** vehicle control; **DXR:** doxorubicin; **MLT:** melatonin.

3.9.8 The effect of daily MLT administration on mitochondrial biogenesis during DXR-induced cardiotoxicity

3.9.8.1 Immunoblot analysis of PGC-1 α protein levels

PGC-1 α is a known marker of mitochondrial biogenesis. PGC-1 α protein levels in rat heart tissue was quantified using immunoblot analysis. PGC-1 α protein levels significantly decreased in DXR-treated rats in comparison to the CTRL ($41.02 \pm 7.219\%$ vs 100% , $p < 0.01$). PGC-1 α protein levels significantly increased in MLT-treated rats in comparison to DXR-treated rats ($106.3 \pm 14.16\%$ vs $41.02 \pm 7.219\%$, $p < 0.001$). Furthermore, PGC-1 α protein levels were significantly increased in DXR+MLT-treated rats in comparison to DXR-treated rats ($135.9 \pm 4.917\%$ vs $41.02 \pm 7.219\%$, $p < 0.001$) (Figure 3.9.8.1).

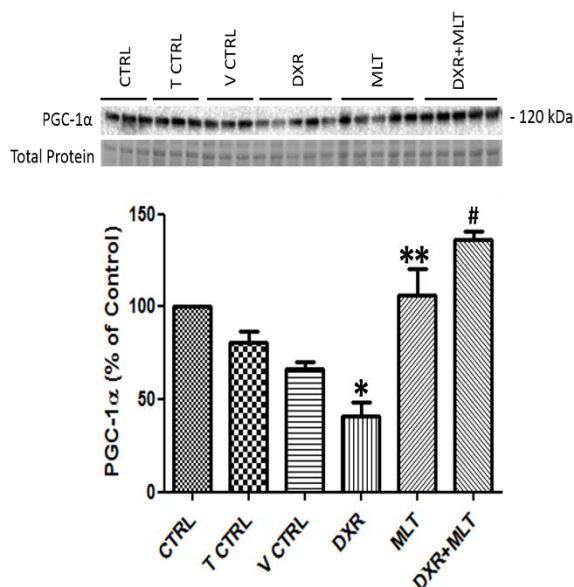


Figure 3.9.8.1: The effect of daily MLT administration on PGC-1 α protein levels during DXR-induced cardiotoxicity. Rats were either treated with MLT (6 mg/kg) or DXR (4 mg/kg) or both MLT and DXR. PGC-1 α protein levels were assessed in rat hearts using immunoblot analysis. Bar graph indicates: PGC-1 α protein levels (normalized to total protein vs control). Values are expressed as a percentage of the control and presented as means \pm SEM (n =minimum of 3), * $p < 0.01$ vs CTRL, ** $p < 0.001$ vs DXR, # $p < 0.001$ vs DXR. Abbreviations- **CTRL**: control; **T CTRL**: tumor control; **V CTRL**: vehicle control; **DXR**: doxorubicin; **MLT**: melatonin.

3.9.9 The effect of daily MLT administration on sirtuin activity during DXR-induced cardiotoxicity

3.9.9.1 Immunoblot analysis of SIRT1 and SIRT3 protein levels

SIRT1 and SIRT3 protein levels in rat heart tissue were quantified using immunoblot analysis. Mitochondria was isolated from rat heart tissue to assess SIRT3 and cell lysates were used to assess SIRT1. SIRT1 protein levels were significantly decreased in DXR-treated rats in comparison to the CTRL ($50.97 \pm 9.920\%$ vs 100% , $p < 0.05$). Interestingly, SIRT1 protein levels were significantly increased in DXR+MLT-treated rats in comparison to DXR-treated rats ($104.1 \pm 10.65\%$ vs $50.97 \pm 9.920\%$, $p < 0.01$) (Figure 3.9.9.1 A). However, no significant changes in SIRT3 levels occurred among the treated groups (Figure 3.9.9.1 B)

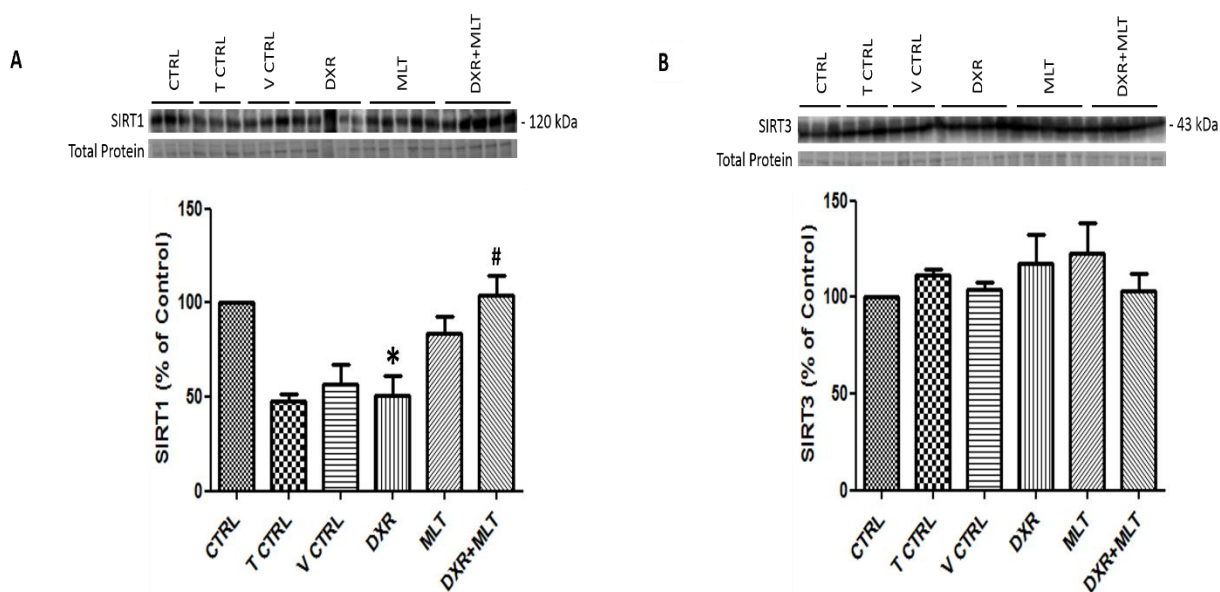


Figure 3.9.9.1: The effect of daily MLT administration on SIRT1 and SIRT3 protein levels during DXR-induced cardiotoxicity. Rats were either treated with MLT (6 mg/kg) or DXR (4 mg/kg) or both MLT and DXR. SIRT1 and SIRT3 protein levels were assessed in rat hearts using immunoblot analysis. Bar graphs show: **A.** SIRT1 and **B.** SIRT3 protein levels (normalized to total protein vs control). Values are expressed as a percentage of the control and presented as means \pm SEM (n =minimum of 3), **A:** * $p < 0.05$ vs CTRL, # $p < 0.01$ vs DXR. **B:** No significant changes. Abbreviations- **CTRL:** control; **T CTRL:** tumor control; **V CTRL:** vehicle control; **DXR:** doxorubicin; **MLT:** melatonin.

Chapter 4

Discussion

4.1 Introduction

Although studies have been conducted on the protective role of melatonin (MLT) in DXR-induced cardiotoxicity, these studies largely lack information regarding the effect of MLT on mitochondrial function during DXR-induced cardiotoxicity. Moreover, there are few studies which use a tumor-bearing model of DXR-induced cardiotoxicity. The aim of the current study was to determine the effect of melatonin on cell death, autophagy/mitophagy, mitochondrial fission and fusion, mitochondrial bioenergetics and biogenesis, sirtuin activity, cardiac function and tumor growth during DXR-induced cardiotoxicity. We hypothesized that pre-treatment with MLT will better preserve mitochondrial function during DXR-induced cardiotoxicity, thereby improving cardiomyocyte survival. Furthermore, we hypothesized that daily MLT administration would improve cardiac function whilst simultaneously exerting its oncostatic properties in our tumor-bearing rat model of DXR-induced cardiotoxicity.

4.2 The effect of MLT on cell viability during DXR-induced cardiotoxicity

It has been well established that DXR-induced cardiotoxicity terminates in the rapid loss of cardiomyocytes via various cell death pathways. In the current study, a concentration of 3 μM of DXR decreased cell viability in H9c2 cells and DXR at a 5 μM concentration equally decreased cell viability (Figure 3.1.1). Since the MTT reductive capacity is dependent on active mitochondrial reductase enzymes (dehydrogenases), the assay not only provides information on cell viability but also on mitochondrial viability in H9c2 cells. Previous work in our group demonstrated a significant decrease in cell viability in H9c2 cells treated with 3 μM of DXR for 24 hours (Sishi *et al.*, 2013). In a clinical setting DXR is administered intravenously over a brief period of time at a dose of 60 - 75 mg/m^2 with plasma concentrations peaking at a range between 5 and 15 μM . Since \pm 75% of DXR is bound by plasma proteins, the peak concentration of free DXR available to induce its apoptotic

effects is between 1.25 and 3.75 μM (Liu, 2008). Since, 3 μM of DXR is within the clinically accepted range of 0.1 - 5 μM *in vitro* (Liu, 2008), this specific concentration was utilized in our study.

There are only a few studies where the effect of MLT on H9c2 cells were investigated. In the current study, a concentration of 10 μM of MLT maintained cell viability to approximately control levels (Figure 3.1.2); therefore this concentration was used in further experiments. It has been demonstrated in clinical trials that plasma levels of MLT vary with age but are relatively maintained at < 10 pg/ml of plasma (Benloucif *et al.*, 2008; Zeitzer *et al.*, 2007). Although, a supra-physiological concentration of MLT was used in this study, there is no evidence supporting the toxicity of MLT at high doses (Venegas *et al.*, 2012; Kasekar *et al.*, 2014). Furthermore, the use of MLT at high doses has been shown to be essential in reaching adequate subcellular concentrations to exert its pharmacological effects (Venegas *et al.*, 2012).

No significant differences in viability were observed in cells treated with MLT either for a period of one hour or for 24 hours (Figure 3.1.3). Since, the plasma half-life of MLT is 20 to 50 minutes (Kasekar *et al.*, 2014), it was expected that pre-treatment with MLT at a concentration of 10 μM for 1 hour followed by DXR treatment would be sufficient to increase cell viability, however, a decrease in cell viability was observed (Figure 3.1.3). On the other hand, considering that H9c2 cells pre-treated with MLT for 24 hours increased cell viability following DXR treatment at 3 μM for 24 hours (Figure 3.1.3), it is possible that a longer exposure time to MLT was required to increase the cells' antioxidant capacity. In support of this notion, Mias and co-workers (2008), previously demonstrated that pre-incubation with MLT for 24 hours increased antioxidant catalase enzymes in a time-dependent manner, with maximum levels of antioxidant catalase enzymes reached at 16 and 24 hours.

To further confirm our findings, pre-treatment with MLT significantly increased the percentage of live cells whereas DXR alone decreased the percentage of live cells (Figure 3.2.1). Therefore, based on these findings, MLT pre-treatment for 24 hours was chosen for subsequent experiments as we aimed to establish a time frame at which H9c2 cells will be offered maximal protection against DXR-induced cardiotoxicity.

4.3 The effect of MLT on apoptosis during DXR-induced cardiotoxicity

Caspases are cysteine aspartate proteins which tightly regulate cell turnover, differentiation and apoptosis (Thornberry, 1998; Elmore, 2007). Caspase-3 is a key downstream effector caspase and the cleavage of caspase-3 initiates apoptotic cell death (Elmore, 2007). Apoptosis is a common feature in the progression of DXR-induced cardiotoxicity. In the current study, the mechanism of cardiomyocyte apoptosis involved during the development of DXR-induced cardiotoxicity, was investigated. In our *in vitro* model of DXR-induced cardiotoxicity, cells pre-treated with MLT significantly reduced caspase3/7 activity (Figure 3.2.2). These results were further validated by immunoblot analysis of cleaved caspase-3 which revealed a significant increase in caspase-3 cleavage following DXR treatment. However, pre-treatment with MLT appeared to protect the cells against the high degree of apoptotic activity induced by DXR as observed by the decrease in caspase-3 cleavage (Figure 3.2.3 A).

Similarly, in our *in vivo* model of DXR-induced cardiotoxicity, cleaved caspase-3 levels were highly expressed in the heart tissue of DXR-treated rats. In contrast, in DXR+MLT-treated rats the expression of caspase-3 cleavage in rat heart tissue was significantly reduced (Figure 3.9.5.1 A). Previous work done in our group supports these findings, as caspase-3 cleavage increased in H9c2 cells treated with DXR at 3 μ M for 24 hours as well as in the hearts of mice which were treated with 10 mg/kg of DXR (Sishi *et al.*, 2013).

Moreover, our results are in accordance with other studies which demonstrated that caspase-3 activation increases during the heart failure stages of DXR-induced cardiotoxicity (Lou *et al.*, 2005; Liu *et al.*, 2008; Shen *et al.*, 2016). Furthermore, MLT has been shown to significantly attenuate DXR-induced apoptosis in a murine model of DXR-induced cardiotoxicity without compromising the antineoplastic activity of DXR (Liu *et al.*, 2002). MLT has also been shown to confer protection during myocardial ischemia/reperfusion injury by downregulating caspase-3 and cleaved caspase-3 expression (Şehirli *et al.*, 2013; Yu *et al.*, 2014).

A major mechanism by which DXR elicits its antitumor activity is via inducing double-stranded DNA breaks. Poly (ADP-ribose) polymerase (PARP) is a nuclear enzyme which is activated in response

to DNA strand breakage. PARP cleavage is initiated by active caspases 3 and 7 during apoptosis and has thus become a useful indicator of apoptotic activity (Gobeil *et al.*, 2001). In both *in vitro* and *in vivo* models in the current study, PARP-cleavage significantly increased in response to DXR treatment (Figure 3.2.3 B and Figure 3.9.5.1 B). These results are in agreement with others studies which demonstrated that DXR also induces apoptosis via PARP-cleavage (Liu *et al.*, 2008; Sishi *et al.*, 2013). However, in our models of DXR-induced cardiotoxicity, pretreatment with MLT attenuated this effect by significantly decreased PARP-cleavage (Figure 3.2.3 B and Figure 3.9.5.1 B). In support of this finding, a recent study conducted by Chua *et al.* (2016) demonstrated that MLT and extendin-4 treatment decreased PARP cleavage in response to DXR treatment in H9c2 cells as well as in a rat model of cardio-renal syndrome.

Taken together, the results in the current study clearly demonstrate that MLT pre-treatment confers cardiac protection by decreasing the expression of apoptotic cell death makers and increasing cell viability during DXR-induced cardiotoxicity. As cell death is central to the clinical limitation of DXR, the underlying mechanisms involved in the anti-apoptotic effects of MLT are worth investigating, as MLT could potentially serve as a cardioprotective agent in the context of DXR-induced cardiotoxicity.

4.4 The effect of MLT on autophagy during DXR-induced cardiotoxicity

Autophagy is characterized by the development of autophagosomes that engulf bulk cytoplasm, damaged organelles and other redundant cellular components before fusing with the lysosome, which results in mass proteolysis (Mizushima *et al.*, 2008). Autophagy at basal levels in the heart is essential for maintaining cardiac contractility and function (Loos *et al.*, 2011). This degradative process may also serve as a double-edged sword in the heart under conditions of stress: on the one hand, it serves as a significant renewal and pro-survival mechanism of cellular organelles and, on the other hand, if autophagy persists beyond a certain threshold, it may lead to cellular demise (de Meyer and Martinet, 2009; Gustaffson and Gottlieb, 2009).

In our *in vitro* study, the effect of MLT on autophagic flux in conjunction with p62 levels were assessed during DXR-induced cardiotoxicity by the addition of bafilomycin A1 (autophagic inhibitor) to the various treatment groups. Autophagic flux is defined as a measure of autophagic degradation

activity (Loos *et al.*, 2014). An increase in autophagic flux was observed in response to both DXR and MLT treatments as indicated by increases in LC3 II levels (Figure 3.3.1 A). In accordance with the increase in autophagic flux induced by DXR in our model, it was demonstrated in a rat model of chronic DXR cardiotoxicity, that increased autophagy contributed to a loss of cardiac myocytes and inhibition of autophagy with 3-methyladenine (3-MA), improved cardiac function, suggesting that autophagy is detrimental in the case of chronic DXR-induced cardiotoxicity (Lu *et al.*, 2009). Interestingly, DXR+MLT treated cells responded with no change in LC3 II levels, which is indicative of an impairment in the autophagic machinery as the autophagosomes are not fusing with lysosomes. It is possible that MLT could possibly be suppressing the increase in autophagic flux induced by DXR. In support of this notion, in a model of liver ischemia/reperfusion (I/R) injury, autophagic flux was increased in response to I/R injury, but this was attenuated by MLT via inhibiting mTOR-dependent autophagy (Kang *et al.*, 2014).

Furthermore, the accumulation of autophagosomes observed in the DXR+MLT treated group does not specifically indicate autophagic cell death. In healthy cells, autophagosomes may also accumulate as a result of hindered processing of autophagosomes and this accumulation does not necessarily have to correspond with an increase in autophagic flux (Codogno and Meijer, 2005). In contrast to the unchanged LC3 II levels in DXR+MLT treated cells, p62 levels was significantly decreased in DXR+MLT treated cells (Figure 3.3.1 B), indicating that autophagosomal degradation is likely occurring in our model. These conflicting results may be attributed to the fact that autophagy is a dynamic process in which LC3 II and p62 levels are constantly changing in a time-dependent manner (Sahani *et al.*, 2014).

In our *in vivo* model, LC3 II and p62 levels in rat heart tissue were assessed but no conclusions on autophagic flux can be deduced from these results as fusion between autophagosomes and lysosomes was not inhibited in our *in vivo* model. The results demonstrated a significant increase in LC3 II levels in rat heart tissue of DXR, MLT and DXR+MLT-treated rats (Figure 3.9.6.1 A). In contrast to the decreased p62 levels in response to DXR+MLT treatment in our *in vitro* model, p62 levels remained highly expressed in rat heart tissue of DXR+MLT-treated rats (Figure 3.9.6.1 B). Since p62 levels decreased in MLT-treated rats but significantly increased in DXR-treated rats, these

results may suggest that DXR is inhibiting autophagic degradation in our *in vivo* model of DXR-induced cardiotoxicity.

To fully elucidate the effect of MLT on autophagy during DXR-induced cardiotoxicity, the autophagic system should be assessed by characterizing each step of the autophagic process as a particular rate in order to accurately assess autophagosomal pool size and autophagic flux as described by Loos *et al.* (2014). Furthermore, cardiac autophagic flux *in vivo* can also be measured using chloroquine as described by Iwai-Kanai *et al.* (2008).

4.5 The effect of MLT on Pink1 and PARKIN during DXR-induced cardiotoxicity

Mitochondrial dysfunction is an apparent hallmark of DXR-induced cardiotoxicity. The selective elimination of damaged or malfunctioning mitochondria by autophagy is referred to as mitophagy which is an essential process for maintaining cellular homeostasis and mitochondrial quality control (Barthe *et al.*, 2010). Pink1 and PARKIN are two critical proteins involved in the execution of mitophagy. Pink1 binds to damaged mitochondria and recruits PARKIN from the cytosol to initiate ubiquitination and mitophagic elimination (Chen and Dorn, 2013). Therefore, in the current study we investigated the effect of MLT pre-treatment on Pink1 and PARKIN protein levels during DXR-induced cardiotoxicity as a potential indication for mitophagic events.

Pink1 protein levels increased in response to both DXR and DXR+MLT treated cells (Figure 3.3.2 A) suggesting that mitochondrial damage is occurring in both treatment groups. In contrast, Pink1 protein levels significantly decreased in the heart tissue of DXR+MLT-treated rats but remained elevated in the heart tissue of DXR-treated rats (Figure 3.9.6.2 A) indicating that there is a higher degree of cardiac mitochondrial damage occurring in DXR-treated rats. Furthermore, PARKIN protein levels significantly increased in response to DXR+MLT treated cells, however PARKIN levels were severely diminished in DXR treated cells (Figure 3.3.2 B), suggesting that although DXR induces autophagy, it may simultaneously be impairing mitochondrial clearance by preventing the recruitment of PARKIN to damaged mitochondria. It has previously been demonstrated that DXR exposure can disrupt the clearance of damaged mitochondria by upregulation of p53 which inhibits the translocation of PARKIN to the mitochondrial outer membrane (Hoshino *et al.*, 2012).

Pre-treatment with MLT appears to restore the function of PARKIN protein (Figure 3.3.2 B). To support this finding, a recent study by Díaz-Casado *et al.* (2016), revealed that MLT restored the normal function and expression of Pink1 and PARKIN in a model of Parkinson-like disease. In contrast, PARKIN protein levels significantly increased in the heart tissue of DXR-treated rats (Figure 3.9.6.2 B) suggesting that damaged mitochondria could possibly be eliminated by autophagy.

The analysis of Pink1 and PARKIN protein levels is, however, insufficient to fully elucidate the effect of MLT pre-treatment on mitophagy during DXR-induced cardiotoxicity in the current study. These results need to be further supported with flow cytometry or microscopy using mitochondrial dyes that allow the assessment of mitochondrial cargo in autophagosomal vesicles (Rodriguez-Enriquez *et al.*, 2002). Furthermore, it would be important to verify that changes in mitochondrial mass are as a result of autophagic activity and not decreased mitochondrial biogenesis. To ensure this, a critical autophagic regulator such as Beclin-1 should be knocked-down (Barthe *et al.*, 2010).

4.6 The effect of MLT on mitochondrial ROS production during DXR-induced cardiotoxicity

Mitochondria are abundant in cardiac tissue, constituting about 45% of the myocardial volume (Marin-Garcia *et al.*, 2001) in comparison with other tissues. The abundance of mitochondria in the heart is mainly attributed to the high energy demand of the heart. DXR targets mitochondria and accumulates in these organelles at concentrations 100-fold higher than in plasma (Tokarska – Schlattner *et al.*, 2007). One major and widely investigated hypothesis of DXR-induced cardiotoxicity is based on the generation of free radicals, which induces oxidative stress (Olson *et al.*, 1981). DXR is known to induce free radical formation in two major ways: (i) through utilizing cellular oxidoreductases (NADH and NADH dehydrogenase of complex I, NADPH and cytochrome P-450 reductases or endothelial nitric oxide synthase); and (ii) by forming complexes with iron in plasma (Tokarska –Schlattner *et al.*, 2006; Doroshov *et al.*, 1980; Minotti *et al.*, 1999). Furthermore, DXR is known to be involved in a 'redox-cycling' process, thereby inducing a vicious cycle of free radical production (Davies and Doroshov, 1986; Zhu *et al.*, 2016). During mitochondrial respiration, free radicals are formed and therefore the heart, in particular, is highly susceptible to DXR-induced oxidative damage as it is abundant in mitochondria, which are both sources and targets for ROS

(Doroshov, 1983; Octavia *et al.*, 2012). To further exacerbate the free radical production induced by DXR, the heart has a limited antioxidant defense systems when compared to other tissues (Doroshov *et al.*, 1980; Quiles *et al.*, 2002).

MLT's potent free-radical scavenging properties have been well documented. MLT appears to be superior to conventional anti-oxidants as its metabolites, namely, AFMK and AMK, have also been reported to possess free radical scavenging properties, creating a free radical scavenging cascade (Tan *et al.*, 2001; Galano *et al.*, 2013). MLT in turn acts to increase the organism's antioxidant defense system as both physiological and pharmacological doses of MLT have resulted in increased gene expression and activities of various cellular antioxidants (GPx, GRd, SOD and CAT) (Antolin *et al.*, 1996; Reiter *et al.*, 2000; Fischer *et al.*, 2013). Furthermore, the most unique property of MLT, which is absent in most antioxidants, is that it does not undergo redox cycling (Tan *et al.*, 2000). Most antioxidants tend to become pro-oxidants when encountered with free radicals, further promoting oxidation and free radical production. Since MLT is an electron-rich molecule, it interacts with free radicals and forms stable end products which are excreted in the urine (Tan *et al.*, 2000). Hence, MLT is considered to be a terminal or suicidal antioxidant distinguishing it from conventional antioxidants (Tan *et al.*, 2000).

Therefore, in the current study the effect of MLT on free radical production induced by DXR was investigated *in vitro*. It was demonstrated in our results that DXR treated H9c2 cells did not significantly increase ROS generation in comparison to the CTRL (Figure 3.4.1 A). This result could possibly be due to the fact that DXR increases the mean intensity of H₂DCFDA in a concentration-dependent manner during DXR-induced cardiotoxicity (Chang *et al.*, 2011). However, pre-treatment with MLT significantly attenuated ROS generation in comparison to the DXR treated cells (Figure 3.4.1 A).

Furthermore, apart from increasing hydroxyl radicals and hydrogen peroxide, DXR is also known to increase reactive nitrogen species (RNS) (Lai *et al.*, 2011). However, RNS is not well detected by H₂DCFDA (Kalyanaraman *et al.*, 2012). The use of H₂DCFDA as a fluorescent probe to measure hydrogen peroxide and other oxidants is debatable since H₂DCFDA does not directly react with

hydrogen peroxide to form the fluorescent product, DCF (Kalyanaraman *et al.*, 2012). Therefore, DCF fluorescence should rather be used as a redox indicator probe (for review see Kalyanaraman *et al.*, 2012). In contrast, MitoSox Red is a more suitable indicator of intracellular oxidants (Kalyanaraman *et al.*, 2012). Mitochondrial ROS generation significantly increased in response to DXR treatment in comparison to the CTRL, whereas pre-treatment with MLT for 24 hours significantly decreased mitochondrial ROS generation in comparison to DXR treated cells (Figure 3.4.1 B). These results suggest that pre-treatment with MLT induced a shift of mitochondria away from the oxidative state induced by DXR. The reduction in oxidative stress induced by MLT is likely attributed to its potent free radical scavenging properties. These results are in accordance with other studies which demonstrated that MLT reduces oxidative stress during DXR-induced cardiotoxicity (Dziegiel *et al.*, 2002; Balli *et al.*, 2004; Eser *et al.*, 2006).

4.7 The effect of MLT on mitochondrial membrane potential during DXR-induced cardiotoxicity

MLT has been reported to protect the mitochondria by preventing cardiolipin oxidation, which would otherwise promote mitochondrial transition pore opening (mPTP), resulting in cell death (Paradies *et al.*, 2010). Furthermore, MLT's preferential juxtaposition to the lipid molecules in membrane lipid layers protects biological membranes against lipid peroxidation (Reiter *et al.*, 2014). In the current study, MLT treatment alone significantly increased mitochondrial membrane potential in comparison to the CTRL (Figure 3.5.1). Considering that cardiac cells have a high energy demand, the high mitochondrial membrane potential observed is required for ATP production (Klingenberg and Rottenberg, 1977) and could have resulted from MLT scavenging free radicals, which are produced during basal mitochondrial respiration. Furthermore, pre-treatment with MLT restored mitochondrial membrane potential reduced by DXR (Figure 3.5.1). This result is consistent with earlier reports that indicated that MLT was able to alleviate reduced mitochondrial potential induced by DXR (Song *et al.*, 2012; Guven *et al.*, 2016). Specifically, in the context of DXR-induced cardiotoxicity, mitochondria in DXR treated myocytes exhibited a collapse in mitochondrial membrane potential, which was prevented with MLT pre-treatment (Xu and Ashraf, 2002).

Increases in oxidative stress is strongly associated with a loss in mitochondrial membrane potential and acts as a trigger for mitophagy (Kim *et al.*, 2007). In fact, changes in mitochondrial redox state and mitochondrial membrane potential have been shown to precede mitochondrial dysfunction during DXR-induced cardiotoxicity (Kuznetsov *et al.*, 2011). A potential mechanism by which DXR disrupts mitochondrial membrane potential is via its binding to cardiolipin. DXR tends to accumulate in mitochondria owing to its cationic nature that has a high affinity for the negatively charged cardiolipin, a major phospholipid component in the inner mitochondrial membrane (Goormaghtigh *et al.*, 1980). The binding of DXR to cardiolipin results in oxidation of this phospholipid, which leads to the formation of an irreversible complex. Cardiolipin forms the structural basis for maintaining mitochondrial membrane potential as demonstrated previously (Paradies *et al.*, 2014; Jiang *et al.*, 2000). In contrast, a deficiency in cardiolipin was shown to increase mitochondrial membrane potential and reduces DXR-induced oxidative stress in human B-Lymphocytes (Aryal and Rao, 2016).

4.8 The effect of MLT on mitochondrial morphology during DXR-induced cardiotoxicity

Since pre-treatment with MLT attenuated mitochondrial ROS formation and restored mitochondrial membrane potential, it was crucial to further examine the effect that MLT pre-treatment has on dynamic changes in mitochondrial morphology. The CTRL and MLT treated cells maintained elongated-shaped mitochondria and an interconnected mitochondrial networks around the perinuclear region of the cell (Figure 3.6.1.1). However, mitochondria were fragmented and spherical-shaped in response to DXR treatment and appeared further dispersed from the perinuclear region of the cell (Figure 3.6.1.1). MLT pre-treatment appeared to significantly reduce the amount of spherical-shaped mitochondria as most cells maintained elongated-shaped mitochondria and an interconnected mitochondrial network (Figure 3.6.1.1).

The form factor analysis performed on the images provided information on the aspect ratio of mitochondria which is the ratio between the major and minor axes of an ellipse equivalent to the shape of mitochondria and the degree of branching of the mitochondrial network (Mortiboys *et al.*, 2008). The observations made regarding the morphology of mitochondria during live-cell imaging

corresponded with the form factor analysis as the major/minor aspect ratio and the degree of mitochondrial branching was significantly reduced in DXR treated cells in comparison to cells which were pre-treated with MLT (Figure 3.6.1.2). These results suggest that pre-treatment with MLT improves mitochondrial morphology during DXR-induced cardiotoxicity.

However, an assessment of mitochondrial morphology is only a snapshot of the dynamic changes in mitochondrial morphology and should be carefully used as indicator for mitochondrial fission and fusion (Galloway *et al.*, 2012). To support this notion, it was indicated in a previous study that mitochondria became elongated under nutrient starvation conditions via the activation of mitochondrial fission proteins (Rambold *et al.*, 2011). Therefore, in the current study we investigated the effect of MLT on mitochondrial fission and fusion proteins during DXR-induced cardiotoxicity.

4.9 The effect of MLT on mitochondrial fission and fusion during DXR-induced cardiotoxicity

In mammalian cells, mitochondrial fusion is a process governed by Mitofusin proteins 1 and 2 (Mfn1 and Mfn2) as well as Optic Atrophy 1 (OPA1). Mitofusin is localized to the outer mitochondrial membrane and facilitates the binding of two distinct mitochondria during early stages of mitochondrial fusion (Lee *et al.*, 2007; Scott and Youle, 2010). OPA1 is a dynamin family GTPase which is localized to the inner mitochondrial membrane and intermembrane space. OPA1 promotes fusion of the inner mitochondrial membrane and regulates the morphology of mitochondrial cristae (Lee *et al.*, 2007; Scott and Youle, 2010). Eight isoforms of OPA1 have been identified, the most dominant isoforms are L-OPA1 (Long-form of OPA1) and S-OPA1 (Short-form of OPA1) (Song *et al.*, 2007; Scott and Youle, 2010). On the other hand, mitochondrial fission is controlled by hFis1 and Drp1. hFis1 is located in the outer mitochondrial membrane and it forms protein-protein interaction sites which protrude into the cytosol (Scott and Youle, 2010). Drp1 is mainly located in the cytosol and upon fission Drp1 is recruited to the mitochondria via hFis1. When Drp1 interacts with hFis1 at fission sites, a collar around the mitochondrion is formed. Constriction of the collar leads to a separation of the outer mitochondrial membrane yielding two independent organelles (Scott and Youle, 2010).

In our study, the expression of L-OPA1 and S-OPA1 isoforms remained unchanged *in vitro* and *in vivo* in response to various treatments (Figure 3.6.2.2 and Figure 3.9.7.1 C). Indeed, a combination of L-OPA1 and S-OPA1 isoforms are critical for mitochondrial fusion activity (Song *et al.*, 2007). However, L-OPA1 has two cleavage sites (S1 and S2) which can be cleaved either by YME1L, an ATP-dependent metalloprotease or OMA1, a zinc-metalloprotease (McBride and Sounbannier, 2010; Thomas *et al.*, 2014) to generate S-OPA1. Under basal conditions, YME1L cleaves L-OPA1 at S2 and generates fusion-competent cells (Song *et al.*, 2007; Thomas *et al.*, 2014). However, in response to stress, OMA1, cleaves L-OPA1 at S1, which inhibits mitochondrial membrane fusion (Head *et al.*, 2009; Thomas *et al.*, 2014). Hence, in the current study it remains unknown if the S-OPA1 band observed (Figure 3.6.2.2 and Figure 3.9.7.1 C) corresponds to the cleavage by YME1L or OMA1. To fully elucidate the role of OPA1 during mitochondrial fusion in our model, the mRNA content from treated cells should be analyzed by qRT-PCR for changes in expression of YME1L and OMA1. Nonetheless, OPA1 has been shown to be dependent on Mfn1 to promote mitochondrial fusion (Cipolat *et al.*, 2004).

In both *in vitro* and *in vivo* models, pre-treatment with MLT significantly increased the expression of mitofusin proteins, which was inhibited by DXR (Figure 3.6.2.1 and Figure 3.9.7.1). Furthermore, MLT pre-treatment significantly attenuated the expression of hFis1 and Drp1 proteins increased by DXR both *in vitro* and *in vivo* (Figure 3.6.2.3 and Figure 3.9.7.2). Thus, the results obtained in the current study suggest that DXR is disrupting mitochondrial fusion and favoring mitochondrial fission as indicated by reduced mitofusin protein (Mfn1 and Mfn2) expression as well as increased mitochondrial fission protein (Drp1 and hFis1) expression. In contrast, pre-treatment with MLT reversed the changes in expression of mitochondrial fission and fusion proteins, favoring mitochondrial fusion during DXR-induced cardiotoxicity.

It was reported in a previous study which investigated the role of mitochondrial fusion and fission in a rat model of DXR-induced hepatic toxicity, that DXR reduced the content of OPA1, Mfn1 and Mfn2, but had no effect on Drp1 and hFis levels (Dirks-Naylor *et al.*, 2014). In contrast, co-administration of DXR with mdivi-1, a mitochondrial fission inhibitor, prevented detrimental effects of DXR via

reduced expression of Drp1 and also prevented an increase in the levels of both p53 and Erk 1/2, in a model of DXR-induced cardiotoxicity (Gharanei *et al.*, 2013). Furthermore, SIRT3-dependent activation of OPA1 contributed to the preservation of mitochondrial networking by favoring mitochondrial fusion and thus protected cardiomyocytes from DXR-induced cell death (Scher *et al.*, 2007).

The variation in results is likely owing to various models and experimental methods used to assess mitochondrial fission and fusion proteins. In our study, mitochondrial isolations from H9c2 cells and rat heart tissue were used to assess the protein levels of mitochondrial fission and fusion proteins whereas other studies tend to use cell or tissue lysates. The use of cell or tissue lysates may not clearly indicate if there are changes in expression of proteins such as Drp1, since Drp1 is located in the cytosol and whether it is recruited to the mitochondria upon fission. There are also a limited number of studies where the effect of MLT on mitochondrial fission and fusion in the context of DXR-induced cardiotoxicity were investigated. MLT has, however, been shown to influence the expression of mitochondrial fission and fusion proteins (Wappler *et al.*, 2012; Stacchiotti *et al.*, 2014; Kang *et al.*, 2016). In a model of hepatotoxicity, MLT attenuated the reduced effect of Drp1 and Mfn2, Pink1, PARKIN and PGC1- α induced by carbon tetrachloride, suggesting that MLT protects against liver fibrosis via upregulation of mitophagy and mitochondrial biogenesis (Kang *et al.*, 2016).

In cardiac cells, mitochondrial fission and fusion are critical processes, which adapt the morphology of mitochondria to meet the high metabolic needs of the heart. Mitochondrial fusion is a common feature of actively respiring cells. The interconnected mitochondrial network formed during fusion, allows for the distribution of respiratory enzymes and metabolites throughout the entire mitochondrial compartment of the cell (Westermann, 2012). The high energy demand of the heart is satisfied during mitochondrial respiration which generates ATP, of which more than 90% is utilized by cardiomyocytes (Tokarska –Schlattner *et al.*, 2006). The underlying molecular mechanisms by which DXR induces a bioenergetic decline in the heart have been well documented in various studies (for review see Tokarska –Schlattner *et al.*, 2006) however, less is known about MLT's effects in the

context of DXR-induced cardiotoxicity. Therefore, in the current study we investigated the effect of MLT on mitochondrial respiration in H9c2 cells, during DXR-induced cardiotoxicity.

4.10 The effect of MLT on mitochondrial bioenergetics and biogenesis during DXR-induced cardiotoxicity

Pre-treatment with MLT caused a significantly increase in cellular ATP levels (Figure 3.7.1.2) but had no effect on basal respiration and ATP-linked respiration in H9c2 cells (Figure 3.7.1.1 A and B). Furthermore, pre-treatment with MLT increased the electron transport system (ETS) capacity and mitochondrial spare respiratory capacity (MSRC) which were reduced by DXR treatment (Figure 3.7.1.1 C and D). The ETS capacity is an unstable state of respiration where the addition of a mitochondrial uncoupler (FCCP) collapses the inner membrane gradient and stimulates increased respiration. Therefore, the ETS capacity is indicative of the substrate oxidation and the maximum activity of the electron transport system that is achievable by the cells during steady state ADP levels (Rose *et al.*, 2014). The MSRC is indicative of the amount of extra ATP that can be produced by oxidative phosphorylation during an increase in energy demand (Desler *et al.*, 2012). Considering that pre-treatment with MLT stabilized mitochondrial membrane potential and increased the ETS capacity in H9c2 cells, it is suggested that MLT maintains mitochondrial function via attenuating the damaging effects of DXR on the electron transport chain. The increase in MSRC observed in cells pre-treated with MLT indicates that MLT is compensating for the loss of ATP induced by DXR. Furthermore, MLT treatment alone maintained cellular ATP at basal levels suggesting that MLT elicits a protective effect on the mitochondria during stressful conditions such as DXR-induced cardiotoxicity.

Interestingly, MLT was also found to influence mitochondrial respiratory complexes I and IV in brain and liver tissues (Martin *et al.*, 2000). In a model of septic heart injury, MLT increased complex IV activity and improved cardiac function (Zhang *et al.*, 2013). In fact, chronic oral administration of MLT increased ATP content of hepatocytes isolated from old Wistar rats (Tresguerres *et al.*, 2012). However, studies where the direct effect of MLT on mitochondrial respiration and ATP generation during DXR-induced cardiotoxicity are investigated, are lacking. Furthermore, the exact mechanisms

by which MLT stabilizes mitochondrial respiration and increases ATP content in cells are not well understood. However, it is suggested in most studies that these effects may be attributed to MLT's antioxidant activity as well as its ability to reduce lipid peroxidation and improve mitochondrial membrane potential as observed in our study.

DXR has a high affinity to cardiolipin, the binding of DXR to cardiolipin leads to the formation of an irreversible complex inhibiting oxidative phosphorylation as it renders cardiolipin incapable of acting as a cofactor for mitochondrial respiratory enzymes (Goormaghtigh *et al.*, 1980; Goormaghtigh *et al.*, 1986). In addition, as the inner mitochondrial membrane represents a critical site for DXR accumulation, the respiratory chain is vulnerable to the toxic effects of DXR. In particular, it was demonstrated in studies which aimed to determine the sensitivity of respiratory complexes, that DXR was mainly located in complexes I, III, and IV, with a specific vulnerability for complexes I (NADH dehydrogenase) and IV (cytochrome c oxidase) (Goormaghtigh *et al.*, 1986; Nicolay *et al.*, 1987; Marcillat *et al.*, 1989).

Various signaling pathways that regulate the enzymatic capacity for fatty-acid β -oxidation, mitochondrial oxidative phosphorylation (OXPHOS) as well as mitochondrial biogenesis and function appear to converge at the transcriptional co-activator peroxisome proliferator-activated receptor-gamma coactivator-1alpha (PGC-1 α). PGC-1 α has been shown to directly influence and modulate the activity of several mitochondrial genes at transcriptional level (Lin *et al.*, 2005; Fernandez-Marcos and Auwerx, 2011). It was demonstrated in PGC-1 α deficient mice that this co-activator diminished postnatal growth of organs abundant in mitochondria such as the heart and was also necessary for the normal expression of various mitochondrial genes (Leone *et al.*, 2005). Cardiac remodeling is apparent in the DXR-challenged heart as DXR is known to initiate a switch in metabolic substrate utilization from fatty acids to glucose (Tokarska –Schlattner *et al.*, 2005; Tokarska –Schlattner *et al.*, 2006) and this subsequently leads to inefficient ATP production as also demonstrated in the our study (Figure 3.7.1.2). Furthermore, DXR has been shown to inhibit the expression of PGC-1 α , leading to the suppression of adipogenesis and resulting in the impaired import of glucose mediated through glucose transporter type 4 (GLUT4) (Arunachalam *et al.*, 2013). Interestingly, MLT has also been shown to influence the expression of PGC-1 α (Guyen *et al.*, 2016; Guo *et al.*, 2014).

In our study, the effect of MLT on PGC-1 α expression was investigated during DXR-induced cardiotoxicity. Pre-treatment with MLT significantly restored PGC-1 α expression that was significantly attenuated in response to DXR treatment in both H9c2 cells and rat heart tissue (Figure 3.7.3.1 and Figure 3.9.8.1). In support of our findings, Guven *et al.* (2016) recently reported that MLT given with DXR increased PGC-1 α and AMPK levels which was reduced by DXR in mouse fibroblasts. Moreover, adult mice hearts deficient in both PGC-1 α and PGC-1 β demonstrated a mitochondrial cristae-stacking abnormality suggestive of a phospholipid abnormality as described in humans with Barth syndrome which is characterized by genetic defects in cardiolipin synthesis (Lai *et al.*, 2014). Genetic profiling in these mice hearts revealed reduced expression of the gene encoding CDP-diacylglycerol synthase 1, an enzyme that catalyzes the proximal step in cardiolipin biosynthesis (Lai *et al.*, 2014) suggesting that PGC-1 α influences the biosynthesis of cardiolipin. Since, DXR directly oxidizes cardiolipin it may also be disrupting the synthesis of cardiolipin and ATP production via the suppression of PGC-1 α in our model.

Furthermore, mitochondrial biogenesis is strongly correlated with mitochondrial fission and fusion. PGC-1 α has been reported to influence the activity of mitochondrial fission and fusion proteins. In particular, PGC-1 α stimulates the expression of Mfn2 under conditions characterized by enhanced energy expenditure (Cartoni *et al.*, 2005; Soriano *et al.*, 2006; Zorano, 2009) such as DXR-induced cardiotoxicity. On the other hand, Mfn2 loss of function has been correlated with the reduced stimulatory effect of PGC-1 α on mitochondrial membrane potential (Soriano *et al.*, 2006). Furthermore, downregulation of PGC-1 α leads to increased expression of the mitochondrial fission protein, Drp1 (Guo *et al.*, 2015). DXR attenuated the expression of Mfn2 and increased the expression of Drp1 in both *in vitro* and *in vivo* models in our study suggesting that DXR could possibly be inducing these effects via reducing PGC-1 α . In summary, apart from MLT's antioxidant activity, pre-treatment with MLT could also be increasing the expression of mitochondrial fusion proteins and promoting cardiolipin synthesis via PGC-1 α activation, thus maintaining mitochondrial membrane potential and an interconnected fused mitochondrial network which subsequently facilitates ATP production during DXR-induced cardiotoxicity.

4.11 The effect of MLT on sirtuin activity during DXR-induced cardiotoxicity

It has been previously demonstrated that sirtuin 1 (SIRT1) is an important upstream regulator of PGC-1 α signaling (Cantó and Auwerx, 2009; Wang *et al.*, 2015; Guo *et al.*, 2015). The sirtuins are a family of proteins that act predominantly as nicotinamide adenine dinucleotide (NAD)-dependent deacetylases (Sack and Finkel, 2012). SIRT1 and SIRT2 can be found in the cytosol, SIRT3, SIRT4 and SIRT5 are localized to the mitochondria and, SIRT6 and SIRT7 are nuclear proteins (Sack and Finkel, 2012).

In our study, pre-treatment with MLT restored the expression of SIRT1 and SIRT3 which were reduced by DXR in H9c2 cells (Figure 3.8.1.1). Interestingly, MLT treatment alone reduced the expression of SIRT1 but not SIRT3 (Figure 3.8.1.1). It is possible that MLT increases SIRT1 expression under conditions of stress such as DXR-induced cardiotoxicity. Furthermore, pre-treatment with MLT increased the expression of SIRT1 in rat hearts reduced by DXR, however no changes in SIRT3 expression was observed in our *in vivo* model (Figure 3.9.9.1). In support of our findings, it was reported in recent studies that SIRT1 expression, stimulated by resveratrol, reduced DXR-induced cardiomyocyte apoptosis and ROS production and that these protective effects were attenuated when SIRT1 was inhibited by nicotinamide (Danz *et al.*, 2009; Ruan *et al.*, 2015; Liu *et al.*, 2016). DXR has also been demonstrated to reduce SIRT3 expression in primary cultures of cardiomyocytes and in mouse hearts (Pillai *et al.*, 2016). SIRT3 overexpression protected the heart from mitochondrial DNA damage and cardiomyocyte cell death induced by DXR (Pillai *et al.*, 2016). Furthermore, the authors reported that SIRT3 deficient mice developed cardiac hypertrophy and died during the course of DXR treatment suggesting that SIRT3 activation protects the heart during DXR-induced cardiotoxicity (Pillai *et al.*, 2016).

In the heart, SIRT1 inhibits the expression of pro-apoptotic proteins Bax and cleaved caspase-3 and enhances the expression of anti-apoptotic protein Bcl-xL (Hsu *et al.*, 2010), suggesting that activation of SIRT1 promotes cardiomyocyte survival during heart failure. A study conducted by Lu *et al.* (2014), revealed that SIRT1 expression was reduced in humans with advanced heart failure. Interestingly, SIRT3 expression was found to be elevated during energy depletion in the heart to

compensate for the loss of ATP by regulating free fatty acid metabolism to meet the high ATP demand in the heart (Ingwall *et al.*, 2009; Pillai *et al.*, 2010). Supporting this notion, the ATP content in the hearts of SIRT3 deficient mice was significantly reduced suggesting that SIRT3 plays a crucial role in regulating ATP production (Ahn *et al.*, 2008). Moreover, SIRT3 reduced oxidative stress by deacetylation of lysine residues on superoxide dismutase 2, a crucial mitochondrial antioxidant (Qiu *et al.*, 2010). SIRT1 and SIRT3 expression is critical for maintaining cardiac function, therefore, in the current study the effect of MLT on SIRT1 and SIRT3 expression during DXR-induced cardiotoxicity was investigated.

There is however a lack of information to support the role of MLT on sirtuin activity in the context of DXR-induced cardiotoxicity. However, in a model of myocardial ischemia/reperfusion injury, MLT has been shown to improve cardiac function, reduce apoptotic protein expression, myocardium superoxide generation, malondialdehyde levels, and increase myocardium superoxide dismutase in a SIRT1 dependent manner as these protective effects were attenuated in the presence of a MLT receptor antagonist, luzindole, or SIRT1 inhibitor, EX527 (Yu *et al.*, 2014). It was found in another study that MLT facilitated adipose-derived mesenchymal based therapy in myocardial infarction by promoting the survival of these stem cells via SIRT1 signaling (Han *et al.*, 2016). It is therefore suggested that MLT elicits anti-apoptotic and antioxidant effects via modulating SIRT1 activity in the heart. There are however no evidence for the role of MLT on SIRT3 expression in the heart. In a model of hepatotoxicity, MLT has been shown to increase superoxide dismutase 2 via upregulation of SIRT3 (Chen *et al.*, 2015). It was revealed in a recent study that MLT enhanced SIRT3 activity and increased the binding of Foxo3a to superoxide dismutase 2 and catalase; thereby reducing oxidative stress during ovarian aging (Song *et al.*, 2016). It is therefore evident from these studies that MLT enhances the expression of mitochondrial antioxidants via modulating SIRT3 activity during oxidative stress.

In summary, our results suggest that pre-treatment with MLT during DXR-induced cardiotoxicity appears to influence both SIRT1 and SIRT3 activity. It is likely that MLT, apart from inducing its free radical scavenging activity during oxidative stress, modulates the activity of SIRT1 and SIRT3 which subsequently stimulates mitochondrial antioxidant defense systems in the heart to counteract the

increase in mitochondrial ROS production induced by DXR as observed in our *in vitro* model. Furthermore, the underlying mechanisms of MLT's anti-apoptotic effects in H9c2 cells and in rat heart tissues exposed to DXR, is possibly associated with the upregulation of SIRT1 during DXR-induced cardiotoxicity. Since SIRT1 has emerged as an upstream regulator of PGC-1 α , MLT could possibly be eliciting its protective mitochondrial effects such as promoting mitochondrial fusion, maintaining mitochondrial membrane potential and increasing ATP production via a SIRT1 and PGC-1 α dependent signaling pathways. However, to validate the effect of MLT pre-treatment on SIRT1 activity during DXR-induced cardiotoxicity, a MLT receptor antagonist such as luzindole or a SIRT1 inhibitor such as EX527 needs to be used in future studies.

4.12 The effect of daily MLT administration on cardiac function, animal body weight and tumor growth during DXR-induced cardiotoxicity

To establish a tumor-bearing rat model of acute DXR cardiotoxicity, female Sprague Dawley rats (16-18 weeks old), received DXR (3 intraperitoneal injections of 4 mg/kg at 3-day intervals, 12 mg/kg cumulative dose) or received MLT (6 mg/kg) daily in their drinking water. The treatment doses used in the current study were chosen based on previous work which showed that MLT treatment (6 mg/kg/day) for two weeks prevented the cardiotoxic side effects of DXR (12 mg/kg) (Balli *et al.*, 2004). It has been previously shown that an optimal accumulative dose of 12.45 mg/kg of DXR is needed to induce congestive heart failure in Wistar rats (Spivak *et al.*, 2013) and doses which exceeded 12.45 mg/kg caused death. In the clinical setting, patients receive DXR in multiple doses between 50-75 mg/m² over several months with a cumulative maximum of 450 mg/m², which is equivalent to approximately 12 mg/kg (Yi *et al.*, 2005), therefore the dose of DXR used in our study is also clinically relevant. The method of administering MLT to rats via their drinking water has been well established and used in various studies (Nduhirabandi *et al.*, 2011; Stacchiotti *et al.*, 2014; Moreira *et al.*, 2015). Since, MLT is usually administered over a long period of time, methods such as oral gavage or intra-peritoneal injections can induce a stress-response in the animals over time. However, a major limitation of administering MLT to rats via their drinking water is that the exact dose of MLT received by each individual rat is unknown.

In the clinical oncology setting, two major types of DXR cardiotoxicity are evident. Acute cardiotoxicity occurs promptly during or shortly after treatment with DXR and manifests as myopericarditis, palpitations, paroxysmal non-sustained supraventricular tachycardia and acute-left ventricular failure, although rare (Takemura and Fujiwara, 2007). The incidence of acute cardiotoxicity is approximately 11% and symptoms are reversible with appropriate treatment (Takemura and Fujiwara, 2007; Shakir and Rasul, 2009; Chatterjee *et al.*, 2010). Chronic cardiotoxicity occurs within 30 days of the last administered dose, but may even occur 6-10 years after the last treatment and manifests as irreversible cardiomyopathic changes leading to congestive heart failure with a poor prognosis. The incidence of DXR-induced cardiomyopathy is approximately 1.7% and is greatly dependent on the accumulative dose of DXR (Takemura and Fujiwara, 2007; Chatterjee *et al.*, 2010). Both acute and chronic administration appear to limit the dose of DXR used to treat cancer patients as a result of its cardiotoxic effects. In the current study an acute model of DXR-induced cardiotoxicity was used to assess the effect of daily MLT administration on cardiac function during DXR-induced cardiotoxicity.

Cardiac function was significantly improved in rats treated with MLT and DXR as shown by the significant increase in cardiac output, total work performance and stroke volume compared to rats that received DXR only (Figure 3.9.4). Although there was a reduction in cardiac output and stroke volume in DXR-treated rats, this was not significant when compared to the CTRL. However, a significant decrease in the total work performance of the heart was observed in DXR-treated rats in comparison to the CTRL (Figure 3.9.4). No significant changes in heart rate were observed among the treated groups. It was recently demonstrated that DXR significantly decreased stroke volume, ejection fraction, cardiac output, and left ventricular systolic pressure in mouse hearts (Mitry and Edwards, 2016). In another study, it was demonstrated that DXR significantly reduced arterial pressure and left ventricular fractional shortening as well as inducing a significant accumulation of ascites; these cardiomyopathy associated changes were ameliorated with MLT treatment (Morishima *et al.*, 1998). Liu and co-workers reported a 50% reduction in heart rate and coronary flow which was reversed with MLT treatment in perfused mouse hearts treated with DXR (Liu *et al.*, 2002). Although the dose of DXR (12 mg/kg) used in this study induced a decline in cardiac function,

the dose was not fatal as none of the animals died during the course of this study. Furthermore, a significant reduction in total body weight and in heart weight were observed in DXR-treated rats which was attenuated in DXR+MLT treated rats (Figure 3.9.1 and Figure 3.9.3). In support of these findings, MLT was shown to attenuate DXR-induced body weight loss in male Sprague Dawley rats (Kim *et al.*, 2005) and attenuate heart weight reduced by DXR (Morishima *et al.*, 1998). Furthermore, DXR has been shown to induce marked atrophy of the hearts in a juvenile mouse model (Zhu *et al.*, 2008).

There are however no studies where the effect of MLT on cardiac function and cancer during DXR-induced cardiotoxicity are assessed in a tumor-bearing rat model. Therefore, the effect of MLT during DXR-induced cardiotoxicity is rarely investigated in a more clinically relevant animal model. In the current study, tumors cells were inoculated in the mammary fat pad of rats to simulate a model of breast cancer to investigate the effect of MLT on tumor growth during DXR-induced cardiotoxicity. Tumors were palpable and decreased in volume in response to MLT treatment alone (Figure 3.9.2). These results suggest that MLT treatment induces an oncostatic effect. Interestingly, tumors were palpable and could not be measured in all ten animals in the DXR+MLT treated group by day 10 (Figure 3.9.2), which suggests that MLT enhances the anti-cancer activity of DXR and the combination of DXR+MLT treatment has a more rapid oncostatic effect on tumor growth than DXR treatment alone.

The effect of MLT on cancer has been widely investigated. A previous study demonstrated that MLT itself inhibits the growth of human breast cancer cells. In addition, the combination of MLT and DXR further reduced the growth of human breast cancer cells, suggesting that MLT improved the antitumor activity of DXR (Kim *et al.*, 2005). In a clinical trial conducted by Lissoni and co-workers, MLT in combination with chemotherapy was shown to significantly increase the overall tumor regression rate and improve the survival outcomes of patients suffering from metastatic non-small cell lung cancer. Patients treated with chemotherapy did not survive after a two year period but 5-year survival was achieved in 6% of patients treated with both MLT and chemotherapy. Moreover, the authors reported that chemotherapy was better tolerated in patients treated with MLT (Lissoni *et al.*, 2003). It was reported in a previous study that MLT elicits its anti-cancer activity via

immunomodulatory action, oncostatic activity, antioxidant properties, anti-inflammatory effects and anti-angiogenic activity (Lissoni *et al.*, 2001). However, further investigations are required to fully elucidate the mechanisms involved in MLT's anti-cancer activity.

In summary, to the best of our knowledge, we are the first to demonstrate that MLT improves cardiac function in a tumor-bearing rat model of acute DXR-induced cardiotoxicity. The underlying mechanisms regarding the cardioprotective effect of MLT during DXR-induced cardiotoxicity is likely attributed to decreased apoptotic activity and the increased expression of mitochondrial fusion proteins as well as PGC-1 α and SIRT1 observed in this study. Furthermore, MLT enhanced the anti-cancer activity of DXR, which suggests that MLT is dually cardioprotective and oncostatic.

Chapter 5

Conclusion

In the clinical oncology setting, doxorubicin (DXR) has proven to be a potent anti-neoplastic agent and is widely used to treat various cancers. Regrettably, it is apparent that this anti-neoplastic agent is a double-edged sword as it is highly toxic to the heart. DXR is known to accumulate in cardiac mitochondria and induce a vicious cycle of free radical production which leads to mitochondrial dysfunction and culminates in cardiomyocyte cell death. In view of this clinical impediment, the pineal indoleamine, melatonin (MLT) has proven to be beneficial in the context of DXR-induced cardiotoxicity as it protects mitochondria against free-radical damage induced by DXR. However, apart from MLT's potent antioxidant activity, other mechanisms by which MLT confers mitochondrial and subsequent cardiac protection during DXR-induced cardiotoxicity remains to be explored.

In our study, we first confirmed the finding of others by demonstrating that pre-treatment with MLT does suppress mitochondrial ROS production and preserve mitochondrial membrane potential during DXR-induced cardiotoxicity. In addition, we have demonstrated that pre-treatment with MLT during DXR-induced cardiotoxicity improves mitochondrial morphology, upregulates mitochondrial fusion, restores the electron transport system (ETS) capacity and the mitochondrial spare respiratory capacity (MSRC) thereby increasing the cellular ATP content in cardiomyocytes. Although we have demonstrated that pre-treatment with MLT increases Pink1 and PARKIN activity during DXR-induced cardiotoxicity, further work needs to be conducted to confirm that pre-treatment with MLT promotes the clearance of damaged mitochondria by mitophagy in our study. The preservation of mitochondrial function by pre-treatment with MLT during DXR-induced cardiotoxicity is strongly associated with decreased cardiomyocyte apoptosis and improved cardiac function. Furthermore, we have demonstrated that MLT enhances the anti-neoplastic activity of DXR and suppresses the growth of tumors whilst maintaining its cardioprotective effects. SIRT3 activation has been shown to promote ATP production in the heart and inhibit ROS production. The effect of pre-treatment with MLT on SIRT3 activation was only observed in our *in*

vitro model of DXR-induced cardiotoxicity and could possibly be influencing the protective mitochondrial effects we have observed in our *in vitro* model. Other studies have reported that the activation of PGC-1 α influences proteins involved in mitochondrial fission and fusion, maintains mitochondrial membrane potential and increases ATP production. Furthermore, it is known that SIRT1 is an upstream regulator of PGC-1 α . SIRT1 activation alone has been shown to suppress apoptotic proteins and decrease ROS production. Since, pre-treatment with MLT increased the expression of SIRT1 and PGC-1 α in both *in vitro* and *in vivo* models of DXR-induced cardiotoxicity in our study, we propose that the underlying mechanisms by which MLT elicits its anti-apoptotic effects and maintains mitochondrial function during DXR-induced cardiotoxicity is possibly via a SIRT1 and PGC-1 α dependent signaling pathway. The effect of MLT on mitochondrial function and the potential mechanisms by which MLT confers mitochondrial protection during DXR-induced cardiotoxicity is summarized in Figure 5.1.

Indeed, the versatile effects of MLT on cardiac mitochondria, its potent antioxidant action as well as its ability to modulate sirtuin activity and cell death regulators has shown to be beneficial in mitigating DXR-induced cardiotoxicity. Moreover, the beneficial effects of melatonin as an adjuvant therapy in reducing the side effects of chemotherapy and improving the survival outcome of cancer patients is well established however, there is a critical need for understanding the dual cardio-protective and oncostatic nature of MLT. Future studies should focus on elucidating the effect that MLT has on mitochondria in the context of oncology using clinically relevant *in vivo* models such as tumor-bearing models of DXR-induced cardiotoxicity. Such studies would aid in further exploiting the use of MLT as an adjuvant therapy and advance the current treatment strategies in the clinical oncology setting.

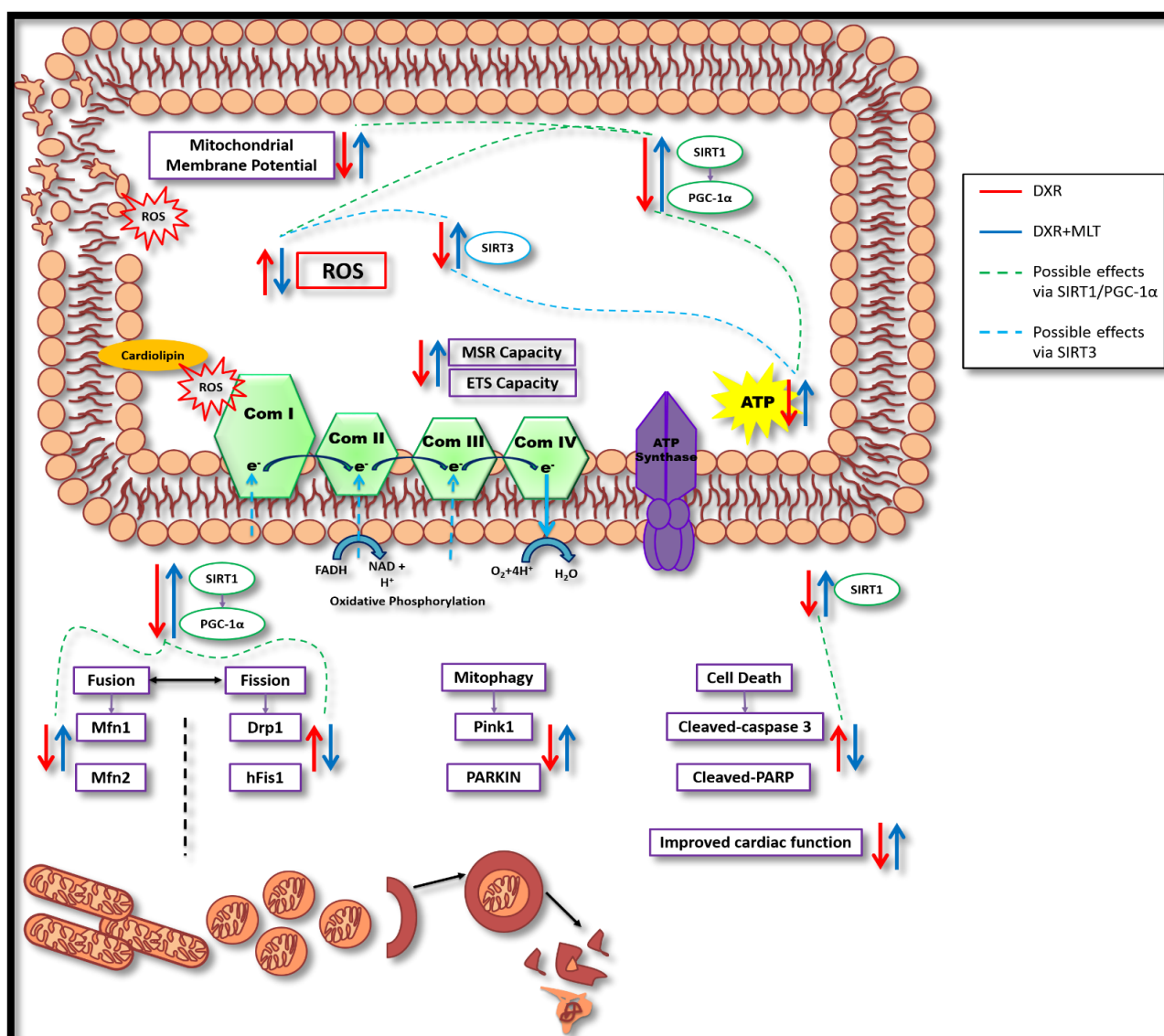


Figure 5.1: The effects of pre-treatment with MLT during DXR-induced cardiotoxicity. The figure summarizes the effects of DXR (red arrows) and DXR+MLT (blue arrows) during that were found in our study. Furthermore, the possible mechanisms by which MLT confers mitochondrial protection and reduces apoptosis is also indicated (green and blue dashed lines). Abbreviations- **DXR**: doxorubicin; **MLT**: melatonin; **ROS**: reactive oxygen species; **ATP**: adenosine tri-phosphate; **ETS**: electron transport capacity; **MSRC**: mitochondrial spare respiratory capacity; **PARP**: poly [ADP-ribose] polymerase; **Drp1**: dynamin-related protein 1; **hFis1**: mitochondrial fission 1 protein; **OPA1**: optic atrophy protein 1; **Mfn1/2**: mitofusin1/2; **SIRT1/3**: sirtuin 1/3; **PGC-1α**: Peroxisome proliferator-activated receptor gamma co-activator 1alpha; **Pink1**: PTEN-induced putative kinase 1; **Parkin**: Parkinson protein.

References

- Abdel-Aleem S, El-Merzabani MM, Sayed-Ahmed M *et al.* Acute and chronic effects of adriamycin on fatty acid oxidation in isolated cardiac myocytes. *J Mol Cell Cardiol.* 1997; 29:789–797.
- Acuna-Castroviejo D, Escames G, VENEGAS C *et al.* Extrapineal melatonin: sources, regulation, and potential functions. *Cell Mol Life Sci.* 2014; 71:2997–3025.
- Ahmed HH, Mannaa F, Elmegeed GA *et al.* Cardioprotective activity of melatonin and its novel synthesized derivatives on doxorubicin-induced cardiotoxicity. *Bioorg Med Chem.* 2005; 13:1847–1857.
- Ahn BH, Kim HS, Song S *et al.* A role for the mitochondrial deacetylase Sirt3 in regulating energy homeostasis. *Proc Natl Acad Sci USA.* 2008; 105:14447-14452.
- Andrabi SA, Sayeed I, Siemen D *et al.* Direct inhibition of the mitochondrial permeability transition pore: a possible mechanism responsible for anti-apoptotic effects of melatonin. *FASEB J.* 2004; 18:869–871.
- Antolin I, Rodrigue C, Sainz RM *et al.* Neurohormone melatonin prevents cell damage: effect on gene expression for antioxidant enzymes. *FASEB J.* 1996; 10:882–890.
- Anwar MM and Meki AR. Oxidative stress in streptozotocin-induced diabetic rats: effects of garlic oil and melatonin. *Comp Biochem Physiol A Mol Integr Physiol.* 2003; 135:539–547.
- Arunachalam S, Tirupathi Pichiah PB and Achiraman S. Doxorubicin treatment inhibits PPAR γ and may induce lipotoxicity by mimicking a type 2 diabetes-like condition in rodent models. *FEBS Lett.* 2013; 587:105–110.
- Aryal B and Rao VA. Deficiency in Cardiolipin Reduces Doxorubicin-Induced Oxidative Stress and Mitochondrial Damage in Human B-Lymphocytes. *PLoS ONE.* 2016; 11(7):e0158376.
- Ashkenazi A and Dixit VM. Apoptosis control by death and decoy receptors. *Curr Opin Cell Biol.* 1999; 11:255–260.
- Bachur NR, Gordon SL and Gee MV. A general mechanism for microsomal activation of quinone anticancer agents to free radicals. *Cancer Res.* 1978; 38:1745–1750.
- Balli E, Mete UO, Tuli A *et al.* Effect of melatonin on the cardiotoxicity of doxorubicin. *Histol Histopathol.* 2004; 19:1101–1108.
- Barth S, Glick D and Macleod KF. Autophagy: assays and artifacts. *J Pathol.* 2010; 221(2):117-124.

- Beer M, Seyfarth T, Sandstede J *et al.* Absolute concentrations of high-energy phosphate metabolites in normal, hypertrophied, and failing human myocardium measured noninvasively with (31)P-SLOOP magnetic resonance spectroscopy. *J Am Coll Cardiol.* 2002; 40:1267–1274.
- Benloucif S, Burgess HJ, Klerman EB *et al.* Measuring melatonin in humans. *J Clin Sleep Med.* 2008; 4(1):66-69.
- Bianchi C, Bagnato A and Paggi MG. Effect of adriamycin on electron transport in rat heart, liver, and tumor mitochondria. *Exp Mol Pathol.* 1987; 46:123–135.
- Bonadonna G, Monfardini S, de Lena M *et al.* Phase I and preliminary phase II evaluation of adriamycin. *Cancer Res.* 1970; 30:2572–2582.
- Bordoni A, Biagi P and Hrelia S. The impairment of essential fatty acid metabolism as a key factor in doxorubicin-induced damage in cultured rat cardiomyocytes. *Biochim Biophys Acta.* 1999; 1440:100–106.
- Cantó C and Auwerx J. PGC-1alpha, SIRT1 and AMPK, an energy sensing network that controls energy expenditure. *Curr Opin Lipidol.* 2009; 20(2):98-105.
- Cardinali DP, Pagano ES, Scacchi Bernasconi PA *et al.* Melatonin and mitochondrial dysfunction in the central nervous system. *Horm Behav.* 2013; 63:322–330.
- Cartoni R, Léger B, Hock MB *et al.* Mitofusins 1/2 and ERR α expression are increased in human skeletal muscle after physical exercise. *J Physiol.* 2005; 567(Pt 1):349-358.
- Chang W-T, Li J, Huang H-H *et al.* Baicalein Protects Against Doxorubicin-Induced Cardiotoxicity by Attenuation of Mitochondrial Oxidant Injury and JNK Activation. *J Cell Biochem.* 2011; 112(10):2873-2881.
- Chatterjee K, Zhang J, Honbo N *et al.* Doxorubicin Cardiomyopathy. *Cardiology.* 2010; 115(2):155-162.
- Chen Y and Dorn GW. PINK1-phosphorylated mitofusin 2 is a Parkin receptor for culling damaged mitochondria. *Science.* 2013; 340(6131):471-475.
- Chen Y, Qing W, Sun M *et al.* Melatonin protects hepatocytes against bile acid-induced mitochondrial oxidative stress via the AMPK-SIRT3-SOD2 pathway. *Free Radic Res.* 2015; 49(10):1275-1284.
- Christofferson DE and Yuan J. Necroptosis as an alternative form of programmed cell death. *Curr Opin Cell Biol.* 2010; 22:263–268.
- Chua S, Lee FY, Chiang HJ *et al.* The cardioprotective effect of melatonin and exendin-4 treatment in a rat model of cardiorenal syndrome. *J Pineal Res.* 2016; 61(4):438-456.

- Cipolat S, de Brito OM, Dal Zilio *et al.* OPA1 requires mitofusin 1 to promote mitochondrial fusion. *Proc Natl Acad Sci USA.* 2004; 101(45):15927-15932.
- Codogno P and Meijer AJ. Autophagy and signaling: their role in cell survival and cell death. *Cell Death Differ.* 2005; 12:1509-1518.
- Coto-Montes A, Boga JA, Rosales-Corral S *et al.* Role of melatonin in the regulation of autophagy and mitophagy: a review. *Mol Cell Endocrinol.* 2012; 361:12–23.
- Danz ED, Skramsted J, Henry N *et al.* Resveratrol prevents doxorubicin cardiotoxicity through mitochondrial stabilization and the Sirt1 pathway. *Free Radic Biol Med.* 2009; 46(12):1589-1597.
- Davies KJ and Doroshov JH. Redox cycling of anthracyclines by cardiac mitochondria. I. Anthracycline radical formation by NADH dehydrogenase. *J Biol Chem.* 1986; 261:3060–3067.
- de Meyer GR and Martinet W. Autophagy in the cardiovascular system. *Biochim Biophys Acta.* 2009; 1793:1485–1495.
- Degterev A, Huang Z, Boyce M *et al.* Chemical inhibitor of nonapoptotic cell death with therapeutic potential for ischemic brain injury. *Nat Chem Biol.* 2005; 1:112–119.
- Desler C, Hansen TL, Frederiksen JB *et al.* Is There a Link between Mitochondrial Reserve Respiratory Capacity and Aging? *J Aging Res.* 2012; 2012:1-10.
- Díaz-Casado ME, Lima E, García JA *et al.* Melatonin rescues zebrafish embryos from the parkinsonian phenotype restoring the parkin/PINK1/DJ-1/MUL1 network. *J Pineal Res.* 2016; 61: 96–107.
- Dirks-Naylor AJ, Kouzi SA, Bero JD *et al.* Doxorubicin alters the mitochondrial dynamics machinery and mitophagy in the liver of treated animals. *Fundam Clin Pharmacol.* 2014; 28(6):633-642.
- Doroshov JH. Anthracycline antibiotic-stimulated superoxide, hydrogen peroxide, and hydroxyl radical production by NADH dehydrogenase. *Cancer Res.* 1983; 43:4543–4551.
- Doroshov JH and Davies KJ. Redox cycling of anthracyclines by cardiac mitochondria. II. Formation of superoxide anion, hydrogen peroxide, and hydroxyl radical. *J Biol Chem.* 1986; 261:3068–3074.
- Doroshov JH, Locker GY and Myers CE. Enzymatic defenses of the mouse heart against reactive oxygen metabolites: alterations produced by doxorubicin. *J Clin Invest.* 1980; 65:128–135.
- Dziegiel P, Jethon Z, Suder E *et al.* Role of exogenous melatonin in reducing the cardiotoxic effect of daunorubicin and doxorubicin in the rat. *Exp Toxicol Pathol.* 2002; 53(6):433-439.
- Eidenschink AB, Schroter G, Muller-Wehrich S *et al.* Myocardial high-energy phosphate metabolism is altered after treatment with anthracycline in childhood. *Cardiol Young.* 2000; 10:610–617.

- Elmore S. Apoptosis: A review of programmed cell death. *Toxicol Pathol.* 2007; 35(4):495-516.
- Escames G, Lopez A, Garcia JA *et al.* The role of mitochondria in brain aging and the effects of melatonin. *Curr Neuropharmacol.* 2010; 8:182–193.
- Eser O, Erbas D, Selcuk Surucu H *et al.* Prevention of doxorubicin-induced cardiotoxicity by melatonin. *Mol Cell Biochem.* 2006; 282:31–37.
- Essmann F, Bantel H, Totzke G *et al.* Staphylococcus aureus alpha-toxin-induced cell death: predominant necrosis despite apoptotic caspase activation. *Cell Death Differ.* 2003; 10:1260-1272.
- Fernandez-Marcos PJ and Auwerx J. Regulation of PGC-1 α , a nodal regulator of mitochondrial biogenesis. *Am J Clin Nutr.* 2011; 93(4):884S-890S.
- Fischer TW, Kleszczyński K, Hardkop LH *et al.* Melatonin enhances antioxidative enzyme gene expression (CAT, GPx, SOD), prevents their UVR-induced depletion, and protects against the formation of DNA damage (8-hydroxy-2'-deoxyguanosine) in ex vivo human skin. *J Pineal Res.* 2013; 54:303–312.
- Frank S, Gaume B, Bergmann-Leitner ES *et al.* The role of dynamin-related protein 1, a mediator of mitochondrial fission, in apoptosis. *Dev Cell.* 2001; 1:515–525.
- Fu JL, Zhang HM, Zhang H *et al.* A melatonin-based fluorescence method for the measurement of mitochondrial complex III function in intact cells. *J Pineal Res.* 2013; 55:364–370.
- Fukazawa R, Miller TA, Kuramochi Y *et al.* Neuregulin-1 protects ventricular myocytes from anthracycline- induced apoptosis via erbB4-dependent activation of PI3-kinase/ Akt. *J Mol Cell Cardiol.* 2003; 35:1473–1479.
- Galano A, Tan DX and Reiter RJ. Cyclic 3-hydroxymelatonin, a key metabolite enhancing the peroxyl radical scavenging activity of melatonin. *RSC Adv.* 2014; 4: 5220–5227.
- Galano A, Tan DX and Reiter RJ. Melatonin as a natural ally against oxidative stress: a physicochemical examination. *J Pineal Res.* 2011; 51:1–16.
- Galano A, Tan DX and Reiter RJ. On the free radical scavenging activities of melatonin's metabolites. AFMK and AMK. *J Pineal Res.* 2013; 54:245–257.
- Galloway CA and Yoon Y. Perspectives on: SGP symposium on mitochondrial physiology and medicine: what comes first, misshape or dysfunction? The view from metabolic excess. *J Gen Physiol.* 2012; 139(6):455-463.
- Ganz PA, Hussey MA, Moinpour CM *et al.* Late cardiac effects of adjuvant chemotherapy in breast cancer survivors treated on Southwest Oncology Group protocol S8897. *J Clin Oncol.* 2008; 26:1223–1230.

- García JJ, Lopez-Pingarrón L, Almeida-Souza P *et al.* Protective effects of melatonin in reducing oxidative stress and in preserving the fluidity of biological membranes: a review. *J Pineal Res.* 2014; 56:225–237.
- Geisler S, Holmström KM, Skujat D *et al.* PINK1/Parkin-mediated mitophagy is dependent on VDAC1 and p62/SQSTM1. *Nat Cell Biol.* 2010; 12:119–131.
- Gharanei M, Hussain A, Janneh O *et al.* Attenuation of doxorubicin-induced cardiotoxicity by mdivi-1: a mitochondrial division/mitophagy inhibitor. *PLoS ONE.* 2013; 8:1–15.
- Ghosh G, De K, Maity S *et al.* Melatonin protects against oxidative damage and restores expression of GLUT4 gene in the hyperthyroid rat heart. *J Pineal Res.* 2007; 42:71–82.
- Gobeil S, Boucher CC, Nadeau D *et al.* Characterization of the necrotic cleavage of poly(ADP-ribose) polymerase (PARP-1): implication of lysosomal proteases. *Cell Death Differ.* 2001; 8:588–594.
- Goormaghtigh E, Chatelain P, Caspers J *et al.* Evidence of a complex between adriamycin derivatives and cardiolipin: possible role in cardiotoxicity. *Biochem Pharmacol.* 1980; 29:3003–3010.
- Goormaghtigh E, Huart P, Brasseur R *et al.* Mechanism of inhibition of mitochondrial enzymatic complex I-III by adriamycin derivatives. *Biochim Biophys Acta.* 1986; 861:83–94.
- Gosalvez M, Blanco M, Hunter J *et al.* Effects of anti-cancer agents on the respiration of isolated mitochondria and tumor cells. *Eur J Cancer.* 1974; 10:567–574.
- Gottlieb RA and Gustafsson AB. Mitochondrial turnover in the heart. *Biochim Biophys Acta.* 2011; 1813:1295–1301.
- Green DR and Reed JC. Mitochondria and apoptosis. *Science.* 1998; 281:1309–1312.
- Gultekin F, Delibas N, Yasar S *et al.* In vivo changes in antioxidant systems and protective role of melatonin and a combination of vitamin C and vitamin E on oxidative damage in erythrocytes induced by chlorpyrifos-ethyl in rats. *Arch Toxicol.* 2001; 75:88–96.
- Guo K, Lu J, Huang Y *et al.* Protective Role of PGC-1 α in Diabetic Nephropathy Is Associated with the Inhibition of ROS through Mitochondrial Dynamic Remodeling. *PLoS ONE.* 2015; 10(40):e0125176.
- Guo P, Pi H, Xu S *et al.* Melatonin Improves Mitochondrial Function by Promoting MT1/SIRT1/PGC-1 Alpha-Dependent Mitochondrial Biogenesis in Cadmium-Induced Hepatotoxicity In Vitro. *Toxicol Sci.* 2014; 142(1):182-195.
- Gustafsson AB and Gottlieb RA. Autophagy in ischemic heart disease. *Circ Res.* 2009; 104:150–158.

- Gustafsson AB and Gottlieb RA. Heart mitochondria: gates of life and death. *Cardiovasc Res.* 2008; 77:334–343.
- Guyen C, Taskin E, Akcakaya H *et al.* Melatonin prevents mitochondrial damage induced by doxorubicin in mouse fibroblasts through Ampk-Ppar Gamma-dependent mechanisms. *Med Sci Monit.* 2016; 22:438-446.
- Han D, Huang W, Li X *et al.* Melatonin facilitates adipose-derived mesenchymal stem cells to repair the murine infarcted heart via the SIRT1 signaling pathway. *J Pineal Res.* 2016; 60(2):178-192.
- Head B, Griparic L, Amiri M *et al.* Inducible proteolytic inactivation of OPA1 mediated by the OMA1 protease in mammalian cells. *J Cell Biol.* 2009; 187: 959–966.
- Hoshino A, Matoba S, Iwai-Kanai E *et al.* p53-TIGAR axis attenuates mitophagy to exacerbate cardiac damage after ischemia. *J Mol Cell Cardiol.* 2012; 52:175–184.
- Hsiao CW, Peng TI, Peng AC *et al.* Long-term A β exposure augments mCa²⁺-independent mROS-mediated depletion of cardiolipin for the shift of a lethal transient mitochondrial permeability transition to its permanent mode in NARP cybrids: a protective targeting of melatonin. *J Pineal Res.* 2013; 54:107–125.
- Hsu CP, Zhai P, Yamamoto T *et al.* Silent information regulator 1 protects the heart from ischemia/reperfusion. *Circulation.* 2010; 122:2170-2182.
- Ichikawa Y, Ghanefar M, Bayeva M *et al.* Cardiotoxicity of doxorubicin is mediated through mitochondrial iron accumulation. *J Clin Invest.* 2014; 124:617–630.
- Iliskovic N, Li T, Khaper N *et al.* Modulation of adriamycin-induced changes in serum free fatty acids, albumin and cardiac oxidative stress. *Mol Cell Biochem.* 1998; 188:161– 166.
- Ingwall JS. Energy metabolism in heart failure and remodelling. *Cardiovasc Res.* 2009; 81:412–419.
- Iwai-Kanai E, Yuan H, Huang C *et al.* A method to measure cardiac autophagic flux *in vivo*. *Autophagy.* 2008; 4(3):322-329.
- Jeyaseelan R, Poizat C, Wu HY *et al.* Molecular mechanisms of doxorubicin-induced cardiomyopathy. Selective suppression of Reiske iron-sulfur protein, ADP/ATP translocase, and phosphofructokinase genes is associated with ATP depletion in rat cardiomyocytes. *J Biol Chem.* 1997; 272:5828–5832.
- Jiang F, Ryan MT, Schlame M *et al.* Absence of Cardiolipin in the *crd1* Null Mutant Results in Decreased Mitochondrial Membrane Potential and Reduced Mitochondrial Function. *J Biol Chem.* 2000; 275: 22387.

- Jimenez-Ortega V, Cano P and Cardinali DP. 24-Hour variation in gene expression of redox pathway enzymes in rat hypothalamus: effect of melatonin treatment. *Redox Rep.* 2009; 14:132–138.
- Jung-Hynes B, Reiter RJ and Ahmad N. Sirtuins, melatonin and circadian rhythms: building a bridge between aging and cancer. *J Pineal Res.* 2010; 48:9–19.
- Jung-Hynes B, Schmit TL, Reagan-Shaw SR *et al.* Melatonin, a novel Sirt1 inhibitor, imparts anti-proliferative effects against prostate cancer in vitro in culture and in vivo in TRAMP model. *J Pineal Res.* 2010; 2:140–149.
- Kaiserova H, Simunek T, Sterba M *et al.* New iron chelators in anthracycline-induced cardiotoxicity. *Cardiovasc Toxicol.* 2007; 7:145–150.
- Kalyanaraman B, Darley-Usmar V, Davies KJ *et al.* Measuring reactive oxygen and nitrogen species with fluorescent probes: challenges and limitations. *Free Radic Biol Med.* 2012; 52(1):1-6.
- Kalyanaraman B, Joseph J, Kalivendi S *et al.* Doxorubicin-induced apoptosis: implications in cardiotoxicity. *Mol Cell Biochem.* 2002; 234–235:119–124.
- Kang JW, Cho HI and Lee SM. Melatonin inhibits mTOR-dependent autophagy during liver ischemia/reperfusion. *Cell Physiol Biochem.* 2014; 33:23–36.
- Kang JW, Hong JM and Lee SM. Melatonin enhances mitophagy and mitochondrial biogenesis in rats with carbon tetrachloride-induced liver fibrosis. *J Pineal Res.* 2016; 60(4):383-393.
- Karbowski M and Youle RJ. Dynamics of mitochondrial morphology in healthy cells and during apoptosis. *Cell Death Differ.* 2003; 10:870–880.
- Kasekar NM, Gupta GJC, Jadhav KR *et al.* Review on melatonin “A miraculous drug and its applications.” *World J Pharm Sci.* 2014; 3(6):1974-1985.
- Kim C, Kim N, Joo H *et al.* Modulation by melatonin of the cardiotoxic and antitumor activities of adriamycin. *J Cardiovasc Pharmacol.* 2005; 46:200–210.
- Kim I, Rodriguez-Enriquez S and Lemasters JJ. Selective degradation of mitochondria by mitophagy. *Arch Biochem Biophys.* 2007; 462:245–253.
- Kim JS, He L and Lemasters JJ. Mitochondrial permeability transition: a common pathway to necrosis and apoptosis. *Biochem Biophys Res Commun.* 2003; 304:463–470.
- Kitagawa K, Takeda K, Saito K *et al.* Differences in fatty acid metabolic disorder between ischemic myocardium and doxorubicin-induced myocardial damage: assessment using BMIPP dynamic SPECT with analysis by the Rutland method. *J Nucl Med.* 2002; 43:1286–1294.

- Klingenberg M and Rottenberg H. Relation between the gradient of the ATP/ADP ratio and the membrane potential across the mitochondrial membrane. *Eur J Biochem.* 1977; 73:125–130.
- Kroemer G and Reed JC. Mitochondrial control of cell death. *Nat Med.* 2000; 6:513–519.
- Kuznetsov AV, Margreiter R, Amberger A *et al.* Changes in mitochondrial redox state, membrane potential and calcium precede mitochondrial dysfunction in doxorubicin-induced cell death. *Biochim Biophys Acta.* 2011; 1813(6):1144-1152.
- L'ecuyer T, Sanjeev S, Thomas R *et al.* DNA damage is an early event in doxorubicin-induced cardiac myocyte death. *Am J Physiol Heart Circ Physiol.* 2006; 291:H1273– H1280.
- Lai HC, Yeh YC, Wang LC *et al.* Propofol ameliorates doxorubicin-induced oxidative stress and cellular apoptosis in rat cardiomyocytes. *Toxicol Appl Pharmacol.* 2011; 257(3):437-448.
- Lai L, Wang M, Martin OJ *et al.* A role for peroxisome proliferator-activated receptor γ coactivator 1 (PGC-1) in the regulation of cardiac mitochondrial phospholipid biosynthesis. *J Biol Chem.* 2014; 289(4):2250-2259
- Lee S, Jeong SY, Lim WC *et al.* Mitochondrial fission and fusion mediators, hFis1 and OPA1, modulate cellular senescence. *J Biol Chem.* 2007; 282(31):22977-22983.
- Leon J, Acuna-Castroviejo D, Escames G *et al.* Melatonin mitigates mitochondrial malfunction. *J Pineal Res.* 2008; 38:1–9.
- Leone TC, Lehman JJ, Finck BN *et al.* PGC-1 α deficiency causes multi-system energy metabolic derangements: muscle dysfunction, abnormal weight control and hepatic steatosis. *PLoS Biol.* 2005; 3(4):e101.
- Li T, Danelisen I and Singal PK. Early changes in myocardial antioxidant enzymes in rats treated with adriamycin. *Mol Cell Biochem.* 2002; 232:19–26.
- Lin J, Handschin C and Spiegelman BM. Metabolic control through the PGC-1 family of transcription coactivators. *Cell Metab.* 2005; 1(6):361-370.
- Lissoni P. The pineal gland as a central regulator of cytokine network. *Neuro Endocrinol Lett.* 1999; 20(6):343-349.
- Liu J, Mao W, Ding B *et al.* ERKs/p53 signal transduction pathway is involved in doxorubicin-induced apoptosis in H9c2 cells and cardiomyocytes. *Am J Physiol Heart Circ Physiol.* 2008; 295:H1956– H1965.

- Liu J, Zheng H, Tang M *et al.* A therapeutic dose of doxorubicin activates ubiquitin-proteasome system-mediated proteolysis by acting on both the ubiquitination apparatus and proteasome. *Am J Physiol Heart Circ Physiol.* 2008; 295(6):H2541-H2550.
- Liu J, Zhou H, Fan W *et al.* Melatonin influences proliferation and differentiation of rat dental papilla cells in vitro and dentine formation in vivo by altering mitochondrial activity. *J Pineal Res.* 2013; 54:170–178.
- Liu MH, Shan J, Li J *et al.* Resveratrol inhibits doxorubicin-induced cardiotoxicity via sirtuin 1 activation in H9c2 cardiomyocytes. *Exp Ther Med.* 2016; 12(2):1113-1118.
- Liu X, Chen Z, Chang CHUAC *et al.* Melatonin as an effective protector against doxorubicin-induced cardiotoxicity. *Am J Physiol Heart Circ Physiol.* 2002; 283:H254– H263.
- Liu Y, Shoji-Kawata S, Sumpter RM Jr *et al.* Autosis is a Na⁺, K⁺-ATPase-regulated form of cell death triggered by autophagy-inducing peptides, starvation, and hypoxia-ischemia. *Proc Natl Acad Sci USA.* 2013; 110:20364–20371.
- Lombard DB, Alt FW, Cheng HL *et al.* Mammalian Sir2 homolog SIRT3 regulates global mitochondrial lysine acetylation. *Mol Cell Biol.* 2007; 27:8807–8814.
- Loos B, du Toit A and Hofmeyr J-HS. Defining and measuring autophagosome flux-concept and reality. *Autophagy.* 2014; 10(11):2087-2096.
- Loos B, Lochner A and Engelbrecht A-M. Autophagy in heart disease: A strong hypothesis for an untouched metabolic reserve. *Med Hypotheses.* 2011; 77(1):52-57.
- Lu L, Wu W, Yan J *et al.* Adriamycin-induced autophagic cardiomyocyte death plays a pathogenic role in a rat model of heart failure. *Int J Cardiol.* 2009; 134:82–90.
- Lu TM, Tsai JY, Chen YC *et al.* Downregulation of Sirt1 as aging change in advanced heart failure. *J Biomed Sci.* 2014; 21:57.
- MacVicar TD and Lane JD. Impaired OMA1-dependent cleavage of OPA1 and reduced DRP1 fission activity combine to prevent mitophagy in cells that are dependent on oxidative phosphorylation. *J Cell Sci.* 2014; 127: 2313-2325.
- Marcillat O, Zhang Y and Davies KJ. Oxidative and non-oxidative mechanisms in the inactivation of cardiac mitochondrial electron transport chain components by doxorubicin. *Biochem J.* 1989; 259:181–189.
- Marin-Garcia J, Michael JG and Gordon WM. Mitochondrial pathology in cardiac failure. *Cardiovasc Res.* 2001; 49:17–26.

- Martin M, Macias M, Escames G *et al.* Melatonin-induced increased activity of the respiratory chain complexes I and IV can prevent mitochondrial damage induced by ruthenium red in vivo. *J Pineal Res.* 2000; 28:242–248.
- Martin M, Macias M, Leon J *et al.* Melatonin increases the activity of the oxidative phosphorylation enzymes and the production of ATP in rat brain and liver mitochondria. *Int J Biochem Cell Biol.* 2002; 34:348–357.
- Martin-Cano FE, Camello-Almaraz C, Acuna-Castroviejo D *et al.* Age-related changes in mitochondrial function of mouse colonic smooth muscle: beneficial effects of melatonin. *J Pineal Res.* 2014; 56:163–174.
- Matsui Y, Takagi H, Qu X *et al.* Distinct roles of autophagy in the heart during ischemia and reperfusion: roles of AMP-activated protein kinase and Beclin 1 in mediating autophagy. *Circ Res.* 2007; 100:914–922.
- Matuszak Z, Reszka K, Chignell CF *et al.* Reaction of melatonin and related indoles with hydroxyl radicals: EPR and spin trapping investigations. *Free Radic Biol Med.* 1997; 23:367–372.
- McBride H and Soubannier V. Mitochondrial function: OMA1 and OPA1, the grandmasters of mitochondrial health. *Curr Biol.* 2010; 20:R274–R276.
- Meininger M, Landschutz W, Beer M *et al.* Concentrations of human cardiac phosphorus metabolites determined by SLOOP 31P NMR spectroscopy. *Magn Reson Med.* 1999; 41:657–663.
- Menendez-Pelaez A, Poeggeler B, Reiter RJ *et al.* Nuclear localization of melatonin in different mammalian tissues: immune-cytochemical and radioimmunoassay evidence. *J Cell Biochem.* 1993; 53:373–382.
- Mias C, Trouche E, Seguelas MH *et al.* Ex vivo pretreatment with melatonin improves survival, proangiogenic/mitogenic activity, and efficiency of mesenchymal stem cells injected into ischemic kidney. *Stem Cells.* 2008; 26(7):1749-57.
- Minotti G, Cairo G and Monti E. Role of iron in anthracycline cardiotoxicity: new tunes for an old song? *FASEB J.* 1999; 13:199–212.
- Minotti G, Menna P, Salvatorelli E *et al.* Anthracyclines: molecular advances and pharmacologic developments in antitumor activity and cardiotoxicity. *Pharmacol Rev.* 2004; 56:185–229.
- Mitchell P and Moyle J. Chemiosmotic hypothesis of oxidative phosphorylation. *Nature.* 1967; 213:137–139.
- Mitry MA and Edwards JG. Doxorubicin induced heart failure: Phenotype and molecular mechanisms. *Int J Cardiol Heart Vasc.* 2016; 31(10):17-24.

Mizushima N, Levine B, Cuervo AM *et al.* Autophagy fights disease through cellular self-digestion. *Nature*. 2008; 451(7182):1069-1075.

Moreira AJ, Ordoñez R, Cerski CT *et al.* Melatonin Activates Endoplasmic Reticulum Stress and Apoptosis in Rats with Diethylnitrosamine-Induced Hepatocarcinogenesis. *PLoS One*. 2015; 10(12):e0144517.

Morishima I, Matsui H, Mukawa H *et al.* Melatonin, a pineal hormone with antioxidant property, protects against adriamycin cardiomyopathy in rats. *Life Sci*. 1998; 63:511-521.

Mortiboys H, Thomas KJ, Koopman WJH *et al.* Mitochondrial function and morphology are impaired in parkin -mutant fibroblasts. *Annals of Neurology*. 2008; 64:555–565.

Mukherjee D, Ghosh AK, Bandyopadhyay A *et al.* Melatonin protects against isoproterenol-induced alterations in cardiac mitochondrial energy metabolizing enzymes, apoptotic proteins, and assists in complete recovery from myocardial injury in rats. *J Pineal Res*. 2012; 53:166–179.

Muraoka S and Miura T. Inactivation of mitochondrial succinate dehydrogenase by adriamycin activated by horseradish peroxidase and hydrogen peroxide. *Chem Biol Interact*. 2003; 145:67–75.

Nduhirabandi F, Du Toit EF, Blackhurst D *et al.* Chronic melatonin consumption prevents obesity-related metabolic abnormalities and protects the heart against myocardial ischemia and reperfusion injury in a prediabetic model of diet-induced obesity. *J Pineal Res*. 2011; 50:171-182.

Nicolay K and de Kruijff B. Effects of adriamycin on respiratory chain activities in mitochondria from rat liver, rat heart and bovine heart. Evidence for a preferential inhibition of complex III and IV. *Biochim Biophys Acta*. 1987; 892:320–330.

Octavia Y, Tocchetti CG, Gabrielson KL *et al.* Doxorubicin-induced cardiomyopathy: from molecular mechanisms to therapeutic strategies. *J Mol Cell Cardiol*. 2012; 52:1213– 1225.

Ogura R, Sugiyama M, Haramaki N *et al.* Electron spin resonance studies on the mechanism of adriamycin-induced heart mitochondrial damages. *Cancer Res*. 1991; 51:3555– 3558.

Olson RD and Mushlin PS. Doxorubicin cardiotoxicity: analysis of prevailing hypotheses. *FASEB J*. 1990; 4:3076–3086.

Olson RD, Boerth RC, Gerber JG *et al.* Mechanism of Adriamycin cardiotoxicity: evidence for oxidative stress. *Life Sci*. 1981; 29:1393–1401.

Ortiz F, García JA, Acuña-Castroviejo D *et al.* The beneficial effects of melatonin against heart mitochondrial impairment during sepsis: inhibition of iNOS and preservation of nNOS. *J Pineal Res*. 2014; 56:71–81.

- Pablo MI, Reiter RJ, Ortiz GG *et al.* Rhythms of glutathione peroxidase and glutathione reductase in brain of chick and their inhibition by light. *Neurochem Int.* 1998; 32:69–75.
- Pablos MI, Agapito MT, Menéndez-Pelaez A *et al.* Iron decreases the nuclear but not the cytosolic content of the neurohormone melatonin in several tissues in chicks. *J Cell Biochem.* 1996; 60:317–321.
- Paradies G, Paradies V, De Benedictis V *et al.* Functional role of cardiolipin in mitochondrial bioenergetics. *Biochim Biophys Acta – Bioenergetics.* 2014; 1837(4):408-417.
- Paradies G, Petrosillo G, Paradies V *et al.* Melatonin, cardiolipin and mitochondrial bioenergetics in health and disease. *J Pineal Res.* 2010; 48:297–310.
- Pillai VB, Bindu S, Sharp W *et al.* Sirt3 protects mitochondrial DNA damage and blocks the development of doxorubicin-induced cardiomyopathy in mice. *Am J Physiol Heart Circ Physiol.* 2016; 310:H962-H972.
- Pillai VB, Sundaresan NR, Kim G *et al.* Exogenous NAD blocks cardiac hypertrophic response via activation of the SIRT3-LKB1-AMP-activated kinase pathway. *J Biol Chem.* 2010; 285:3133–3144.
- Pozo D, Reiter RJ, Calvo JR *et al.* Inhibition of cerebellar nitric oxide synthase and cyclic GMP production by melatonin via complex formation with calmodulin. *J Cell Bio-chem.* 1997; 65:430–442.
- Qiu X, Brown K, Hirschey MD *et al.* Calorie restriction reduces oxidative stress by SIRT3-mediated SOD2 activation. *Cell Metab.* 2010; 12:662-667.
- Quiles JL, Huertas JR, Battino M *et al.* Antioxidant nutrients and adriamycin toxicity. *Toxicology.* 2002; 180:79– 95.
- Rabinowitz JD and White E. Autophagy and metabolism. *Science.* 2010; 330:1344–1348.
- Rambold AS, Kostecky B and Lippincott-Schwartz J. Fuse or die. Shaping mitochondrial fate during starvation. *Commun Integr Biol.* 2011; 4:752–754.
- Rambold AS, Kostecky B, Elia N *et al.* Tubular network formation protects mitochondria from autophagosomal degradation during nutrient starvation. *Proc Natl Acad Sci USA.* 2011; 108(25):10190-10195.
- Reiter RJ, Paredes SD, Korkmaz A *et al.* Melatonin combats molecular terrorism at the mitochondrial level. *Inter-discip Toxicol.* 2008; 1:137–149.
- Reiter RJ, Tan D-X and Galano A. Melatonin reduces lipid peroxidation and membrane viscosity. *Front Physiol.* 2014; 5:377.

- Reiter RJ, Tan DX, Osuna C *et al.* Actions of melatonin in the reduction of oxidative stress. *J Biomed Sci.* 2000; 7:444–458.
- Reiter RJ, Tan DX, Sainz RM *et al.* Melatonin protects the heart against both ischemia/reperfusion injury and chemotherapeutic drugs. *Cardiovasc Drugs Ther.* 2002; 16:5–6.
- Rodriguez C, Mayo JC, Sainz RM *et al.* Regulation of antioxidant enzymes: a significant role for melatonin. *J Pineal Res.* 2004; 36:1–9.
- Rodriguez-Enriquez S, Kim I, Currin RT *et al.* Tracker dyes to probe mitochondrial autophagy (mitophagy) in rat hepatocytes. *Autophagy.* 2006; 2(1):39-46.
- Rosales-Corral S, Tan D-X, Reiter RJ *et al.* Orally administered melatonin reduces oxidative stress and pro-inflammatory cytokines induced by amyloid-beta peptide in rat brain: a comparative, in vivo study versus vitamin C and E. *J Pineal Res.* 2003; 35:80–84.
- Rose S, Frye RE, Slattery J *et al.* Oxidative stress induces mitochondrial dysfunction in a subset of autism lymphoblastoid cell lines in a well-matched case control cohort. *PLoS One.* 2014; 9(1):e85436.
- Rozov SV, Filatova EV, Orlov AA *et al.* N1- acetyl-N2-formyl-5-methoxykynuramine is a product of melatonin oxidation in rats. *J Pineal Res.* 2004; 35:245–259.
- Ruan Y, Dong C, Patel J *et al.* SIRT1 Suppresses Doxorubicin-Induced Cardiotoxicity by Regulating the Oxidative Stress and p38MAPK Pathways. *Cell Physiol Biochem.* 2015; 35:1116-1124.
- Sack MN and Finkel T. Mitochondrial Metabolism, Sirtuins, and Aging. *Cold Spring Harb Perspect Biol.* 2012; 4(12):a013102.
- Sack MN. Emerging characterization of the role of SIRT3-mediated mitochondrial protein deacetylation in the heart. *Am J Physiol Heart Circ Physiol.* 2011; 301:2191–2197.
- Sahani MH, Itakura E and Mizushima N. Expression of the autophagy substrate SQSTM1/p62 is restored during prolonged starvation depending on transcriptional upregulation and autophagy-derived amino acids. *Autophagy.* 2014; 10(3):431-441.
- Sahna E, Palakinar H, Ozer MK *et al.* Melatonin protects against myocardial doxorubicin toxicity in rats: role of physiological concentrations. *J Pineal Res.* 2003; 35:257–261.
- Sainz RM, Mayo JC, Rodriguez C *et al.* Melatonin and cell death: differential actions on apoptosis in normal and cancer cells. *Cell Mol Life Sci.* 2003; 60:1407–1426.

- Saito K, Takeda K, Okamoto S *et al.* Detection of doxorubicin cardiotoxicity by using iodine-123 BMIPP early dynamic SPECT: quantitative evaluation of early abnormality of fatty acid metabolism with the Rutland method. *J Nucl Cardiol.* 2000; 7:553–561.
- Sayed-Ahmed MM, Shouman SA, Rezk BM *et al.* Propionyl-L-carnitine as potential protective agent against adriamycin-induced impairment of fatty acid beta-oxidation in isolated heart mitochondria. *Pharmacol Res.* 2000; 41:143– 150.
- Schaper J, Meiser E and Stammli G. Ultrastructural morphometric analysis of myocardium from dogs, rats, hamsters, mice and from human hearts. *Circ Res.* 1985; 56:377–391.
- Scher MB, Vaquero A, Reinberg D *et al.* SirT3 is a nuclear NAD⁺-dependent histone deacetylase that translocates to the mitochondria upon cellular stress. *Genes Dev.* 2007; 21:920–928.
- Schwer B and Verdin E. Conserved metabolic regulatory functions of sirtuins. *Cell Metab.* 2008; 7:104–112.
- Scott I and Youle RJ. Mitochondrial fission and fusion. *Essays Biochem.* 2010; 47:85–4798.
- Sehested M, Jensen PB, Sørensen BS *et al.* Antagonistic effect of the cardioprotector (+)-1, 2-bis (3, 5-dioxopiperazi-nyl-1-yl) propane (ICRF-187) on DNA breaks and cytotoxicity induced by the topoisomerase II directed drugs daunorubicin and etoposide (VP-16). *Biochem Pharmacol.* 1993; 46:389–393.
- Şehirli AÖ, Koyun D, Tetik Ş *et al.* Melatonin protects against ischemic heart failure in rats. *J Pineal Res.* 2013; 55(2):138-148.
- Shakir DK and Rasul KI. Chemotherapy Induced Cardiomyopathy: Pathogenesis, Monitoring and Management. *J Clin Med Res.* 2009; 1(1):8-12.
- Shen L, Lu S, Zhou Y *et al.* Developing a rat model of dilated cardiomyopathy with improved survival. *J Zhejiang Univ-Sci B.* 2016; 17(12):975-983.
- Singal PK, Iliskovic N, Li T *et al.* Adriamycin cardiomyopathy: pathophysiology and prevention. *FASEB J.* 1997; 11:931–936.
- Sishi BJN, Loos B, van Rooyen J *et al.* Autophagy upregulation promotes survival and attenuates doxorubicin-induced cardiotoxicity. *Biochem Pharmacol.* 2013; 85: 124–134.
- Siveski-Iliskovic N, Hill M, Chow DA *et al.* Probucol protects against adriamycin cardiomyopathy without interfering with its antitumor effect. *Circulation.* 1995; 91:10–15.
- Sokolove PM. Interactions of adriamycin aglycones with mitochondria may mediate adriamycin cardiotoxicity. *Int J Biochem.* 1994; 26:1341–1350.

- Song C, Peng W, Yin S *et al.* Melatonin improves age-induced fertility decline and attenuates ovarian mitochondrial oxidative stress in mice. *Sci Rep.* 2016; 6:35165.
- Song N, Kim AJ, Kim HJ *et al.* Melatonin suppresses doxorubicin-induced premature senescence of A549 lung cancer cells by ameliorating mitochondrial dysfunction. *J Pineal Res.* 2012; 53(4):335-343.
- Song Z, Chen H, Fiket M *et al.* OPA1 processing controls mitochondrial fusion and is regulated by mRNA splicing, membrane potential, and Yme1L. *J Cell Biol.* 2007; 178(5):749-755.
- Soriano FX, Liesa M, Bach D *et al.* Evidence for a mitochondrial regulatory pathway defined by peroxisome proliferator-activated receptor-gamma coactivator-1 alpha, estrogen-related receptor-alpha, and mitofusin 2. *Diabetes.* 2006; 55(6):1783-1791.
- Spallarossa P, Garibaldi S, Altieri P *et al.* Carvedilol prevents doxorubicin-induced free radical release and apoptosis in cardiomyocytes in vitro. *J Mol Cell Cardiol.* 2004; 37:837–846.
- Spivak M, Bubnov R, Yemets I *et al.* Doxorubicin dose for congestive heart failure modeling and the use of general ultrasound equipment for evaluation in rats. Longitudinal in vivo study. *Med Ultrason.* 2013; 15(1):23-28
- Stacchiotti A, Favero G, Giugno L *et al.* Mitochondrial and Metabolic Dysfunction in Renal Convoluted Tubules of Obese Mice: Protective Role of Melatonin. *PLoS ONE.* 2014; 9(10): e111141.
- Steinherz LJ, Steinherz PG, Tan CT *et al.* Cardiac toxicity 4 to 20 years after Completing anthracycline therapy. *JAMA.* 1991; 266:1672–1677.
- Suen DF, Norris KL and Youle RJ. Mitochondrial dynamics and apoptosis. *Genes Dev.* 2008; 22:1577–1590.
- Sundaresan NR, Samant SA, Pillai VB *et al.* SIRT3 is a stress-responsive deacetylase in cardiomyocytes that protects cells from stress-mediated cell death by deacetylation of Ku70. *Mol Cell Biol.* 2010; 28:6384–6401.
- Szewczyk A and Wojtczak L. Mitochondria as a pharmacological target. *Pharmacol Rev.* 2002; 54:101–127.
- Takemura G and Fujiwara H. Doxorubicin-induced cardiomyopathy from the cardiotoxic mechanisms to management. *Prog Cardiovasc Dis.* 2007; 49(5):330-352.
- Tan DX, Hardeland R, Manchester LC *et al.* Cyclic-3-hydroxymelatonin (C3HOM), a potent antioxidant, scavenges free radicals and suppresses oxidative reactions. *Curr Med Chem.* 2014; 21:1557–1565.

- Tan DX, Manchester LC and Burkhardt S. N1-acetyl-N2-formyl-5-methoxykynuramine, a biogenic amine and melatonin metabolite, functions as a potent antioxidant. *FASEB J.* 2001; 15:2294–2296.
- Tan DX, Manchester LC, Liu X *et al.* Mitochondria and chloroplasts as the original sites of melatonin synthesis: a hypothesis related to melatonin's primary function and evolution in eukaryotes. *J Pineal Res.* 2013; 54:127–138.
- Tan DX, Manchester LC, Reiter RJ *et al.* Melatonin directly scavenges hydrogen peroxide: a potentially new metabolic pathway of melatonin biotransformation. *Free Radic Biol Med.* 2000; 29:1177–1185.
- Tan DX, Manchester LC, Reiter RJ *et al.* Significance of melatonin in antioxidative defense system: reactions and products. *Biol Signals Recept.* 2000; 9(3-4):137-159.
- Tengattini S, Reiter RJ, Tan D-X *et al.* Cardiovascular diseases: protective effects of melatonin. *J Pineal Res.* 2008; 44:16–25.
- Terman A and Brunk UT. Autophagy in cardiac myocyte homeostasis, aging, and pathology. *Cardiovasc Res.* 2005; 68:355–365.
- Thomas C, Carr AC and Winterbourn CC. Free radical inactivation of rabbit muscle creatinine kinase: catalysis by physiological and hydrolyzed ICRF-187 (ICRF-198) iron chelates. *Free Radic Res.* 1994; 21:387–397.
- Thornberry NA. Caspases: key mediators of apoptosis. *Chem Biol.* 1988; 5:97-103.
- Tokarska-Schlattner M, Dolder M and Gerber I *et al.* Reduced creatine-stimulated respiration in doxorubicin challenged mitochondria: particular sensitivity of the heart. *Biochim Biophys Acta.* 2007; 1767:1276–1284.
- Tokarska-Schlattner M, Zaugg M, da Silva R *et al.* Acute toxicity of doxorubicin on isolated perfused heart: response of kinases regulating energy supply. *Am J Physiol Heart Circ Physiol.* 2005; 289:H37–H47.
- Tokarska-Schlattner M, Zaugg M, Zuppinger C *et al.* New insights into doxorubicin-induced cardiotoxicity: the critical role of cellular energetics. *J Mol Cell Cardiol.* 2006; 41:389–405.
- Tresguerres JA, Kireev R, Forman K *et al.* Effect of chronic melatonin administration on several physiological parameters from old Wistar rats and SAMP8 mice. *Curr Aging Sci.* 2012; 5(3):242-53.
- Urata Y, Honma S, Goto S *et al.* Melatonin induces gamma glutamylcysteine synthetase mediated by activator protein-1 in human vascular endothelial cells. *Free Radic Biol Med.* 1999; 27:838–847.
- Venegas C, García JA, Escames G *et al.* Extrapineal melatonin: analysis of its subcellular distribution and daily fluctuations. *J Pineal Res.* 2012; 52:217–227.

- Ventura-Clapier R, Garnier A and Veksler V. Energy metabolism in heart failure. *J Physiol*. 2004; 555:1–13.
- Verma M, Shulga N and Pastorino JG. Sirtuin-4 modulates sensitivity to induction of the mitochondrial transition pore. *Biochim Biophys Acta*. 2013; 1827:38–49.
- Vidal RF, Eksborg S, Sundberg M *et al*. Doxorubicin and daunorubicin-induced energy deprivation and nucleotide degradation in isolated cardiomyocytes. *Toxicology*. 1996; 114:1–10.
- Von Hoff DD, Layard MW, Basa P *et al*. Risk factors for doxorubicin-induced congestive heart failure. *Ann Intern Med*. 1979; 91:710–717.
- Wahab MH, Akoul ES and Abdel-Aziz AA. Modulatory effects of melatonin and vitamin E on doxorubicin-induced cardiotoxicity in Ehrlich ascites carcinoma-bearing mice. *Tumori*. 2000; 86:157–162.
- Wakasugi S, Fischman AJ, Babich JW *et al*. Myocardial substrate utilization and left ventricular function in adriamycin cardiomyopathy. *J Nucl Med*. 1993; 34:1529–1535.
- Wallace KB. Doxorubicin-induced cardiac mitochondrionopathy. *Pharmacol Toxicol*. 2003; 93:105–115.
- Wang K and Klionsky DJ. Mitochondria removal by autophagy. *Autophagy*. 2011; 7:297–300.
- Wang S, Zhao X, Chen W *et al*. Sirtuin 1 activation enhances the PGC-1 α /mitochondrial antioxidant system pathway in status epilepticus. *Mol Med Rep*. 2015; 11(1):521-526.
- Wappler EA, Katz PS, Katakam PVG *et al*. Melatonin affects the expression of mitochondrial fission-fusion proteins in cultured neurons. *FASEB J*. 2012; 26:711-716.
- Weiss RB. The anthracyclines: will we ever find a better doxorubicin? *Semin Oncol*. 1992; 19:670–686.
- Westermann B. Bioenergetic role of mitochondrial fusion and fission. *Biochim Biophys Acta - Bioenergetics*. 2012; 1817(10):1833-1838.
- Xie Z and Klionsky DJ. Autophagosome formation: core machinery and adaptations. *Nat Cell Biol*. 2007; 9:1102–1109.
- Xu M and Ashraf M. Melatonin protection against lethal myocyte injury induced by doxorubicin as reflected by effects on mitochondrial membrane potential. *J Mol Cell Cardiol*. 2002; 34(1):75-79.
- Xu X, Chua CC, Zhang M *et al*. The role of PARP activation in glutamate-induced necroptosis in HT-22 cells. *Brain Res*. 2010; 1343:206–212.

- Xua MF, Tang BPL, Qianb ZM *et al.* Effects by doxorubicin on the myocardium are mediated by oxygen free radicals. *Life Sci.* 2001; 68:889–901.
- Yamamoto HA and Mohanan PV. Melatonin attenuates brain mitochondria DNA damage induced by potassium cyanide in vivo and in vitro. *Toxicology.* 2002; 179:29–36.
- Yen HC, Oberley TD, Vichitbandha S *et al.* The protective role of manganese superoxide dismutase against adriamycin-induced acute cardiac toxicity in transgenic mice. *J Clin Invest.* 1996; 98:1253–1260.
- Yi X, Bekeredjian R, DeFilippis NJ *et al.* Transcriptional analysis of doxorubicin-induced cardiotoxicity. *Am J Physiol Heart Circ Physiol.* 2005; 290:H1098-H1102.
- Yorimitsu T and Klionsky DJ. Autophagy: molecular machinery for self-eating. *Cell Death Differ.* 2005; 12:1542–1552.
- Yu L, Sun Y, Cheng L *et al.* Melatonin receptor-mediated protection against myocardial ischemia/reperfusion injury: role of SIRT1. *J Pineal Res.* 2014; 57:228–238.
- Yu SW, Wang H, Poitras MF *et al.* Mediation of poly (ADP-ribose) polymerase-1-dependent cell death by apoptosis-inducing factor. *Science.* 2002; 297:259–263.
- Zeitzer JM, Duffy JF, Lockley SW *et al.* Plasma melatonin rhythms in young and older humans during sleep, sleep deprivation, and wake. *Sleep.* 2007; 30(11):1437-1443.
- Zhang H, Liu D, Wang X *et al.* Melatonin improved rat cardiac mitochondria and survival rate in septic heart injury. *J Pineal Res.* 2013; 55:1–6.
- Zhang YW, Shi J and Li YJ. Cardiomyocyte death in doxorubicin-induced cardiotoxicity. *Arch Immunol Ther Exp.* 2009; 57:435–445.
- Zhao S, Xu W, Jiang W *et al.* Regulation of cellular metabolism by protein lysine acetylation. *Science.* 2010; 327:1000–1004.
- ZHU H, Sarkar S, Scott L *et al.* Doxorubicin Redox Biology: Redox Cycling, Topoisomerase Inhibition, and Oxidative Stress. *ROS.* 2016; 1(3):89–198.
- Zhu P, Liu J, Shi J *et al.* Melatonin protects ADSCs from ROS and enhances their therapeutic potency in a rat model of myocardial infarction. *J Cell Mol Med.* 2015; 19(9):2232-2243.
- Zhu W, Shou W, Payne RM *et al.* A mouse model for juvenile doxorubicin-induced cardiac dysfunction. *Pediatr Res.* 2008; 64(5):488-494.
- Zorzano A. Regulation of mitofusin-2 expression in skeletal muscle. *Appl Physiol Nutr Metab.* 2009; 34(3):433-439.

Zweier JL, Gianni L, Muindi J *et al.* Differences in O₂ reduction by the iron complexes of Adriamycin and daunomycin: the importance of the side chain hydroxyl group. *Biochim Biophys Acta.* 1988; 884:326–336.